

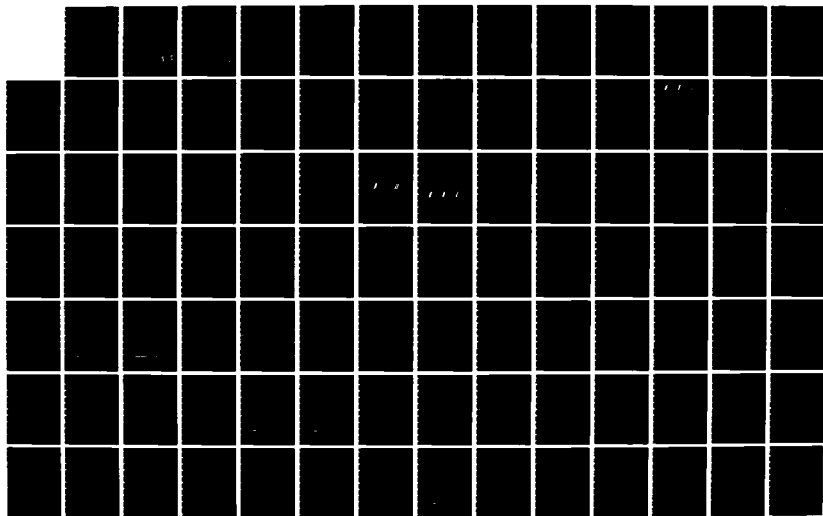
AD-A136 896

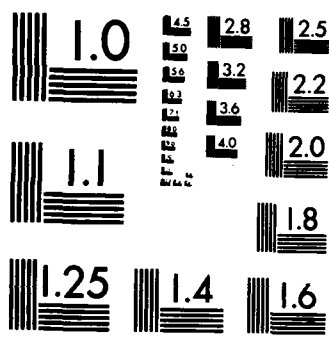
ROUGHNESS EFFECTS ON COMPRESSOR BLADE PERFORMANCE IN
CASCADE AT HIGH REYN. (U) AIR FORCE INST OF TECH
WRIGHT-PATTERSON AFB OH SCHOOL OF ENGI... F J TANIS
NOV 83 AFIT/GAE/AA/83D-23 F/G 20/4

1/2

UNCLASSIFIED

NL





MICROCOPY RESOLUTION TEST CHART
NATIONAL BUREAU OF STANDARDS-1963-A

AD A136896



ROUGHNESS EFFECTS ON COMPRESSOR
BLADE PERFORMANCE IN CASCADE
AT HIGH REYNOLDS NUMBER

THESIS

AFIT/GAE/AA/83D-23 Frederick J. Tanis Jr.
2Lt. U.S. Air Force

DTIC
ELECTE
JAN 18 1984
S E D

DEPARTMENT OF THE AIR FORCE
AIR UNIVERSITY

AIR FORCE INSTITUTE OF TECHNOLOGY

Wright-Patterson Air Force Base, Ohio

84 01 17 071

This document has been approved
for public release and sale; its
distribution is unlimited.

AFIT/GAE/AA/83D-23

ROUGHNESS EFFECTS ON COMPRESSOR
BLADE PERFORMANCE IN CASCADE
AT HIGH REYNOLDS NUMBER

THESIS

AFIT/GAE/AA/83D-23 Frederick J. Tanis Jr.
2Lt. U.S. Air Force

DTIC
ELECTE
JAN 18 1984
S E D

Approved for public release; distribution unlimited

AFIT/GAE/AA/83D-23

ROUGHNESS EFFECTS ON COMPRESSOR
BLADE PERFORMANCE IN CASCADE
AT HIGH REYNOLDS NUMBER

THESIS

Presented to the Faculty of the School of Engineering
of the Air Force Institute of Technology
Air University
in Partial Fulfillment of the
Requirements for the Degree of
Master of Science in Aeronautical Engineering

Frederick J. Tanis Jr., B.S.
Second Lieutenant, USAF

November 1983

Approved for public release; distribution unlimited

PREFACE

I would like to thank my thesis committee members, Capt Wesley Cox, Dr. Milton Franke and particularly my principal advisor Dr. William C. Elrod for all the time they spent working with me in order to get this study compleated. I would also like to thank Maj. John Vonada for all of his help in getting acquainted with the Cascade Test Facility and keeping it alive throughout the course of this study. I am also very grateful for the the support of the members of the AFIT Fabrication Branch and the technicians in the Department of Aeronautics and Astronautics, with special thanks going to Mr. John Brohaus and Mr. Harley Linville. My deepest thanks go to my wife Melinda for her understanding and support during my long hours away from home during the course of this study.

Frederick J. Tanis Jr.



Accession For	
NTIS GRA&I	<input checked="checked" type="checkbox"/>
DTIC TAB	<input type="checkbox"/>
Unannounced	<input type="checkbox"/>
Justification	
By _____	
Distribution/	
Availability Codes	
Dist	Avail and/or Special
A-1	

CONTENTS

Preface.....	ii
LIST OF FIGURES.....	iv
LIST OF SYMBOLS.....	vii
LIST OF TABLES.....	ix
ABSTRACT.....	x
I. INTRODUCTION.....	1
BACKGROUND.....	1
OBJECTIVES AND SCOPE.....	2
II. APPERATUS AND PROCEDURE.....	4
CASCADE TEST FACILITY.....	4
TEST SECTION.....	4
INSTRUMENTATION.....	5
HOT FILM SENSOR CALIBRATION.....	7
EXIT PLANE TRAVERSER.....	10
BLADE ROUGHNESS CONFIGURATIONS.....	11
DATA ACQUISITION AND PROCESSING.....	12
III. DATA REDUCTION.....	14
EXIT VELOCITY.....	14
TOTAL PRESSURE LOSS.....	16
TURBULENCE INTENSITY.....	19
IV. RESULTS AND DISCUSSION.....	20
LOCATION EFFECTS.....	21
ROUGHNESS MAGNITUDE EFFECTS.....	37
REPEATABILITY.....	48
V. CONCLUSIONS AND RECOMMENDATIONS.....	50
CONCLUSIONS.....	50
RECOMMENDATIONS.....	50
BIBLIOGRAPHY.....	52
APPENDIX A: ROUGHNESS DEFINITIONS.....	54
APPENDIX B: VELOCITY AND TURBULENCE INTENSITY PROFILES.....	57
VITA.....	98

LIST OF FIGURES

<u>Figure</u>	<u>Page</u>
1. Test Section.....	5
2. Hot Wire Calibration Curve.....	9
3. Standard Data Window.....	10
4. Blade Roughness Configurations.....	12
5. Roughness Configurations 2 and 3.....	21
6. Roughness Configurations 5, 7 and 8.....	22
7. Velocity and Turbulence Intensity Profile Conf#1 Eval#6: Smooth Baseline blade Traverse#1..	26
8. Velocity and Turbulence Intensity Profile Conf#1 Eval#6: Smooth Baseline blade Traverse#2..	27
9. Velocity and Turbulence Intensity Profile Conf#1 Eval#6: Smooth Baseline blade Traverse#3..	28
10. Velocity and Turbulence Intensity Profile Conf#1 Eval#6: Smooth Baseline blade Traverse#4..	29
11. Velocity and Turbulence Intensity Profile Conf#1 Eval#6: Smooth Baseline blade Traverse#5..	30
12. Velocity and Turbulence Intensity Profile Traverse#1 Conf#5 Eval#2: 20 micro-meter Ra Roughness from L.E.-1/4Chord.....	32
13. Velocity and Turbulence Intensity Profile Traverse#1 Conf#7 Eval#1: 20 micro-meter Ra Roughness from 1/8-3/8Chord.....	33
14. Velocity and Turbulence Intensity Profile Traverse#1 Conf#8 Eval#1: 20 micro-meter Ra Roughness from 1/4-1/2Chord.....	34
15. Velocity and Turbulence Intensity Profile Traverse#1 Conf#2 Eval#1: 27 micro-meter Ra Roughness from L.E.-1/4Chord.....	35
16. Velocity and Turbulence Intensity Profile Traverse#1 Conf#3 Eval#1: 44 micro-meter Ra Roughness from 1/2Chord-T.E.....	36

17.	Loss in Non-Dimensional Total Pressure with Ra Roughness.....	39
18.	Loss in Non-Dimensional Total Pressure with Rtm Roughness.....	40
19.	Loss in Non-Dimensional pressure with Rpm Roughness.....	41
20.	Velocity and Turbulence Intensity Profile Traverse#1 Conf#1 Eval#6: Smooth Baseline blade.	44
21.	Velocity and Turbulence Intensity Profile Traverse#1 Conf#6 Eval#2: 3 micro-meter Ra Roughness from L.E.-1/4Chord.....	45
22.	Velocity and Turbulence Intensity Profile Traverse#1 Conf#5 Eval#2: 20 micro-meter Ra Roughness from L.E.-1/4Chord.....	46
23.	Velocity and Turbulence Intensity Profile Traverse#1 Conf#2 Eval#1: 27 micro-meter Ra Roughness from L.E.-1/4Chord.....	47
24.	Arithmetic Average Roughness.....	54
25.	Three different surfaces with equal Ra.....	54
26.	Derivation of Rtm roughness.....	55
27.	Derivation of Rpm roughness.....	55
28.	Velocity and Turbulence Intensity Profile Conf#1 Eval#7: Smooth Baseline blade.....	58
29.	Velocity and Turbulence Intensity Profile Conf#2 Eval#1: 27 micro-meter Ra Roughness from L.E.-1/4Chord.....	63
30.	Velocity and Turbulence Intensity Profile Conf#3 Eval#1: 44 micro-meter Ra Roughness from 1/2Chord-T.E.....	68
31.	Velocity and Turbulence Intensity Profile Conf#5 Eval#2: 20 micro-meter Ra Roughness from L.E.-1/4Chord.....	73
32.	Velocity and Turbulence Intensity Profile Conf#6 Eval#2: 3 micro-meter Ra Roughness from L.E.-1/4Chord.....	78
33.	Velocity and Turbulence Intensity Profile Conf#7 Eval#1: 20 micro-meter Ra Roughness from 1/8-3/8Chord.....	83

34.	Velocity and Turbulence Intensity Profile Conf#8 Eval#1: 20 micro-meter Ra Roughness from 1/4-1/2Chord.....	88
35.	Velocity and Turbulence Intensity Profile Conf#8 Eval#2: 20 micro-meter Ra Roughness from 1/4-1/2Chord.....	93

LIST OF SYMBOLS

<u>Symbol</u>	<u>Name</u>	<u>units</u>
A	Area	in
C	Chord	in
Cp	Specific Heat at Constant Pressure	B/lbm-R
dA	Differintial Area	in
dY	Differintial Length	in
γ	Ratio of Specific Heats	NONE
L	Sample Length	micro-meters
m	Mass Flow Rate	lbm/sec
Nu	Nusselt Number	NONE
$\bar{\omega}$	Non-Dimensional Total Pressure Loss	NONE
P	Pressure	lbf/in
P	Mass Averaged Pressure	lbf/in
Ra	Arithmetic Average Roughness	micro-meters
Re	Reynolds Number	NONE
ρ	Density	lbm/cubic-ft
Rpm	Average Maximum Peak to Mean Roughness	micro-meters
Rtm	Average Maximum peak to Valley Roughness	micro-meters
s	Scaling Factor	NONE
T	Temperature	R
TI	Turbulence Intensity	percent
V	Velocity	ft/sec
V'	Corrected Velocity	ft/sec

Subscripts

1	Inlet
2	Exit
S	Static
T	Total

Abbreviations

AFIT	Air Force Institute of Technology
CTF	Cascade Test Facility
HP	Hewlet Packard

LIST OF TABLES

Table		Page
I.	PERFORMANCE DATA FOR ROUGHNESS LOCATION TESTS.....	23
II.	PERFORMANCE DATA FOR ROUGHNESS MAGNITUDE TESTS.....	38

ABSTRACT

An experimental investigation of the effects of roughness on compressor blade performance in cascade at high Reynolds numbers was performed. A ~~seven~~^{9 1/2} blade cascade of NACA 64-A905 blades with a chord of 2 in. and an aspect ratio of 1 was tested in a linear cascade. The blades were mounted with a stagger angle of 31 deg and an angle of attack of 15 deg. The spacing between blades was 1.33 inches which gave a solidity of 1.5.

This study was divided into two parts; first to determine the importance of the location of roughness on blade performance; and ~~second~~⁹ to determine how the degree of roughness affects blade performance. The velocity and turbulence intensity profiles of the flow region downstream of the center blade and the non-dimensional total pressure loss parameter ^(omega bar) ~~59~~ were used to evaluate blade performance. Hot wire anemometry ² was used to measure the velocity and turbulence intensity profiles downstream of the blade. The measured exit velocity and static pressure were used to derive the exit total pressure.

Roughness located near the leading edge of the blade caused the greatest impact on ~~omega~~⁵⁹ and the velocity and turbulence intensity profiles. Changes in the magnitude of the roughness did not affect the blade performance until a threshold was exceeded; then the performance decreased rapidly.

I. INTRODUCTION

BACKGROUND

The wide operating range of today's military aircraft engine has led to a flow regime characterized by a high Reynolds number in the last few stages of the high pressure ratio compressor. In this regime the loss in performance is thought to be a function of roughness alone. This is in comparison to the low Reynolds number flow where the efficiency is a function of the Reynolds number and not as heavily dependent on roughness. The lack of good cascade data for use in specifying blade surface finishes in order to minimize the loss in total pressure across the blade row has led to increased research in this area. One performance parameter that of particular use to the compressor designer is the total pressure loss coefficient (Ref.15).

In recent years the Air Force Institute of Technology in conjunction with the Air Force Wright Aeronautical Laboratories, AFWAL/POTC, has been studying the effects of roughness on compressor blades at a high Reynolds number. This study was initiated in order to characterize the effects of roughness on the performance of axial flow compressor blades in cascade. The ultimate goal would be to find a technically quantifiable surface finish that will optimize the thrust specific fuel consumption (TSFC) and the maintenance time of the gas turbine engine. With this accomplished the Air Force could save millions of dollars in

reduced operating costs.

The research began in 1981 with the design and construction of a cascade test facility at the Air Force Institute of Technology's School of Engineering (Ref.2). The following year a study of the roughness effects of compressor exit guide vanes at a high angle of attack was conducted. This study showed that there was minimal effect of roughness on the blades because of a large separated flow region on the suction surface of the blade. The losses from the separation greatly over shadowed any losses due to the roughness (Ref.6).

OBJECTIVE AND SCOPE

The basic objectives of this investigation are as follows:

1. Locate the region on the blade where roughness affects the loss in total pressure the greatest.
2. Evaluate how the total pressure loss coefficient varies with changes in the magnitude of the roughness.

The approach used to evaluate the effects that roughness has on blade performance was to build a cascade of roughened blades then perform a wake survey to evaluate

blade total pressure loss in non-dimensional form. In addition to the total pressure loss coefficient the velocity and turbulence intensity profiles of the blade wake will be compared.

The surface roughness parameters chosen for this investigation are the arithmetic average roughness, R_a , the average maximum peak to valley roughness, R_{tm} , and the average maximum peak to mean roughness, R_{pm} (see Appendix A for roughness definitions).

II. EXPERIMENTAL APPARATUS AND PROCEDURE

CASCADE TEST FACILITY

The cascade test facility (CTF) at the Air Force Institute of Technology School of Engineering was used for this investigation. This apparatus, which was described in detail by Allison (Ref.2), consists of an air supply coupled to a diffuser and stilling chamber with provisions for mounting a 2 in by 8 in test section. The air supply for the CTF consists of a 40 horsepower centrifugal blower with a name plate rating of 3000 cubic feet per minute at 26 ounces of head. The blower brings cool air from outside and mixes it with warm recirculated air in order to control the test section temperature. The air is then filtered using an electrostatic cleaner to remove particles that would be detrimental to a hot wire anemometer sensor. A flow straightening system consisting of two fiber filters and a honeycomb is located in the stilling chamber. The air is then delivered to the test section with turbulence intensities of less than 2%, and a Reynolds number per foot in excess of two million.

TEST SECTION

The test section, as depicted in Fig. 1, was a cascade containing seven NACA 64-A905 blades with a chord of 2 in and an aspect ratio of 1. The blades were mounted with a stagger angle of 31 deg and an angle of attack of 15 deg.

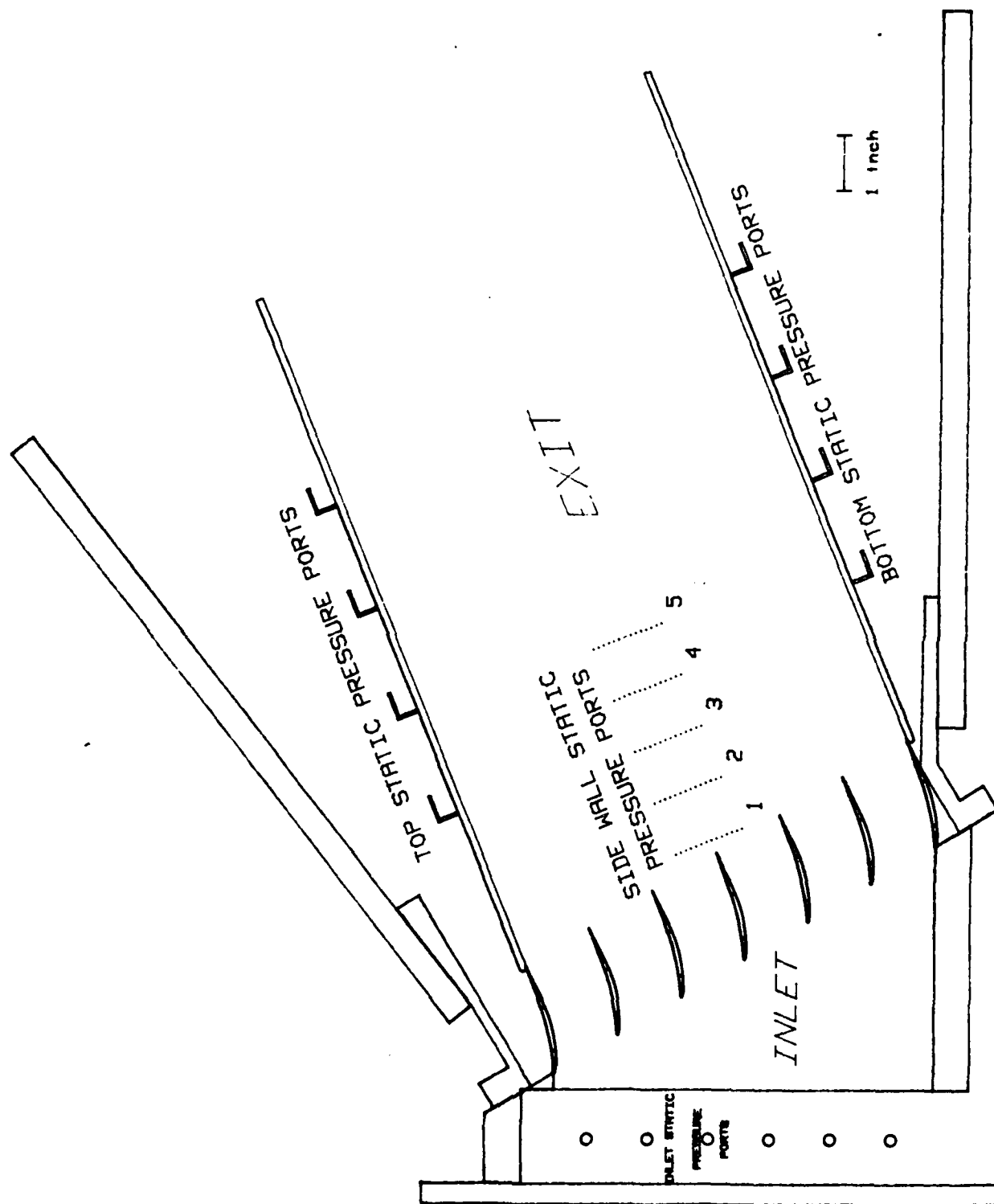


Figure 1: Test section

This produced a nominal turning angle of 22 deg. The spacing between the blades was 1.33 in which gave a solidity of 1.5.

The cascade of blades was followed by a 13 in long adjustable channel that could be used either as a constant area or a diffusing channel. The top and bottom end walls of the channel are fitted with static pressure ports that are used in aligning the exit channel with the free stream direction. When the end walls were parallel to the free stream direction, the static pressure at the respective static ports on the top and bottom end walls were in agreement and the inlet velocity profile was uniform. In addition there are static pressure ports in the side walls of the channel to measure the local static pressure at each traverse location. The inlet duct to the cascade is also fitted with static pressure ports that are used to calculate the inlet velocity and check the profile during alignment of the exit channel.

INSTRUMENTATION

The CTF was instrumented with four pressure transducers, two thermocouples, a hot wire anemometer and numerous manometers. The pressure transducers were used to measure stilling chamber (test section inlet) total, inlet static, exit static, and ambient pressures. The thermocouples were used to measure stilling chamber total and control room ambient temperatures. The hot wire anemometer was used to measure both the X and Y components

of the velocity and turbulence (fluxuating velocity) in the region downstream from the blades. The hot wire system consisted of a TSI Model 1241-10 hot film X-sensor in conjunction with two TSI Model 1050 constant temperature anemometers. Manometers were used to monitor the static pressure on the top and bottom end walls of the exit channel to insure that this channel was properly aligned with the free stream.

HOT FILM SENSOR CALIBRATION

The hot film sensors were calibrated using a temperature compensation procedure that is described briefly as follows. First the operating resistance of the sensor was determined for temperature range of interest assuming an over heat ratio of 1.5 as recommended by TSI (Ref.16). Once the operating resistance was determined the anemometers were set-up and calibration data were recorded at various velocities and temperatures in the expected test range. Usually four temperatures and ten velocities were recorded in the expected range. The following data were recorded at each calibration point: 1) calibrator total pressure, 2) calibrator total temperature, 3) exit static pressure (ambient), and 4) voltage outputs from each channel of the anemometer. This data provided the necessary information to determine the velocity, adiabatic wall temperature, heat transfer rate and mean boundary layer properties of the hot film sensor. From this information the Reynolds number

(based on the diameter of the hot film sensor and mean boundary layer properties) and the Nusselt number could be determined. The calibration curve for the sensor is a plot of the Reynolds number raised to the 0.51 power (Ref.4) versus the product of the Nusselt number with the ratio of the mean boundary layer temperature and free stream static temperatures raised to an exponent that would collapse the calibration data for the various velocities and temperatures into a straight line as seen in Fig.2. The exponent used to collapse the data, X_0 , was found by assuming a value and running the data through a least squares curve fitting routine until a good fit of the data was obtained. The exponent was usually found to be approximately 0.03 in the range of velocities for this study. Once the exponent, X_0 , was found, the data were plotted and the slope and Y intercept of the linear calibration curve were found and stored for future use. In order to use the calibration curve the voltage from the bridge circuit of the anemometer must be converted to a Nusselt number then multiplied by the appropriate temperature ratio raised to the X_0 power before reading the Reynolds number from Fig.2. The velocity is then determined from the Reynolds number obtained from Fig.2 using the appropriate mean boundary layer properties of the flow in the test section where the hot film sensor is located. The above procedure was programmed into the HP 3052 Data Acquisition System in order to reduce the time required to calibrate the hot film sensors.

Hot Wire Probe Calibration

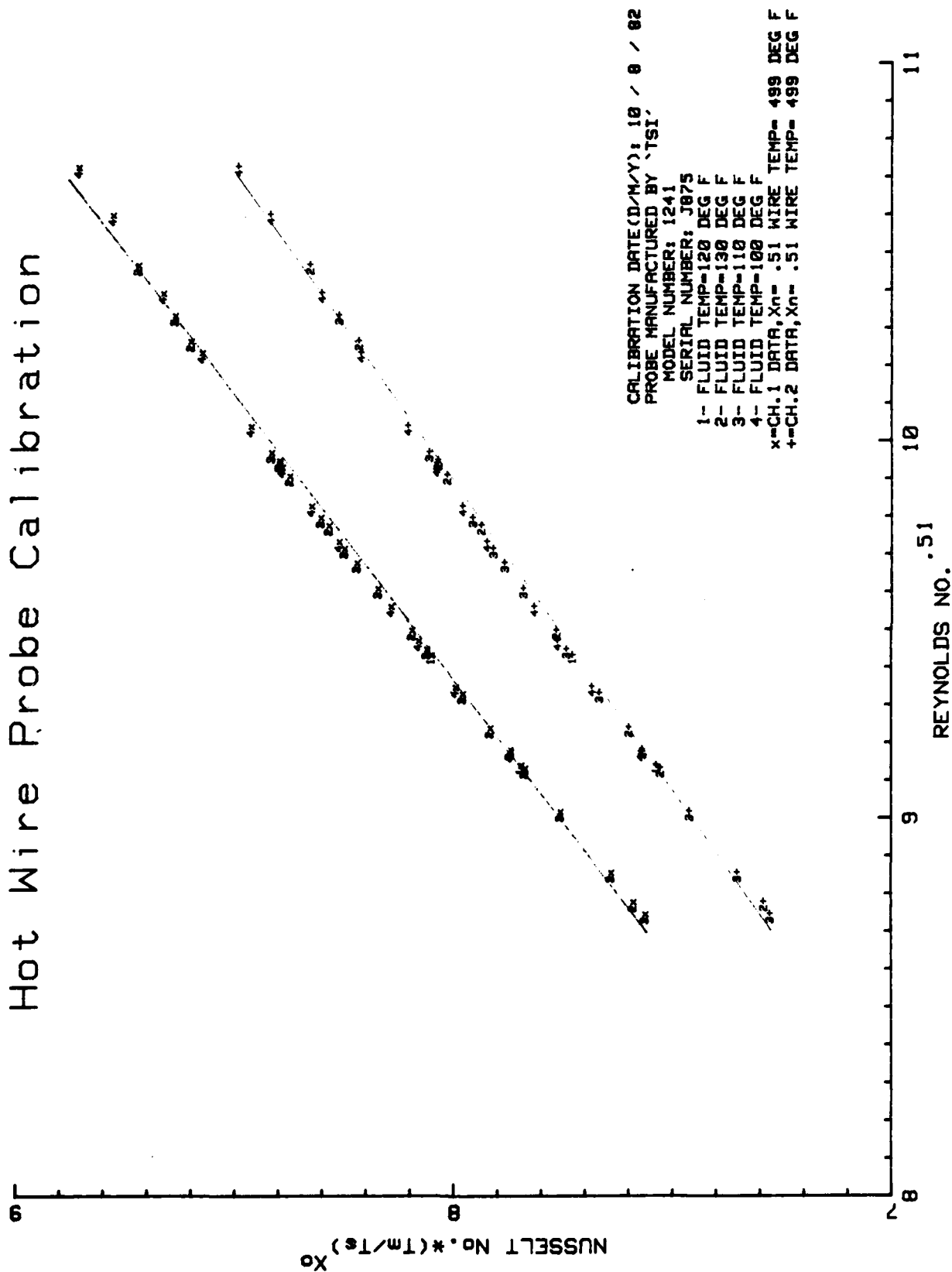


Figure 2: Hot Wire Calibration Curve

EXIT PLANE TRAVERSER

The CTF includes a computer controlled X-Y axis traverser that positioned the hot film sensor in the desired location in the region behind the blades to within 0.002 in in the X and 0.001 in in the Y directions. The traverser mount was integrated with the test section design so that its X-axis could be aligned with the free stream direction for the flow leaving the compressor blade cascade (See Fig.1). Once aligned the entire flow field behind the cascade could be probed with the hot film sensor.

After some initial testing on a smooth blade, a standard data window was established behind the center blade. This data window is comprised of five traverses in the Y-direction at 1 inch intervals starting 0.25 in behind the trailing edge of the center blade. Each traverse contained 133 points located at 0.01 in intervals beginning 0.6 in below the center blade (Fig.3). The length of each traverse was 1.33 in which corresponded to a single blade spacing.

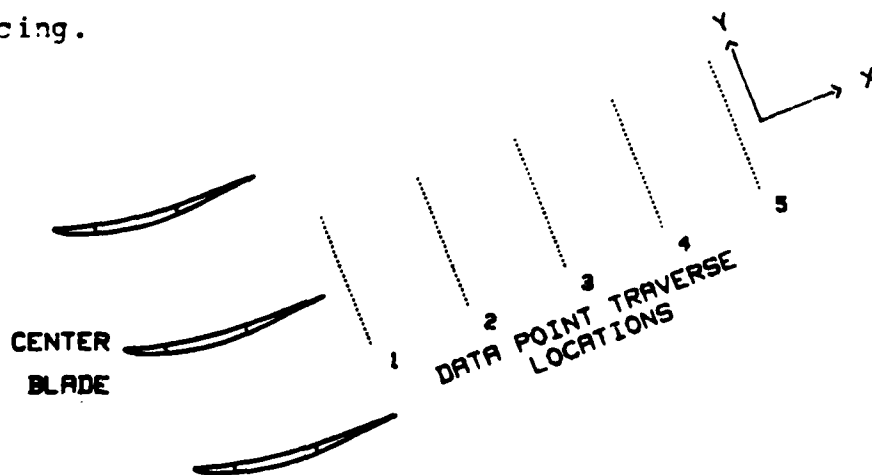


Figure 3: Standard Data Window

BLADE ROUGHNESS CONFIGURATIONS

The effects of surface roughness were studied in two parts in order to determine the importance of location and degree of roughness. In the first part a strip of roughness was applied at discrete locations. The strip was 1/2 inch wide and its leading edge was located at 1/4 inch intervals along the chord (Fig.4). The second part of the study used blades with roughness applied from the leading edge to the 1/4 chord on the suction surface (Fig.4a). At this location the magnitude of the roughness was varied from 0.5 micro-meters Ra for the unroughened blades to 27 micro-meters Ra for the roughened blades. In both parts of the study, roughness was only applied to the suction surface of the blade where the boundary layer and wake region are thought to be greatly impacted by small changes in surface roughness.

The blades were cast from epoxy and then the surface was roughened to the desired finish. The roughening was accomplished by one of two methods. The first method was to coat the blade, or a portion there of, with a very thin layer of adhesive and blow on a fine grit. The other method used was to sand blast the blade to produce cavities in the surface. When applying the roughness extreme care had to be excersized as not to alter the shape of the blade. The majority of the blade configurations investigated were roughened by the first method as a wider range of roughness could be created.

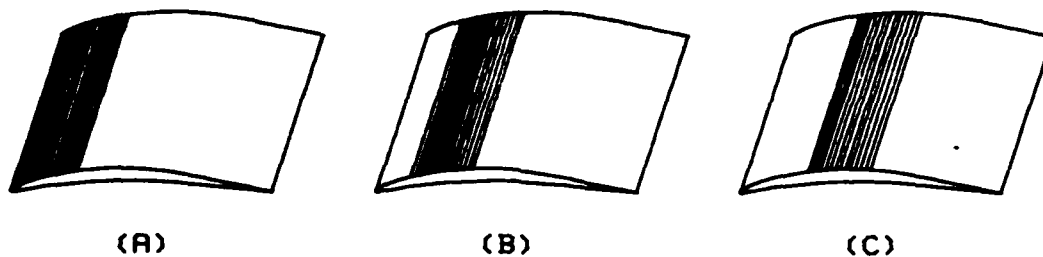


Figure 4: Blade Roughness Configurations

To measure the R_a , R_{tm} and R_{pm} values for the roughened blades a profilometer manufactured by Rank Taylor Hobson was used with the parameter and recorder modules attached. The blades were measured for R_a , R_{tm} and R_{pm} at various locations on the blade and an average of these measurements was used to characterize the roughness for this investigation.

DATA ACQUISITION AND PROCESSING

The acquisition and processing of the data were accomplished using a Hewlet-Packard(HP) 3052A Automatic Data Acquisition System which is integral to the CTF. The data acquisition system consisted of a HP 9845B Computer which controlled a HP 3455A Digital Voltmeter, a HP 3437A System Voltmeter, a HP 3495A Scanner, and two HP 9895 Disk Drives. Also integral to the system were a HP 9874A Digitizer, a HP 9871A Daisy Wheel Printer, and a HP 9872S Plotter for input and output of data. The various software packages designed for the system allowed for the maximum utilization of the systems capability. The data acquisition software allow the experimenter to specify the number and location of the data

points to be taken. The computer would then direct the traverser to move the hot film sensor to the desired location. Once the sensor was in place the scanner would step the voltmeter through the various channels and record the voltage outputs from the various transducers. The voltages were then stored on magnetic storage disk as "raw" data. The "raw" data were later reduced into usable form as pressures, temperatures, and velocities and recorded on magnetic storage disk as "engineering" data for use in evaluating various performance parameters.

III. DATA REDUCTION

The parameters used in evaluating the effect of roughness on blade performance were the exit velocity profile, non-dimensionalized total pressure loss coefficient, and the turbulence intensity profile of the blade's wake. The total pressure loss across the cascade was evaluated from the pressure and velocity data obtained from the survey across one blade spacing centered on the center blade in the cascade.

EXIT VELOCITY

The exit velocity as measured by the hot wire anemometer experienced small changes in magnitude with changes in temperature and humidity of the outside air supply to the CTF. The changes were first noticed as shifts in the velocity profiles of two tests of the same blade configurations on different days. The shift was later noticed when the exit total pressure calculated from the measured exit velocity was greater than the measured total pressure in the stilling chamber. The shift in velocity is thought to come primarily from a change in resistance of the hot wire probe support with a change in temperature, and a change in heat transfer rate with a change in humidity. Tests run using a single sensor probe support, which had a lower resistance than the double sensor support primarily used (0.05 vs. 0.16 ohms), did not show the same size shifts

that had previously occurred when the double sensor probe support had been used. The 40 deg temperature increase in the probe support's environment that occurred when the sensor was moved from the calibration (control) room to the test section would cause an increase in the resistance of the probe support as the temperature increased. Preliminary experiments run to define how the resistance of the probe support changed with temperature were unsuccessful. The humidity problem has been studied by Larsen and Busch (Ref.7) with the conclusions that humidity increases the heat transfer rate between 0.5% and 2%, corresponding to an increase in apparent velocity between 1 and 5% but no quantitative relationships were found.

In order to correct the hot film velocity data a continuity check was performed. If the calculated mass flow entering the cascade based on pressure data differed from the mass flow leaving the cascade based on the hot wire data, a correction factor was applied to the exit velocity data to force continuity through the cascade. The mass flow rate exiting the cascade was evaluated by numerically integrating the following relation:

$$\dot{m}_2 = \int_2 \rho v_2 dy \quad (1)$$

Where \dot{m}_2 is the exit mass flow rate, ρ is the local density evaluated using the ideal gas law, v_2 is the exit velocity as measured by the hot wire and dy is the differential exit

area assuming unit width. The inlet mass flow rate was evaluated using:

$$\dot{m}_1 = \rho V_1 A_1 \quad (2)$$

Where \dot{m}_1 is the inlet mass flow rate, ρ is the local inlet density, A_1 is the inlet area and V_1 is the average inlet velocity evaluated as follows with the known inlet total and static pressures and total temperature.

$$V_1 = \sqrt{2 C_p T_T \left[1 - \left(\frac{P_2}{P_T} \right)^{\frac{\gamma-1}{\gamma}} \right]} \quad (3)$$

If the derived exit mass flow rate did not equate to the inlet mass flow rate a scale factor was applied to the hot wire velocity data as follows to force the equality.

$$V_2' = s V_2 \quad (4)$$

Where V_2' is the corrected exit velocity, s is the scale factor that equates the exit mass flow rate to the inlet mass flow rate, and V_2 is the exit velocity as measured by the hot wire. The scale factor s was evaluated by a numerical trial and error scheme and was found to vary from 0.90 to 0.95.

TOTAL PRESSURE LOSS

The total pressure loss across the cascade was

calculated from the measured inlet total pressure and the exit total pressure as calculated from the exit static pressure and velocity. The total pressure at each data point behind the cascade was calculated using the following isentropic compressibility relation:

$$P_{t2} = P_s \left[1 + \frac{V_2'^2}{2 C_p T_T} \right]^{\frac{\gamma}{1-\gamma}} \quad (5)$$

where V_2' is the corrected exit velocity, P_s is the static pressure as measured by the wall static pressure ports, and T_s is the total temperature as measured in the stilling chamber. The total temperature of the flow was assumed constant through the test section.

The overall exit total pressure was calculated from a mass-averaging of the total pressure of the individual data points in a single traverse. The mass-averaging was accomplished with the following relation:

$$\bar{P}_{t2} = \frac{\int P_{t2} \rho V_2' dA}{\int \rho V_2' dA} \quad (6)$$

where \bar{P}_{t2} is the mass-averaged value of the total pressure, P_{t2} is the total pressure at a single data point in the traverse being evaluated, ρ is the local density evaluated using the ideal gas law, and dA is the differential exit area. The double integrals over the exit area were reduced to a single

integral by assuming no variations in the span wise direction of the blade. For unit width of the blade, the equation then reduces to:

$$\bar{P}_{T_2} = \frac{\int_2 P_{T_2} \rho V_2' dy}{\int_2 \rho V_2' dy} \quad (7)$$

The integrals were numerically evaluated using the trapezoidal rule with dy being the step size in the Y-direction (0.01 in).

Having calculated the exit total pressure, the loss in total pressure across the cascade can be evaluated using:

$$\Delta P_T = P_{T_1} - \bar{P}_{T_2} \quad (8)$$

The total pressure loss can be non-dimensionalized by the inlet dynamic head to give $\bar{\omega}$, the desired performance parameter.

$$\bar{\omega} = \frac{\Delta P_T}{\frac{1}{2} \rho V_1^2} \quad (9)$$

where ρ is the inlet density evaluated using the ideal gas law and V_1 is the inlet velocity evaluated in equation 3. The total pressure loss was calculated for each traverse and an average of all five traverses were taken as the total pressure loss parameter in this study. It is realized that

mixing losses occur in the wake but the error of the instrumentation was greater than any mixing losses and an average loss parameter was thought to be a better representation of the blade losses.

TURBULENCE INTENSITY

The definition of turbulence intensity for this investigation is the ratio of the RMS velocity (AC output of the anemometer as indicated by a TRUE RMS voltmeter) to the stream wise component of the local mean velocity (DC output from the anemometer).

$$TI = \frac{V_{rms}}{V_{x,mean}} \quad (10)$$

Turbulence intensity would not normally be negative but because of the configuration of the X-sensor probe used to measure the components of the velocity the two sensors allow the orientation of the fluctuations to be determined. As a result, positive value of the turbulence intensity indicates that the fluctuations are occurring in a plane rotated in a positive direction about the Z axes from the positive XZ plane, and, conversely, a negative Y turbulence intensity indicates a negative rotation from the positive XZ plane (Ref.17).

IV. RESULTS AND DISCUSSION

The objectives of the study were to determine the importance of position and magnitude of roughness on the loss in total pressure across a cascade of compressor blades. Eight blade configurations were tested in the AFIT CTF with sand type roughness applied at various locations along the chord and with varying magnitudes. The cascade used for this study did not use boundary layer removal therefore the cascade could not be considered two dimensional according to Erwin and Emery (Ref.5). The results being presented are good for making comparisons between smooth and rough blades but should not be considered design cascade data.

The non-dimensional total pressure loss coefficient, $\bar{\omega}$, as defined below, was used as the primary means of evaluating the blade total pressure losses.

$$\bar{\omega} = \frac{P_{T1} - P_{T2}}{\frac{1}{2} \rho V_1^2} \quad (11)$$

In addition, the velocity and turbulence intensity profiles of the blade's wake were studied to evaluate the effect that roughness had on the wake. The surface roughness was evaluated using a profilometer to measure R_a , R_{tm} , and R_{pm} values of the surface roughness (see Appendix A for definitions of the above roughness parameters).

LOCATION EFFECTS

Five blade configurations with roughness on portions of the suction surface were tested to determine the importance of the roughness location on the loss of total pressure across the blade. Initially two blades were tested; one with roughness from the leading edge to the 1/4 chord (Conf#2) with an Ra value of 26.9 micro-meter, the other configuration with roughness from the mid-chord to the trailing edge (Conf#3) with an Ra value of 44.1 micro-meters Figs.5a&b. The loss in total pressure across the blade, as

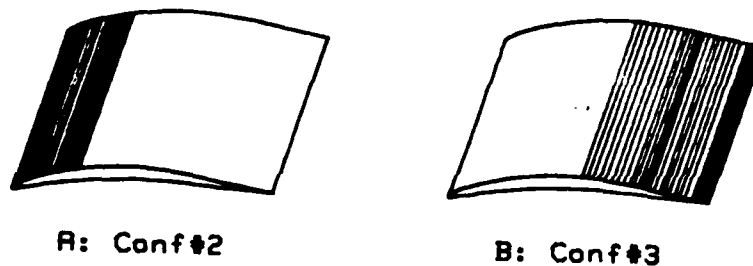


Figure 5: Roughness Configurations 2 and 3

measured by ω , increased from 0.0963 for the blade with the roughness near the trailing edge to 0.1037 for the blade with the roughness beginning at the leading edge. The blade with the roughness beginning at the leading edge thus experienced an 11% greater loss in ω based on ω of the smooth blades. The increase in ω occurred even though the magnitude of the roughness was less on the blade configuration with the roughness beginning at the leading edge compared to the blade with the roughness near the

trailing edge. These tests showed that roughness located near the leading edge, on the suction surface, is critical to the performance of the blade. Further testing showed that by moving the roughness location away from the leading edge even small percentages of the chord caused a decreases in ζ . Table I shows the decrease in ζ that accompanies the movement of the roughness away from the leading edge. For these tests blade configurations 5,7,&8 were used which consisted of a 1/2 in band of 20 micro-meter Ra roughness applied to the suction surface of the blade. The leading edge of the strip of roughness was initially at the blade's leading edge (Conf.5) Fig.6a but was progressively moved away from the blade's leading edge in 1/8 chord intervals (Confs.7&8) Figs.6b&c.

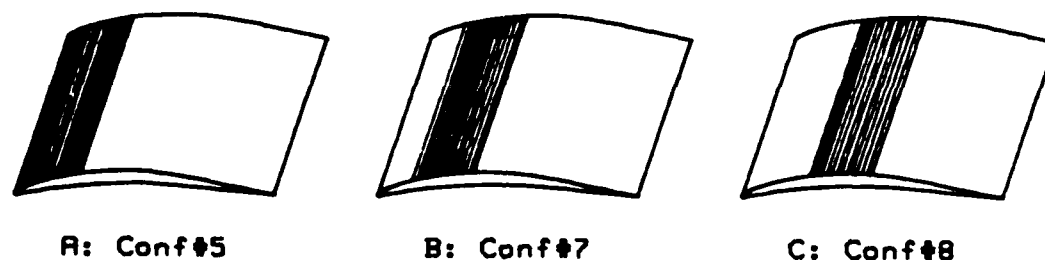


Figure 6: Roughness Configurations 5, 7 and 8

Moving the strip 1/8 chord from the leading edge decreased ζ from 0.0973 for the blade with the roughness begining at the leading edge (Conf#5) to 0.0918. Moving the roughness back another 1/8 chord decreased ζ to 0.0870.

A cause for the high loss in total pressure when

TABLE I: PERFORMANCE DATA FOR ROUGHNESS LOCATION TESTS

Conf#	Eval#	Ra	Rtm micro-meters	Rpm	$\bar{\omega}$	Re/ft Million	Blade discription
1	6	0.5	2.11	1.31	0.0775	2.71	smooth
2	1	26.9	155.8	78.8	0.1037	2.58	1st 1/4Cord rough
3	1	44.1	>199.9	139.5	0.0963	2.57	Last 1/2Cord rough
5	2	19.79	115.1	61.65	0.0973	2.69	1st 1/4Cord rough
7	1	20.87	122.4	59.8	0.0918	2.74	1/4Cord rough 1/8Cord removed from L.E.
8	1	20.13	119.5	59.7	0.0870	2.76	1/4Cord rough 1/4Cord removed from L.E.
8	2	20.13	119.5	59.7	0.0870	2.74	(Same)

roughness begins at the leading edge of the blade is that the size of the roughness is large in comparison to the boundary layer thickness. On this premise, when the peaks of the roughness extend through the laminar sublayer of the boundary layer, a significant increase in the boundary layer growth results. As the boundary layer grows along the blade, the peaks of the roughness become submerged in the boundary layer and their effects on the boundary layer decrease. Similar effects have been seen on a flat plates where the coefficient of skin friction decreased as the roughness was moved away from the leading edge (Ref.11). Schlichting points out that the reduction in the coefficient of skin friction is due to a reduction in the size of the roughness in comparison to the local boundary layer thickness.

The effects of the location of roughness on the wake down stream of the blade can be seen by inspection of the velocity and turbulence intensity profiles in this region. The measured velocity and turbulence intensity data for the X and Y directions have been resolved into vectors with magnitude and direction. The vectors were then plotted using the point at which the data were taken as the origin and drawing a vector in the appropriate direction. The solid line vectors are the velocity vectors and the dotted line vectors are the turbulence intensity vectors. The magnitude of the vectors can be determined by measuring the length of the vector using the down stream position scale as a measure of length and applying the appropriate scale factor. The

scale factors for the velocity and turbulence intensity vectors are 540 ft/sec/in and 20 percent/in respectively. As can be seen in the set of the velocity and turbulence intensity profiles for the smooth blade (Conf.1), Figs.7,8,9,10,&11, both the velocity and turbulence intensity profiles are fairly uniform in the free stream but exhibit large changes in magnitude and direction in the blade wake region. The velocity profile exhibits a small narrow decrement accompanied by high levels of turbulence as seen in the traverse located 1/8 chord from the blade's trailing edge (Fig.7). As the traverse location moves down stream (Figs.8,9,10,&11) the velocity decrement becomes wider and shallower accompanied by decrease of the levels of turbulence but this is accompanied by a spreading of the turbulence into the free stream. All the blade configurations tested exhibited the same trends as the smooth blades but with changes in the relative sizes of the velocity decrement and turbulence levels. The following discussion of the effects of the location and magnitude of roughness on the blade's wake will only deal with the traverse located 1/8 chord behind the trailing edge of the blade with the understanding that events similar to those of the smooth blades also occur downstream of the roughened blades. In order to verify that these trends do occur the reader is referred to Appendix B which contains a complete set of the velocity and turbulence intensity profiles for each configuration tested.

1 VANE WAKE: CONF. NO.1, EVAL. NO.6

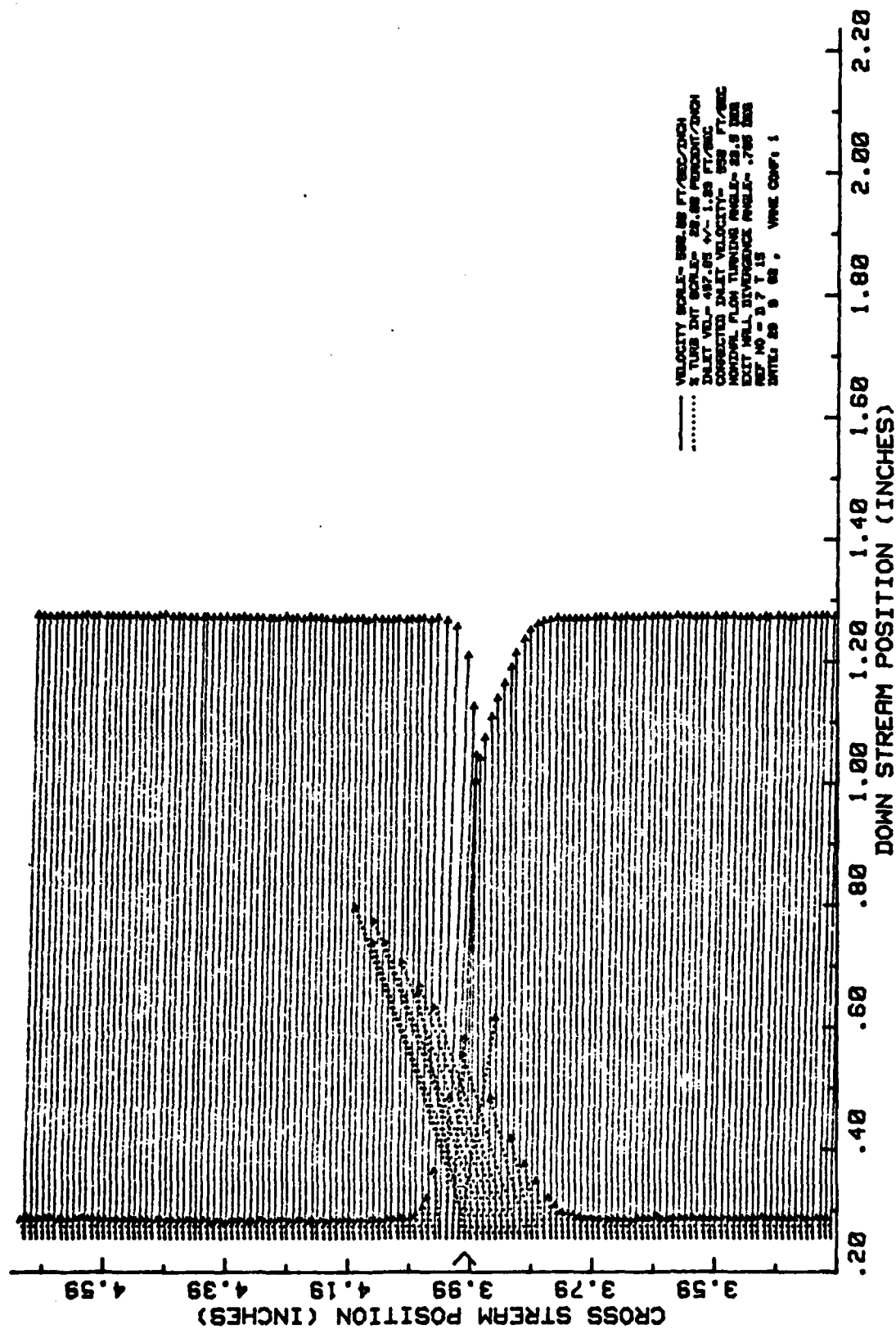


Figure 7: Velocity and Turbulence Intensity Profile
 Conf#1 Eval#6: Smooth baseline blade Traverse#1

VANE WAKE: CONF. NO.1, EVAL. NO.6

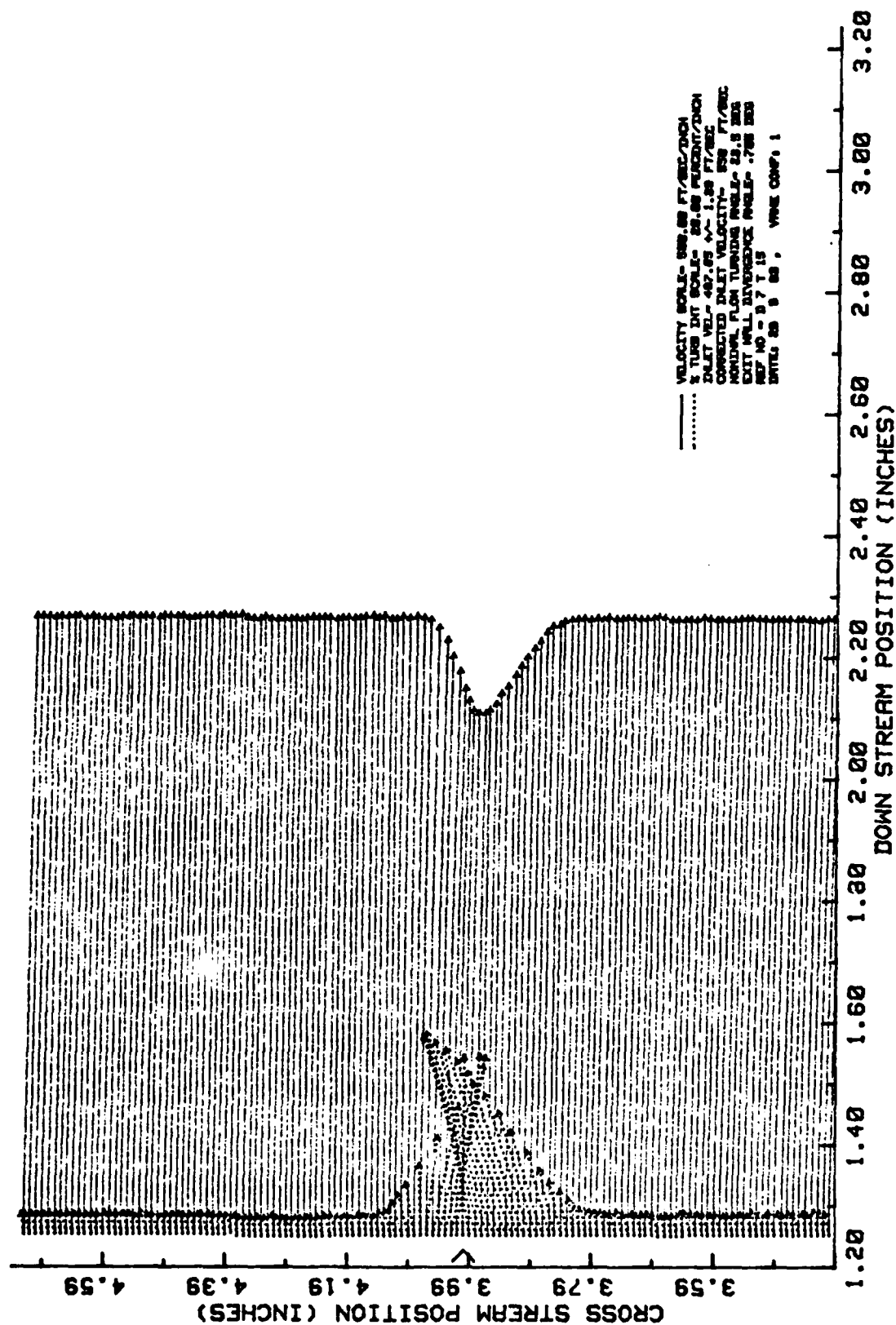
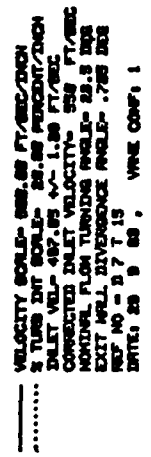


Figure 8: Velocity and Turbulence Intensity Profile
Conf#1 Eval#6: Smooth Baseline blade Traverse#2



**Figure 9: Velocity and Turbulence Intensity Profile
Conf#1 Eval#6: Smooth Baseline Blade Traverse#3**

VANE WAKE: CONF. NO.1, EVAL. NO.6

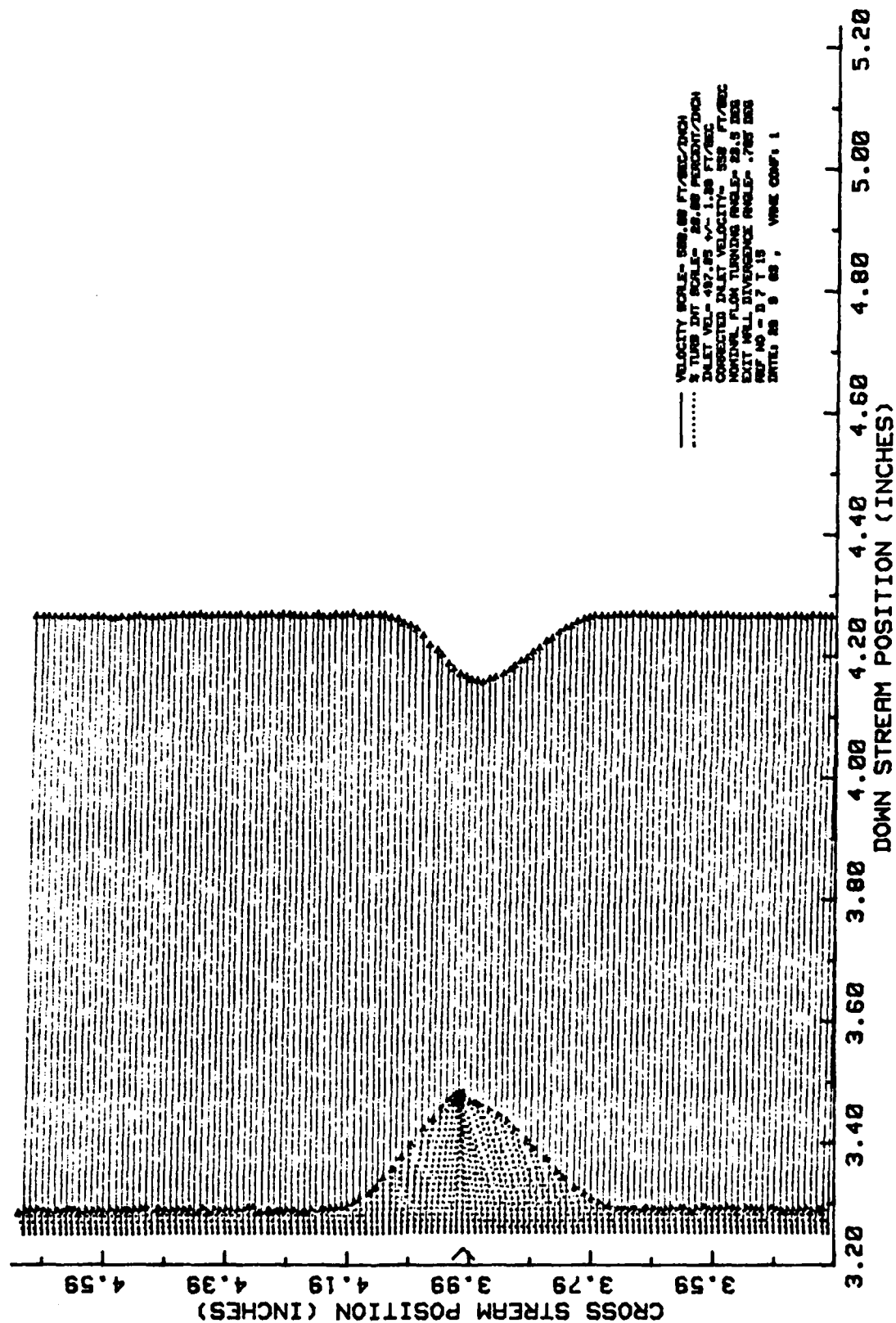


Figure 10: Velocity and Turbulence Intensity Profile
Conf#1 Eval#6: Smooth Baseline Blade Traverse#4

VANE WAKE: CONF. NO.1, EVAL. NO.6

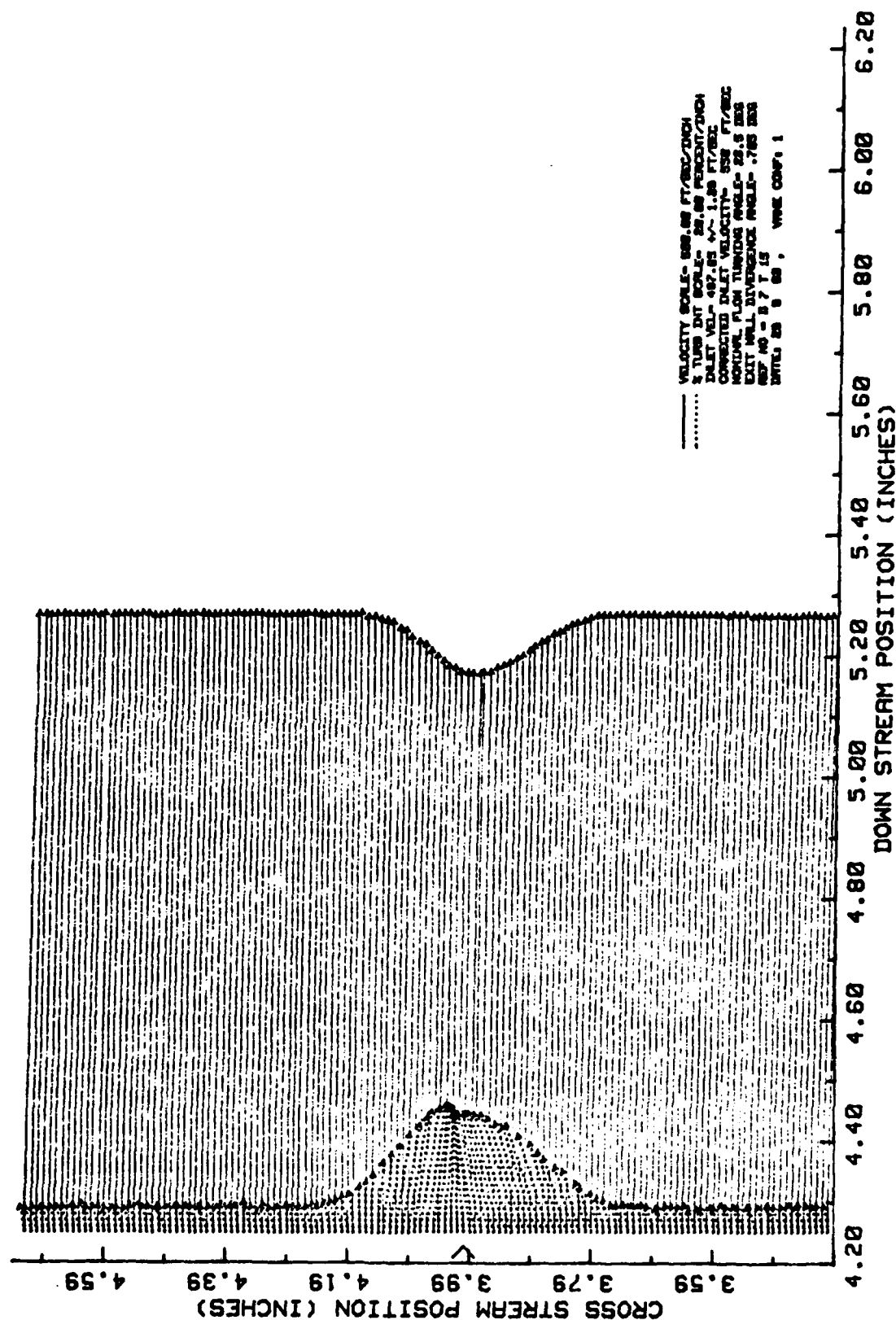


Figure 11: Velocity and Turbulence Intensity Profile
Conf#1 Eval#6: Smooth Baseline Blade Traverse#5

The velocity and turbulence intensity profiles for the blade configurations where the roughness started at the leading edge and was moved away in $1/8$ chord intervals (Conf#5,7,&8) showed a large change in the blade's wake from that of the smooth blade but did not show any difference between themselves. This is seen by the large increase in the depth of the velocity decrement and the increase in the magnitude of the turbulence levels when Figs.12,13,&14 are compared to Fig.7. When Figs.12,13,&14 are compared to each other no significant difference can be seen. The velocity and turbulence intensity profiles for the blade configuration that has roughness beginning at the leading edge and extending to the $1/4$ chord (Conf#2) and the one with roughness from the mid chord to the trailing edge (Conf#3), Figs.15&16 respectively, show a large change in the blade's wake. When these profiles are compared Conf#2 exhibits a larger velocity decrement than conf#3 but a smaller level of turbulence. A possible cause for the increase in turbulence intensity, when roughness is applied from the mid-chord to the trailing edge of the blade, is the position at which the boundary layer becomes separated. When the boundary layer experiences roughness after the mid-chord it may immediately separate due to a unstabilizing effect of the roughness on the boundary layer in a unfavorable pressure region. The separated flow over the blade would account for the high turbulence intensity levels. If the boundary layer experiences roughness before the mid-chord,

VANE WAKE: CONF. NO.5, EVAL. NO.2

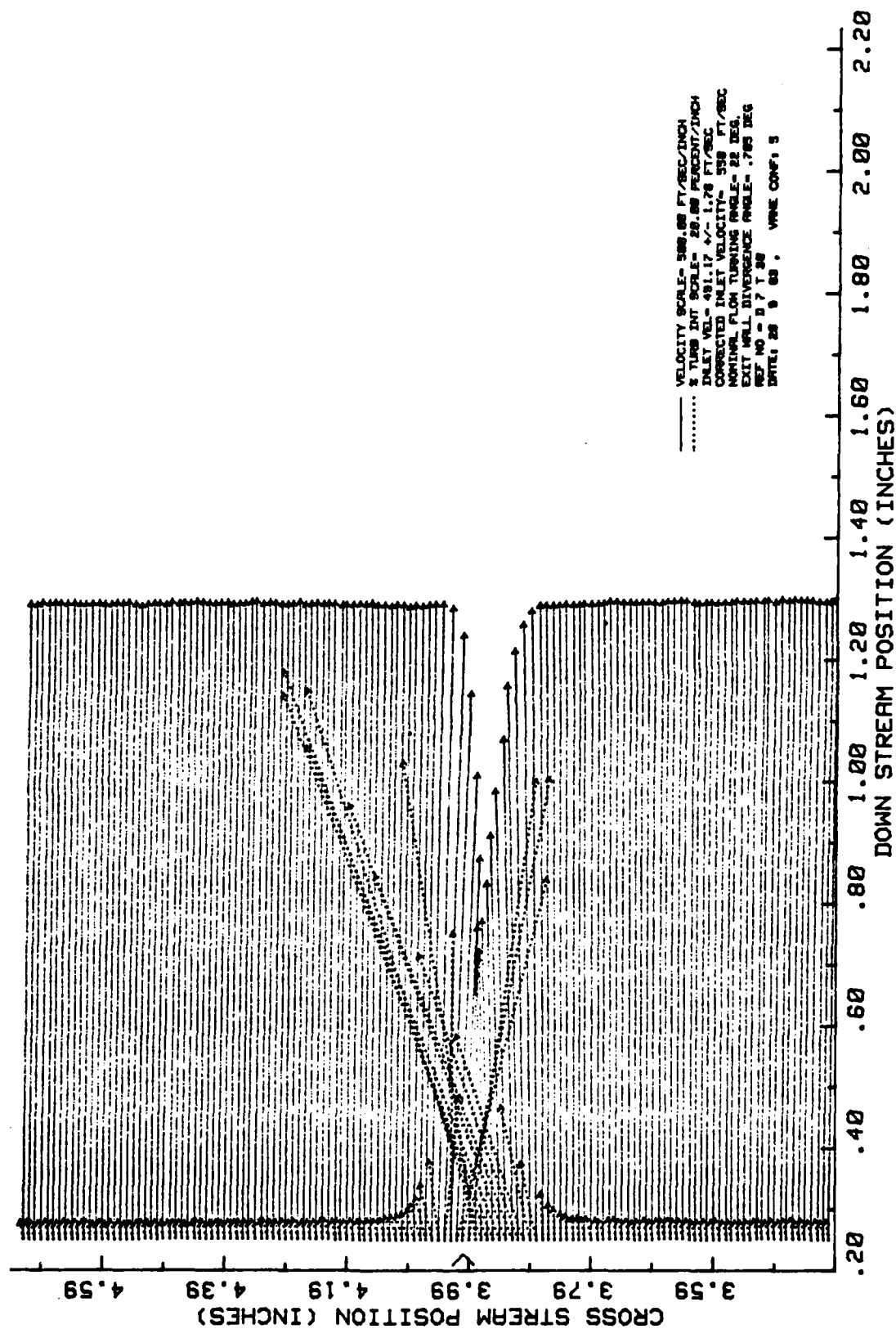


Figure 12: Velocity and Turbulence Intensity Profile; Traverse#1
Conf#5 Eval#2: 20 micro-meter Ra Roughness from L.E.-1/4Chord

VANE WAKE: CONF. NO.7, EVAL. NO.1

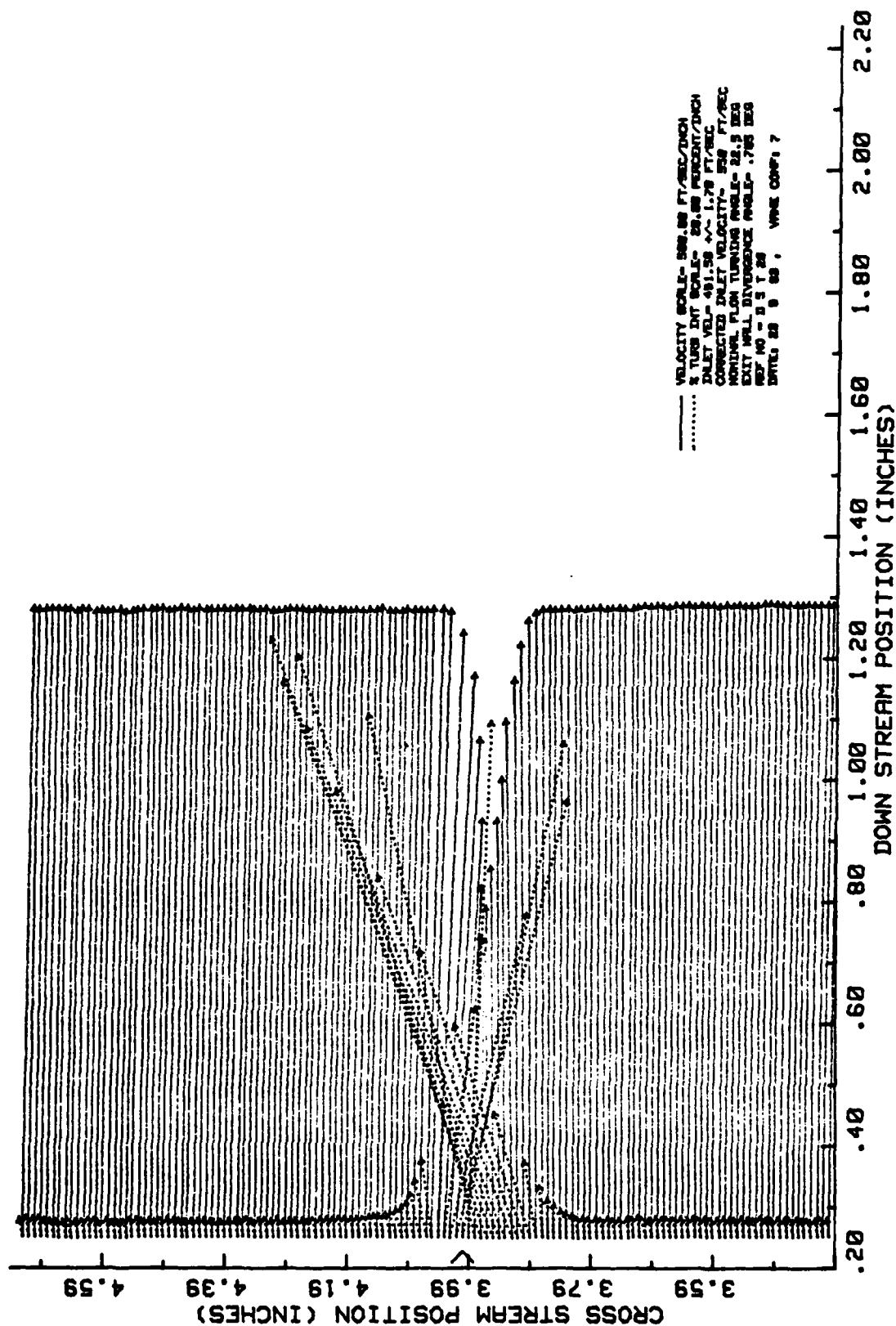


Figure 13: Velocity and Turbulence Intensity Profile; Traverse#1
 Conf#7 Eval#1: 20 micro-meter Ra Roughness from 1/8.-3/8Chord

VANE WAKE: CONF. NO.8, EVAL. NO.1

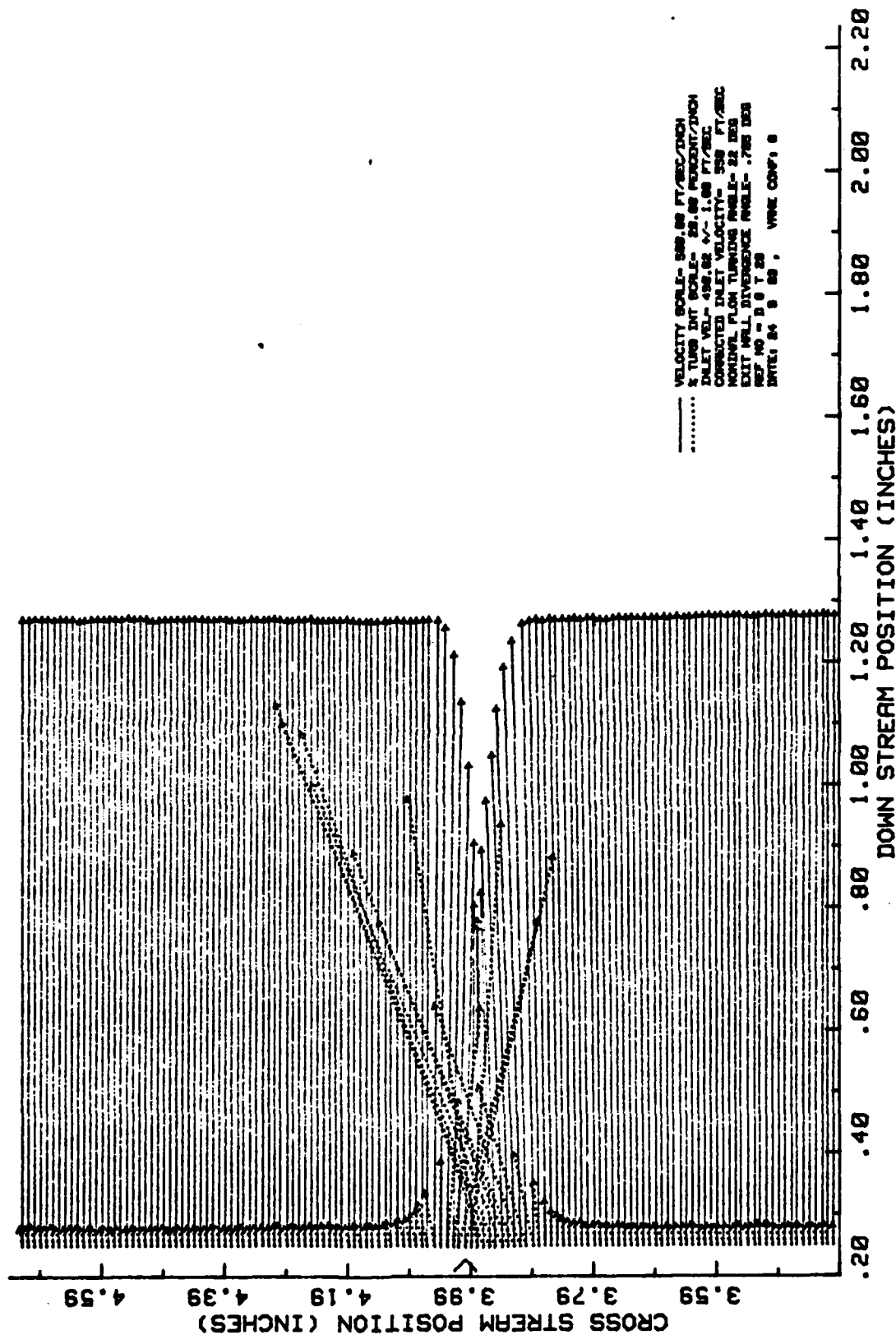


Figure 14: Velocity and Turbulence Intensity Profile; Traverse #1
Conf#8 Eval#1: 20 micro-meter Ra Roughness from 1/4.-1/2Chord

VANE WAKE: CONF. NO.2, EVAL. NO.1

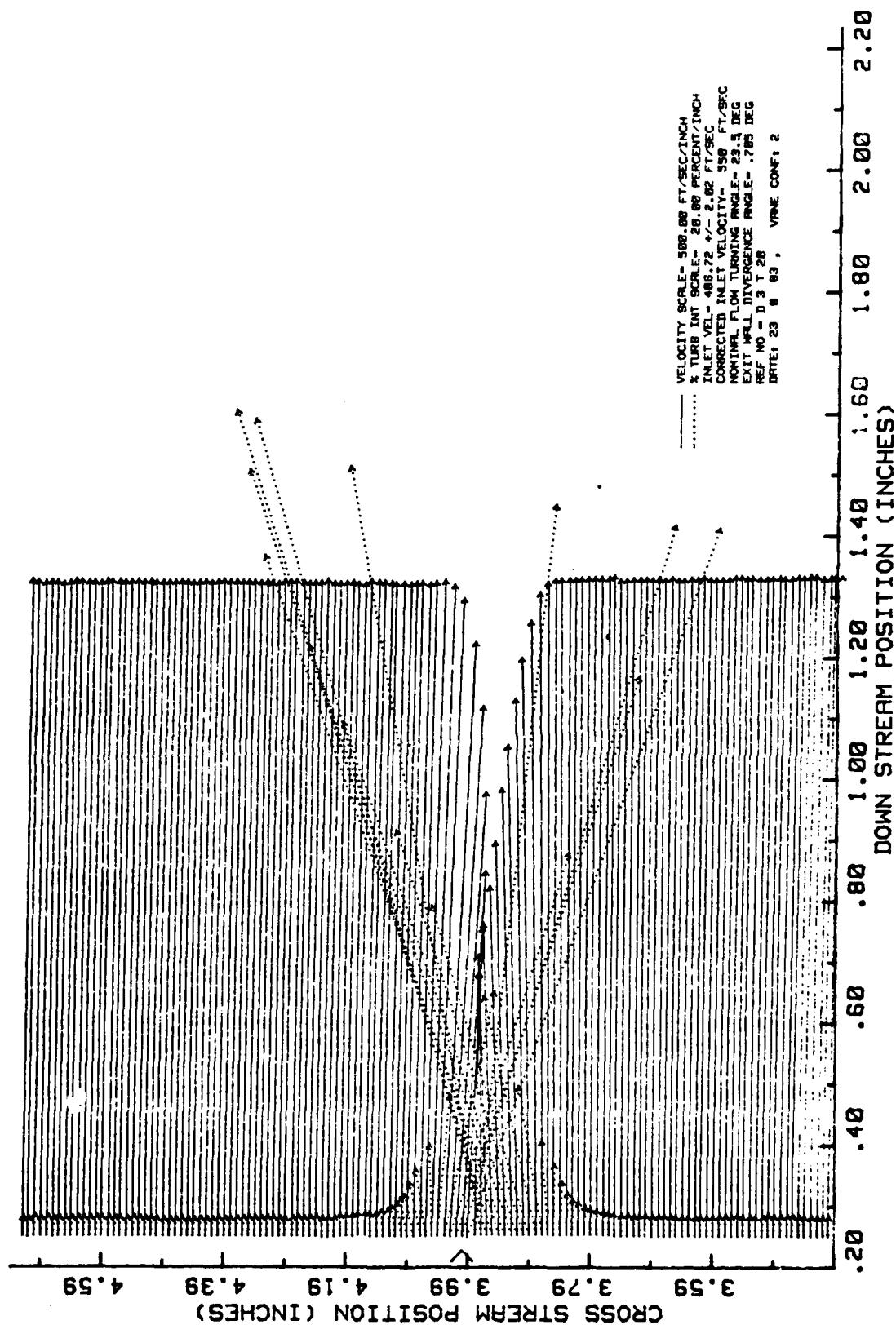


Figure 15: Velocity and Turbulence Intensity Profile; Traverse #1
 Conf#2 Eval#1: 27 micro-meter Ra Roughness from L.E.-1/4Chord

VANE WAKE: CONF. NO.3, EVAL. NO.1

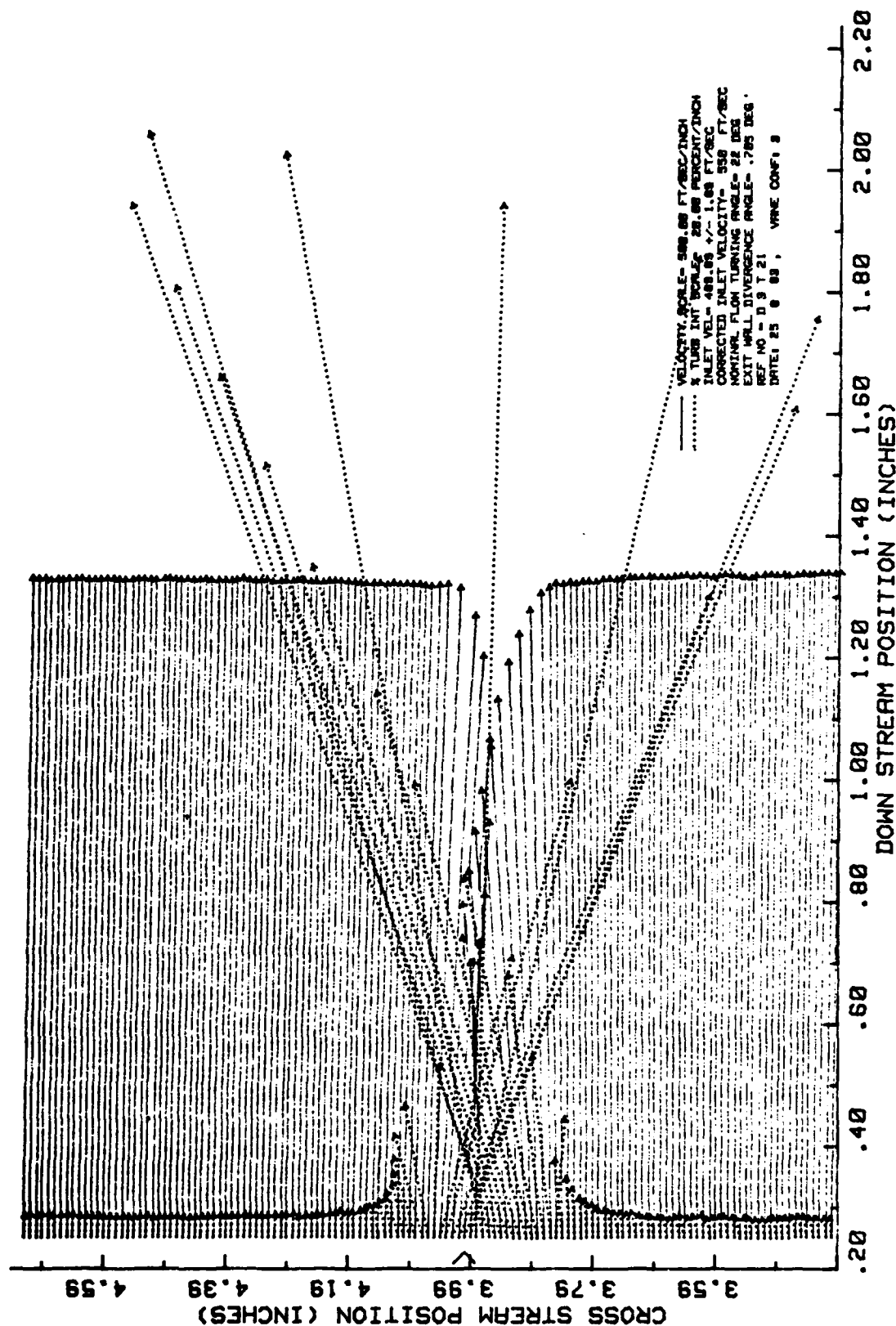


Figure 16: Velocity and Turbulence Intensity Profile; Traverse #1
 Conf#3 Eval#1: 44 micro-meter Ra Roughness from 1/2Chord-T.E.

in a region where the flow is accelerating around the blade, the boundary layer may not separate immediately due to the favorable pressure gradient but remain attached along the blade. The closer to the leading edge that the boundary layer becomes detached, the greater the separation region thus the larger the turbulence levels particularly if it is unstable.

ROUGHNESS MAGNITUDE EFFECTS

Four blade configurations with roughness applied to the first 1/4 chord were tested to determine the effects of varying the magnitude of roughness on the loss in total pressure across the cascade of compressor blades. The results of these tests are presented in Table II but can be seen best in graphical form. Figures 17, 18, & 19 are plots of the increase in non-dimensional total pressure loss that accompanied an increase in roughness as measured by R_a , R_{tm} , and R_{pm} roughness parameters. Even though the size of the values for the roughness parameters change from one plot to the next the relative trend remains the same as can be seen in Figs. 17, 18, & 19. The sand type roughness used in this study created such a uniform randomness that the method of evaluating roughness did not affect the trend. For this reason the following discussion will only deal with R_a values of roughness. R_{tm} and R_{pm} values of roughness could have just as easily been used and would have led to the same conclusions.

TABLE II: PERFORMANCE DATA FOR ROUGHNESS MAGNITUDE EFFECTS

Conf #	Eval #	Ra	Rtm micro-meter	Rpm	$\bar{\omega}$	Re/ft Million
1	6	0.5	2.11	1.31	0.0775	2.71
1	7	0.5	2.11	1.31	0.0765	2.66
6	2	2.7	17.01	6.75	0.0767	2.72
5	2	19.8	115.1	61.65	0.0973	2.69
2	1	26.9	155.8	78.8	0.1037	2.58

NOTE: All of the above blade configurations consist of a 1/4 Cord strip of roughness located from the leading edge of the blade back to the 1/4 Cord

LOSS OF PERFORMANCE WITH Ra ROUGHNESS

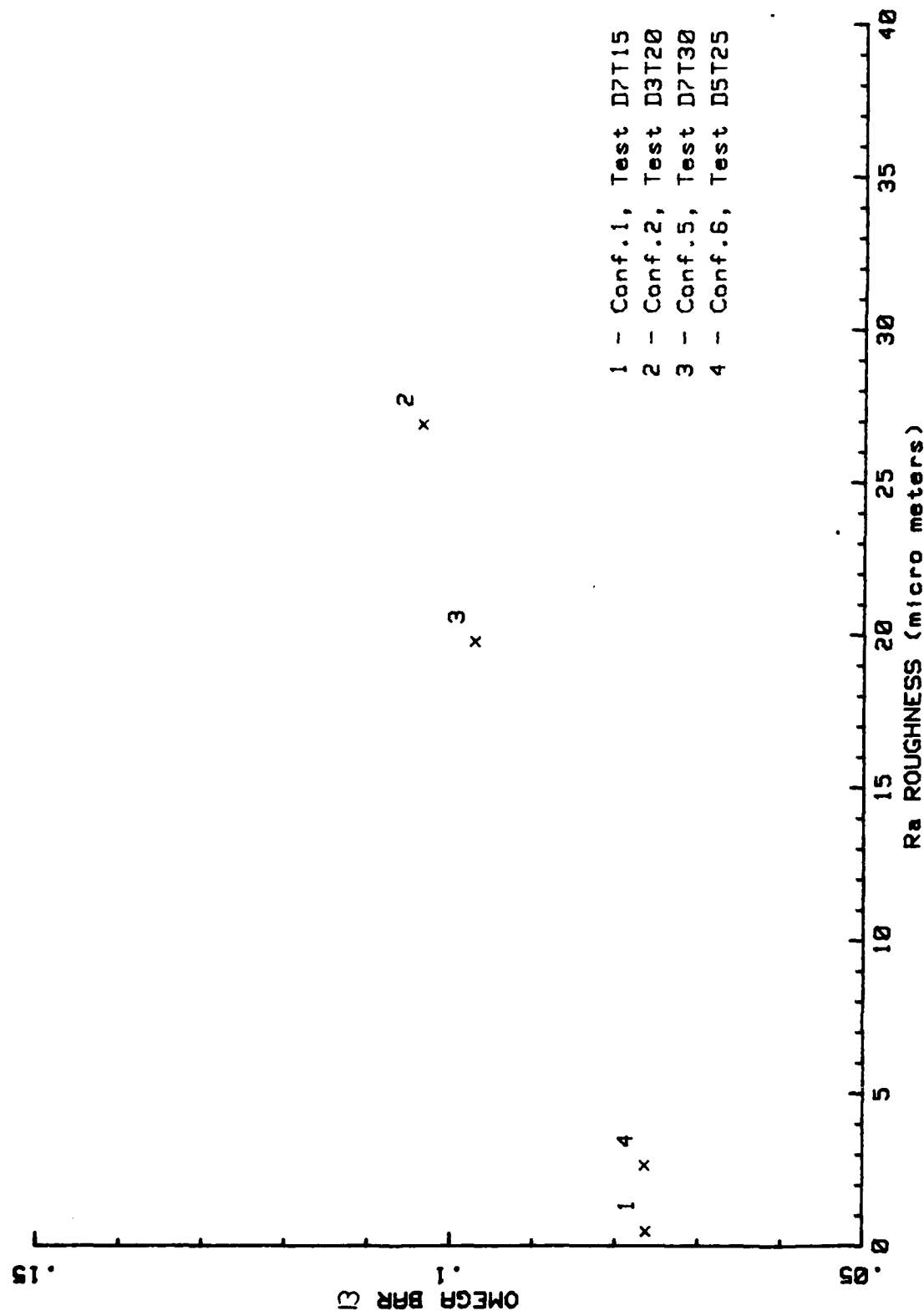


Figure 17: Loss in Non-Dimensional Total Pressure with Ra Roughness

LOSS OF PERFORMANCE WITH R_{tm} ROUGHNESS

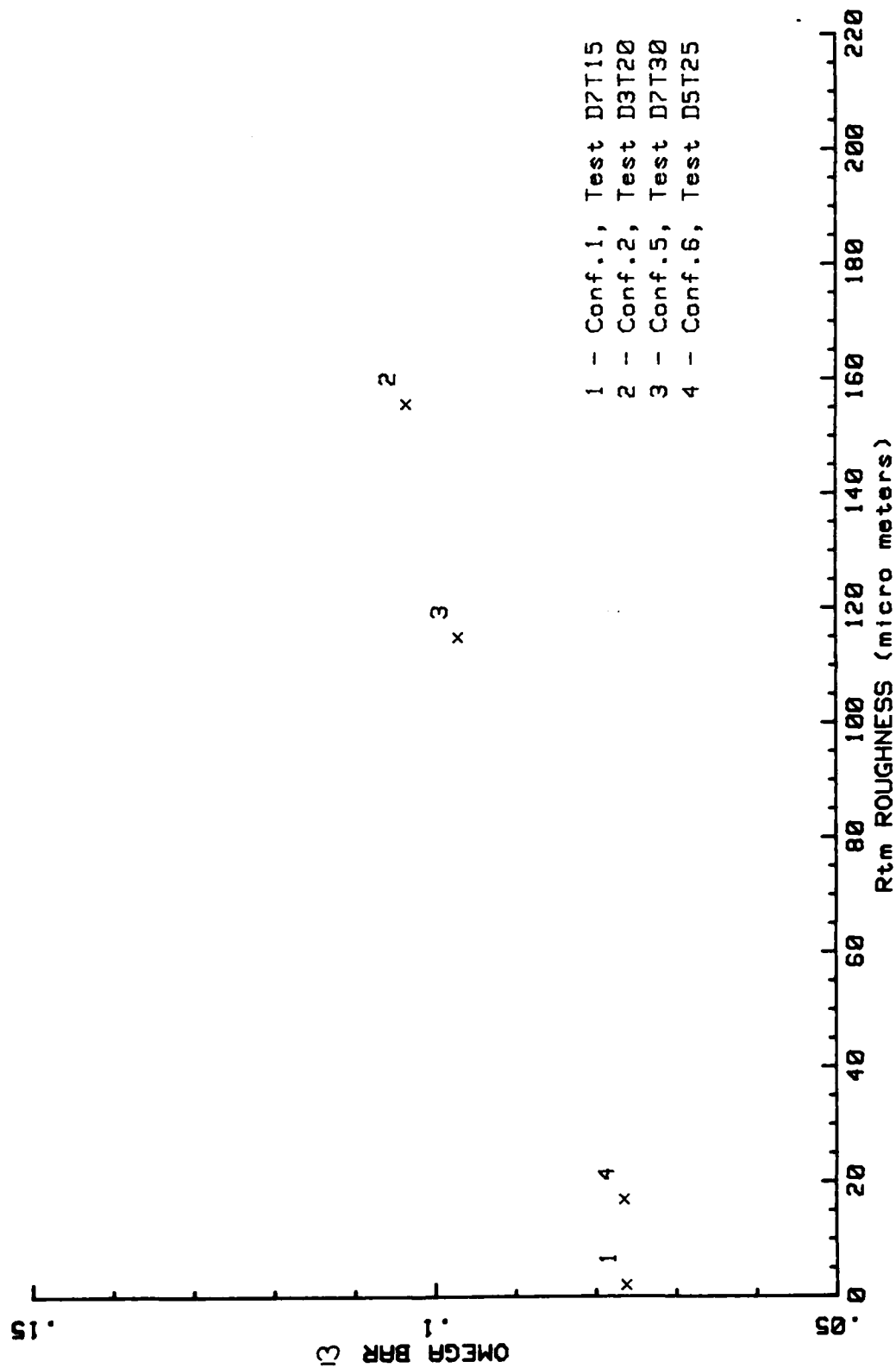


Figure 18: Loss in Non-Dimensional Total Pressure with R_{tm} Roughness

LOSS OF PERFORMANCE WITH Rpm ROUGHNESS

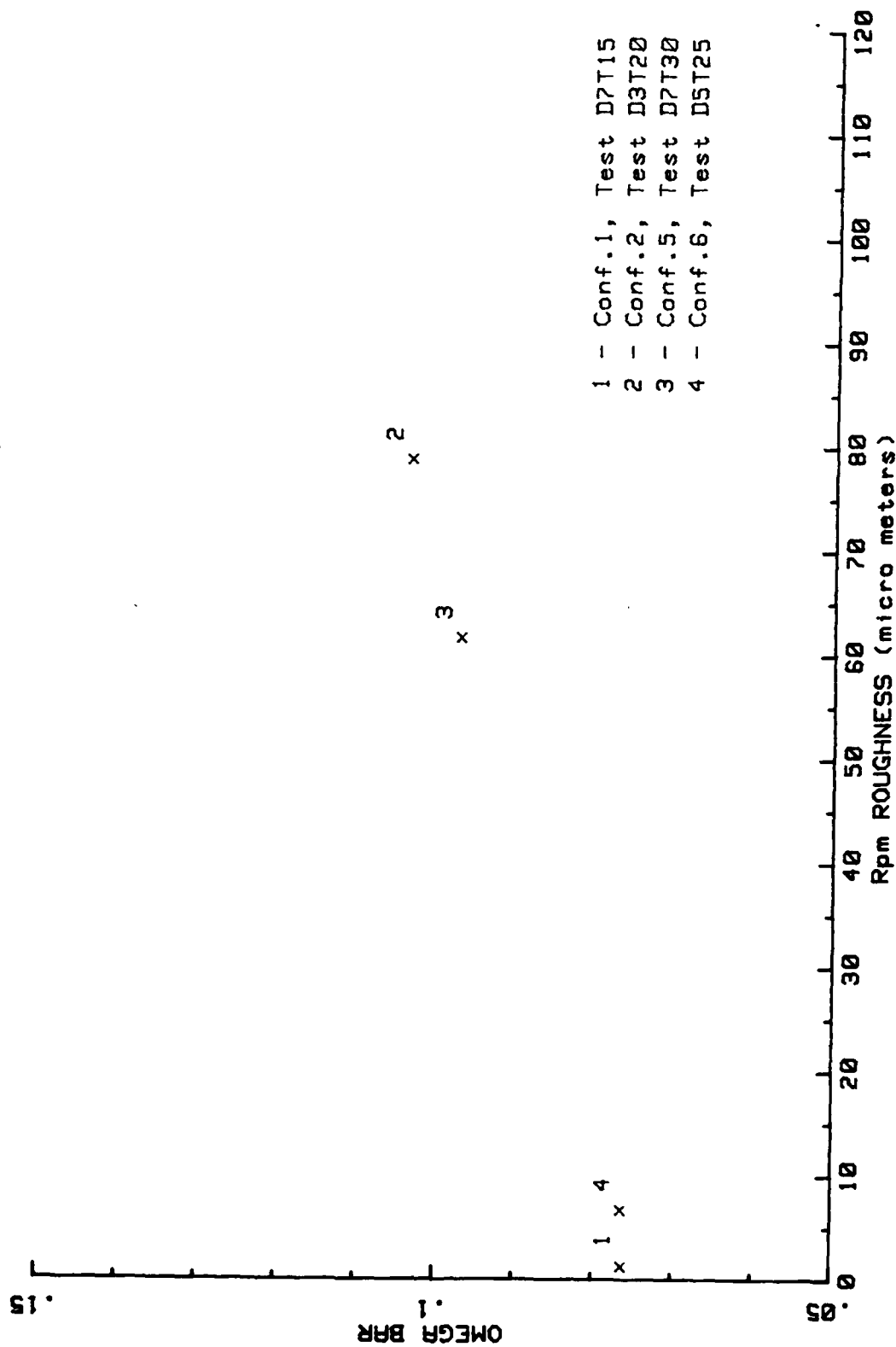


Figure 19: Loss in Non-Dimensional Total Pressure with Rpm Roughness

The change in total pressure loss across the cascade as measured by $\bar{\omega}$ can easily be seen in Fig.17. As the roughness magnitude varies from 0.5 micro-meter Ra for the smooth blade (Conf#1) to 26.9 micro-meter Ra for the roughest leading edge configuration (Conf#2) $\bar{\omega}$ changed from 0.0775 to 0.1037. For small values of Ra the change in $\bar{\omega}$ was negligible, as the Ra value of the roughness increased the non-dimensional total pressure loss, $\bar{\omega}$, showed an increase. When the $\bar{\omega}$ values for the blade configuration with a leading edge roughness of 2.7 micro-meters Ra (Conf#6) is compared to that of a blade configuration with a leading edge roughness of 19.8 micro-meters Ra (Conf#5) a 27% increase in total pressure loss is experienced. The percent increase is based on the difference between $\bar{\omega}$ for the two tests in comparison to $\bar{\omega}$ for the smooth blades (Conf#1). A further increase in roughness to a Ra value of 26.9 micro-meters brings an additional 8.3% increase in non-dimensional total pressure loss.

The increase in $\bar{\omega}$ with roughness is thought to be caused by the peaks of the roughness extending through the boundary layer and causing a significant increase in the growth of the boundary layer. On this premise, when the Ra value of the roughness was small the peaks of the roughness did not extend through the boundary layer, thus the insignificant change in $\bar{\omega}$ with roughness as seen in Fig.17. As the magnitude of the roughness on the blade increases, the peaks begin to extend through the laminar sublayer of

the boundary layer and the loss in total pressure starts to increase. The data seems to indicate that there should be some Ra value of roughness at which point the peaks just start to penetrate the laminar sublayer of the boundary layer. At this point the blade's surface transitions from a hydrodynamicly smooth surface, where the roughness is submerged in the boundary layer and the performance is not a function of the roughness, to a hydrodynamicly rough surface, where the peaks of the roughness extend through the boundary layer and large losses in performance are experienced with changes of roughness. This transition point could not be investigated due to the lack of sand of the necessary size. Similar affects of roughness on the total pressure loss of compressor blades was found in a study by Schaffler. Schaffler found that the polytropic efficiency of a compressor decreased as the magnitude of roughness increased past a critical value. At this point the surface of the blades transitioned from a hydrodynamicly smooth to a hydrodynamicly rough surface (Ref.10).

When the velocity and turbulence intensity profiles are examined for configurations 1,6,5,&2 (Figs. 20,21,22,&23), an enlarging of the wake region is noticed. These configurations correspond to blades with roughness located from the leading edge to the 1/4 chord with Ra values of 0.5, 2.7, 19.8 and 26.9 micro-meters respectively. When the profiles of the first traverse of Conf#1 (Fig.20) are compared to those of Conf#6 (Fig.21) no significant

VANE WAKE: CONF. NO.1, EVAL. NO.6

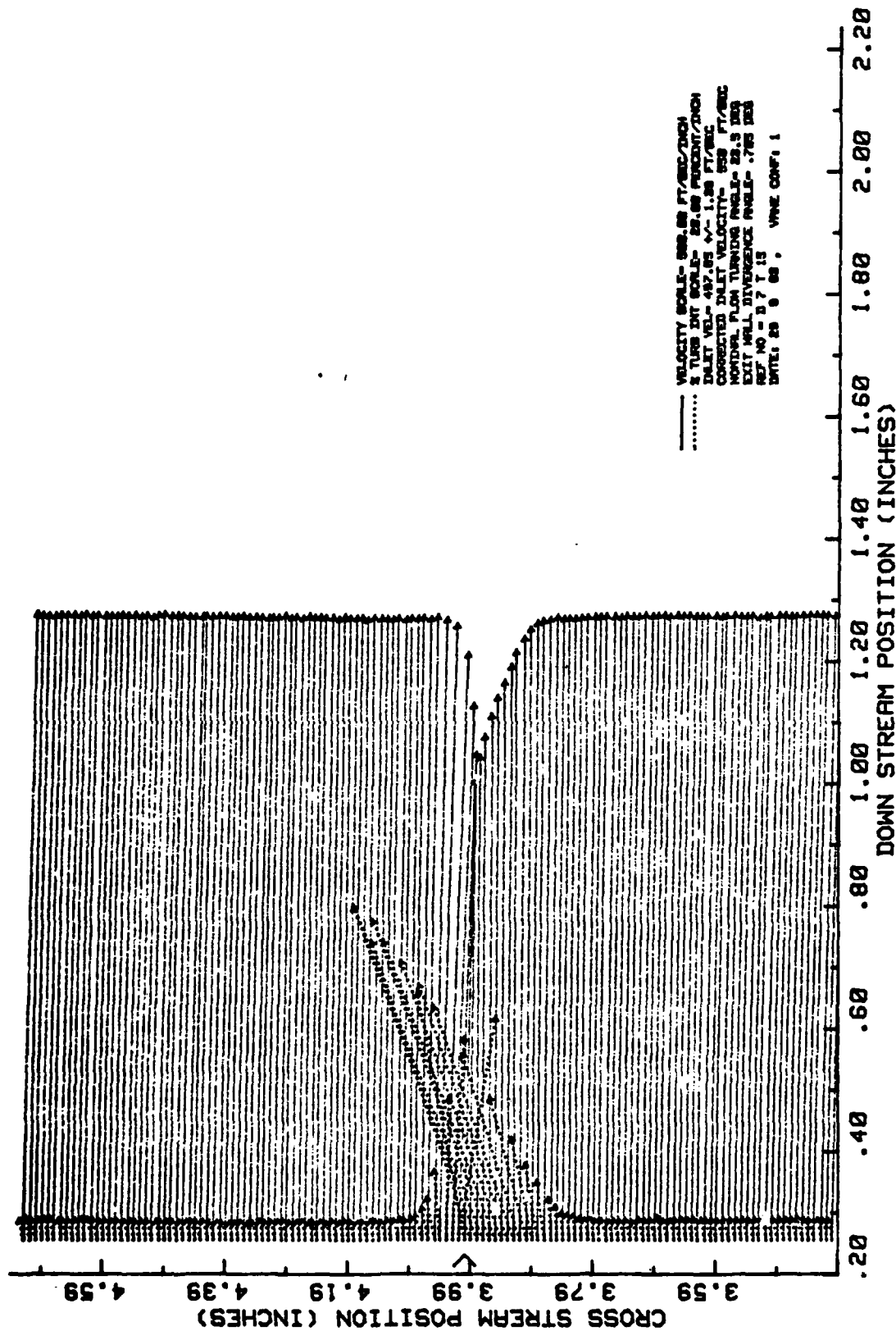


Figure 20: Velocity and Turbulence Intensity Profile; Traverse #1
 Conf#1 Eval#6: Smooth Baseline Blade

VANE WAKE: CONF. NO.6, EVAL. NO.2

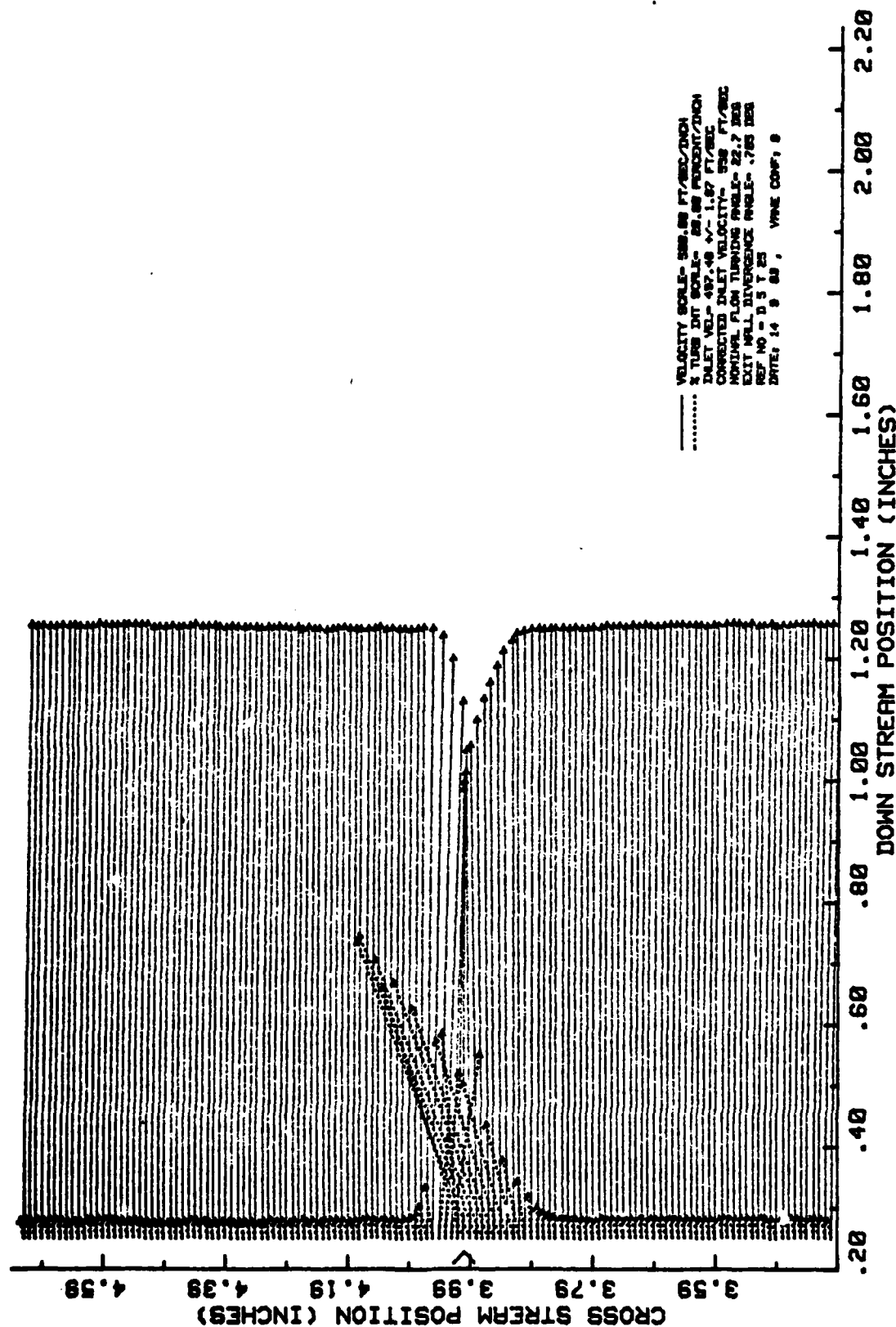


Figure 21: Velocity and Turbulence Intensity Profile; Traverse#1
 Conf#6 Eval#2: 3 micro-meter Ra Roughness from L.E.-1/4Chord

VANE WAKE: CONF. NO.5, EVAL. NO.2

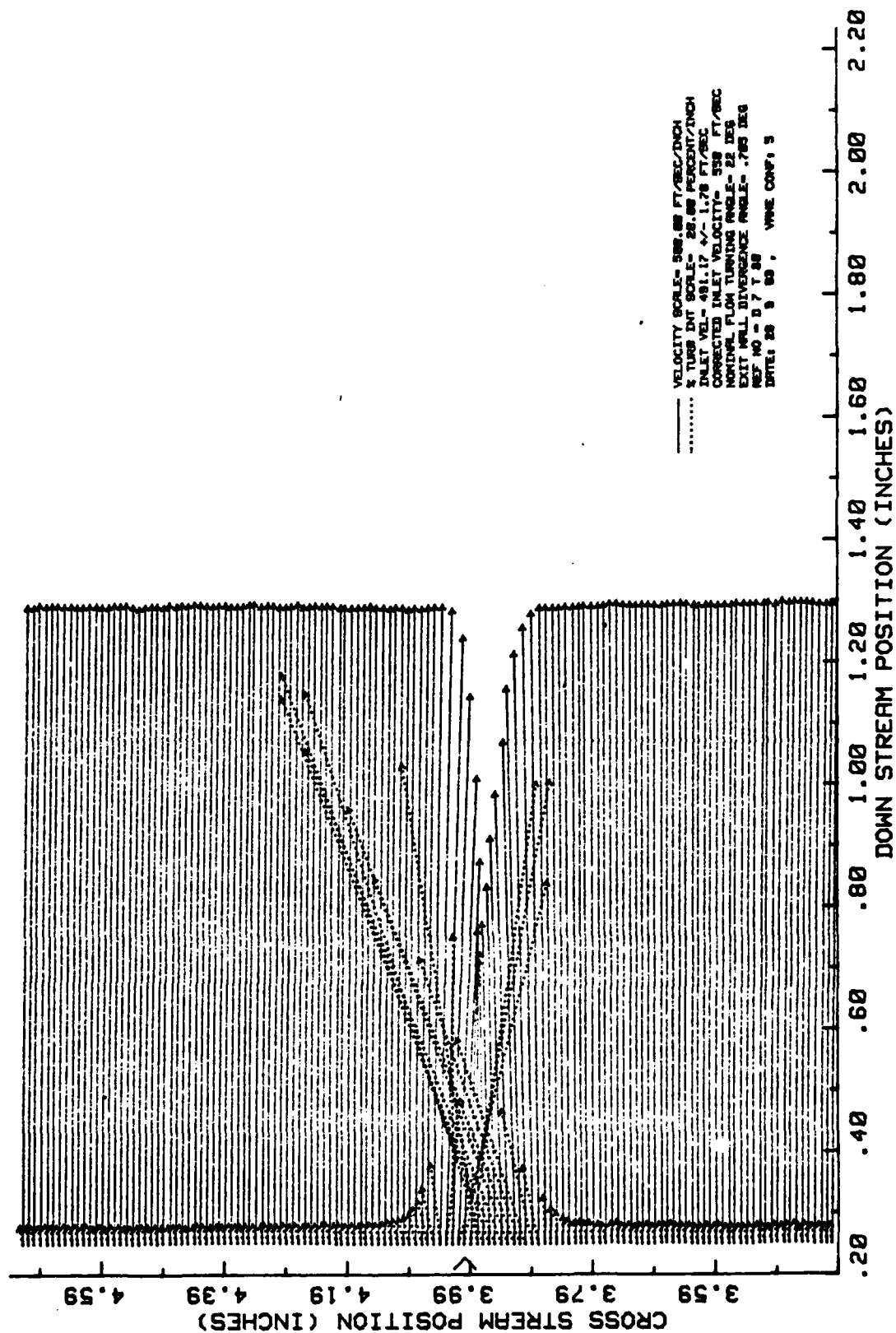


Figure 22: Velocity and Turbulence Intensity Profile; Traverse #1
 Conf #5 Eval #2: 20 micro-meter Ra Roughness from L.E.-1/4 Chord

VANE WAKE: CONF. NO.2, EVAL. NO.1

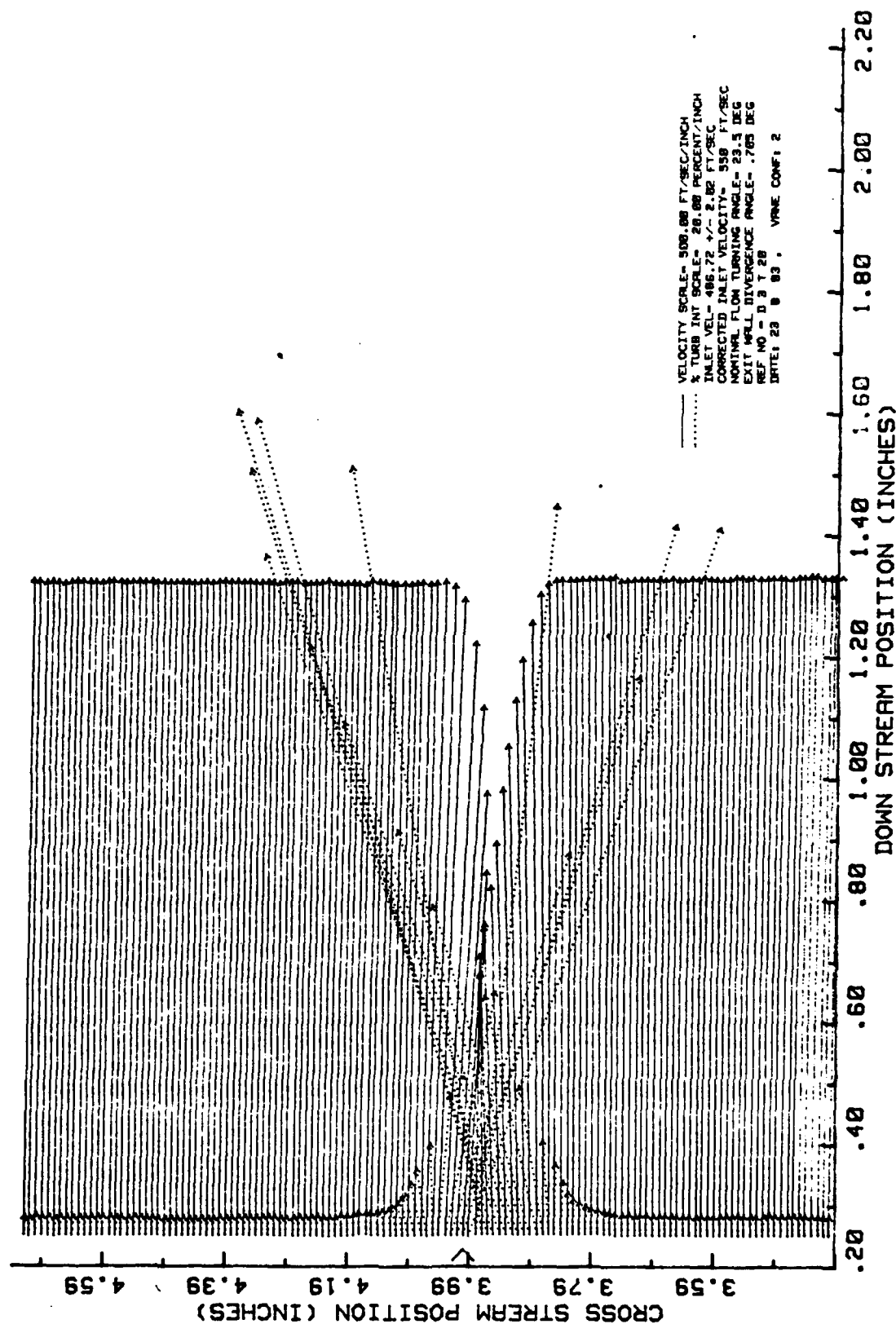


Figure 23: Velocity and Turbulence Intensity Profile; Traverse#1
Conf#2 Eval#1: 27 micro-meter Ra Roughness from L.E.-1/4Chord

differences can be noticed. The velocity decrement in both cases have the same general shape, characterized by the steep gradient on the pressure side of the wake (upper portion of the velocity decrement) and the gentle gradient on the suction side (lower portion of the velocity decrement). The depth of the velocity decrement and the magnitude and direction of the turbulence intensity vectors are also the same. When configurations 5 and 2 (Figs. 22 & 23) are compared to configurations 1 and 6 a large difference in their wake regions is noticed. Configurations 5 and 2, with their larger magnitudes of roughness (19.8 and 26.9 micro-meters Ra respectively as compared to 0.5 and 2.11 micro-meters Ra for configurations 1 and 6), exhibit a deeper velocity decrement with larger gradients on the sides than configurations 1 and 6. The turbulence intensity vectors for configurations 5 and 2 also show an increase in magnitude over configurations 1 and 6.

The velocity and turbulence intensity profiles suggest that as the roughness level increases there is an insignificant change in the flow over to the blade until a threshold is achieved. Once this threshold is passed a significant increase in the boundary layer growth occurs and a loss of performance is experienced.

REPEATABILITY

During the testing of the various blade configurations great care was taken to insure constant test conditions

during a run. It was found practically impossible to duplicate test conditions from run to run because of changes in the weather that affected the air supply's humidity and temperature. These changes in the air supply primarily affected the hot wire system by increasing the heat transfer from the sensor and the resistance of the probe support. These changes caused a uniform shift in the measured velocity data from 3 to 7 percent. This increase in the hot wire velocity data caused the calculated exit mass flow rate to be greater than the inlet mass flow rate as derived from the inlet static and total pressure data. The pressure transducers having been very stable over the course of the study were assumed correct and the inlet mass flow calculated from the pressure data was therefore assumed correct. To correct the calculated exit mass flow a scaling factor was applied to the hot wire velocity data that caused the derived exit mass flow to equal that of the inlet.

To estimate the total error of the system duplicate tests were run on configurations 1 & 8 and compared for repeatability. After the mass flow correction factor was applied to the measured velocity the average performance parameter, ζ , was within 3% for duplicate tests of the same blade configuration as was the velocity data. The turbulence intensity data differed by no more than 5% between the duplicate tests.

V. CONCLUSIONS AND RECOMMENDATIONS

CONCLUSIONS

The effect of roughness on the performance of compressor blades was studied in a seven blade cascade of NACA 64-A905 blades. The cascade used did not use boundary layer removal therefore could not be considered two dimensional according to Erwin and Emery (Ref.5). The results of this investigation showed that roughness has significant affect on the loss of total pressure across the cascade of blades but the data presented in this report should not be considered hard fast design data.

Roughness affects the loss in total pressure across the compressor blades as follows:

1. The greatest loss in total pressure occurred with roughness located near the leading edge of the blade.
2. The loss in total pressure across the blade is dependent on the degree of roughness only after a threshold level of roughness is exceeded.

RECOMMENDATIONS

A better understanding of how roughness affects the loss in total pressure across compressor blades could be accomplished if the boundary layer thickness of the blade were evaluated and compared to the size of the roughness. One possible method for evaluating the boundary layer thickness would be to physically measure it with a hot wire

anemometer. Before evaluating the boundary layer thickness a new test section should be made that employs continuous boundary layer removal along the side walls of the cascade. Without boundary layer removal the cascade can not be considered two dimensional according to the NACA report 1016 (Ref.5). In addition to the continuation of the present investigation, a study of the effects that humidity have on the heat transfer rate of hot film sensors and the effects of a temperature change on the resistance of the hot wire probe support should be initiated.

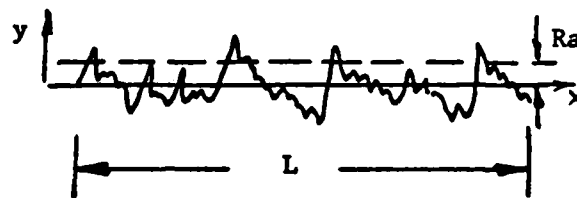
BIBLIOGRAPHY

1. Abbott, I.H., von Doenhoff, A.E., and Stivers, L.S., Jr., Report No 824, National Advisory Committee for Aeronautics, p. 258.
2. Allison, Dennis M. Design and Evaluation of a Cascade Test Facility, Unpublished MS Thesis. Wright-Patterson AFB, Ohio: Air Force Institute of Technology, June 1982.
3. Bammert, K. and Sandstede, H. "Influences of Manufacturing Tolerances and Surface Roughness of Blades on the Performance of Turbines", Journal of Engineering for Power (January 1976).
4. Bradshaw, P. An Introduction to Turbulence and Its Measurement, New York; Pergamon Press, INC., 1971.
5. Erwin, John R. and Emery, James C., "Effects of Tunnel Configuration and Testing Technique on Cascade Performance", Report No. 1016 National Advisory Committee on Aeronautics, P. 263.
6. Genovese, David T. Roughness Effects on Compressor Outlet Guide Vanes at High Reynolds and High Angle of Attack, Unpublished MS Thesis. Wright-Patterson AFB, Ohio: Air Force Institute of Technology, December 1982.
7. Larsen, Soren E. and Busch, Niels E. "On the Humidity Sensitivity of Hot Wire Measurements". DISA Information No. 25: 4-5 (February 1980).
8. Perry, A.E. and Schofield, W.H. "Rough Wall Turbulent Boundary Layers", Journal of Fluid Mechanics, Vol.37 (1969).
9. Pope, Alan. Wind-Tunnel Testing, New York; John Wiley and Sons, INC., 1954.
10. Schaffler, A. "Experimental and Analytical Investigation of the Effects of Reynolds Number and Blade Surface roughness on Multistage Axial Flow Compressors", Journal of Engineering For Power, 102:5-13 (January 1980)
11. Schlichting, Hermann. Boundary-Layer Theory, New york; McGraw-Hill Book Co., 1979.

12. Smith, A. and Clutter, D. "The Smallest Height of Roughness Capable of Affecting Boundary-Layer Transition", Journal of the Aero/Space Sciences, Vol.26 (April 1959).
13. Stiles, R.J. Roughness Effects in Axial Compressors-An Emperical Model-. Unpublished Report. Wright-Patterson AFB, Ohio: Wright Aeronautical Laboratories, 1980.
14. Taylor Hobson. Surtronic 3. Operating Instructions. Leicester, England: Rank Taylor Hobson, (undated).
15. Thomas, M.W. and Evans, D.C. General Electric Gas Turbine Fundamentals Vol II, Unpublished report, General Elictric Co. Evansdale Ohio, July 1973.
16. TSI, General System Information For 1050 Series Anemometry, TSI Incorporated, 500 Cardigan Rd, St. Pual, Minnesota, 55164.
17. Vonada, John A. and Elrod, William C. Wake Mixing Investigation of Crenelated Trailing Edge Blades in Cascade, Unpublished report. Wright-Patterson AFB, Ohio: Air Force Institute of Technology, October 1983.

APPENDIX A: ROUGHNESS DEFFINITIONS

Surface roughness is defined as the finer irregularities in the repetitive or random deviations from an intended surface contour (Ref.13). These random deviations which look like a series of peaks and valleys are most commonly characterized in terms of "Arithmetic Average Roughness, R_a " as defined below.



$$R_a = \frac{1}{L} \int |y| dx$$

(12)

Figure 24: Arithmetic Average Roughness

Arithmetic Average Roughness does not completely characterize the surface for there could be several surfaces with equal R_a but have different appearances and different hydrodynamic characteristics Fig.25.

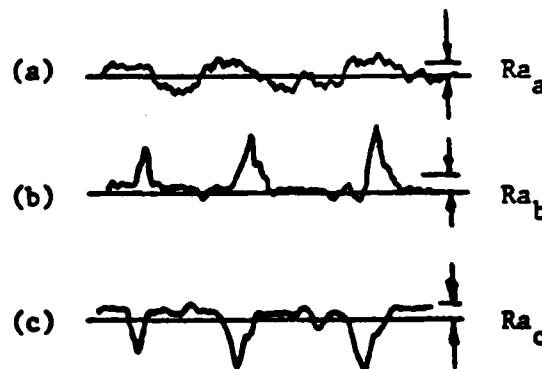


Figure 25: Three different surfaces of equal R_a (Ref.13)

For this reason two other roughness parameters will be defined Average Maximum Peak to Valley, R_{tm} ; and Average Maximum Peak to Mean, R_{pm} .

The R_{tm} roughness parameter characterizes the surface by measuring the maximum distance between peaks and valleys over several measuring lengths and then averages these maximums for the total traverse Fig.26.

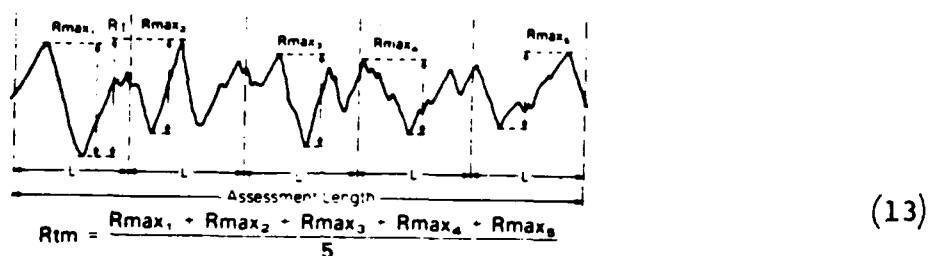


Figure 26: Derivation of R_{tm} Roughness (Ref.14)

The R_{tm} roughness parameter defines the maximum average peak to valley distance, which is important when studying the hydrodynamic character of a surface, but does not distinguish between a surface primarily of valleys or peaks as in Fig 25b&c. A third roughness parameter, Average Maximum Peak to Mean Roughness, R_{pm} is defined in Fig.27 similar to R_{tm} but only measuring the peaks of the roughness.

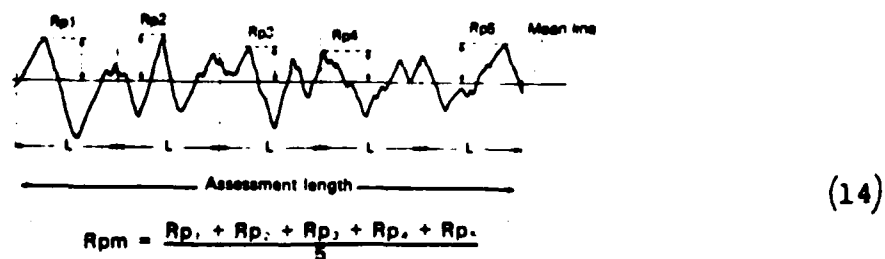
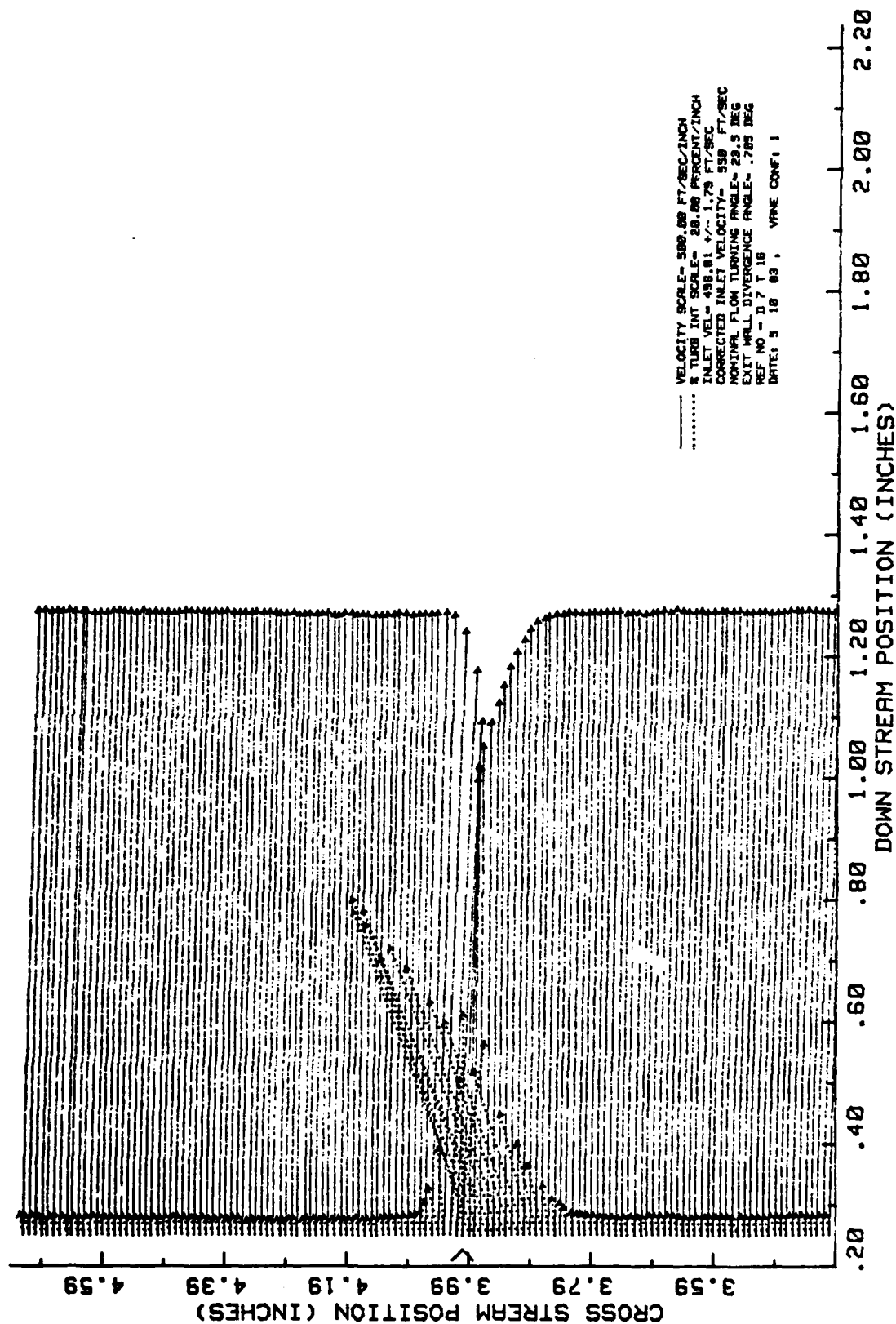


Figure 27: Derivation of R_{pm} roughness

With the three roughness parameters R_a , R_{tm} , and R_{pm} the surface's hydrodynamic characteristics can be adequately defined.

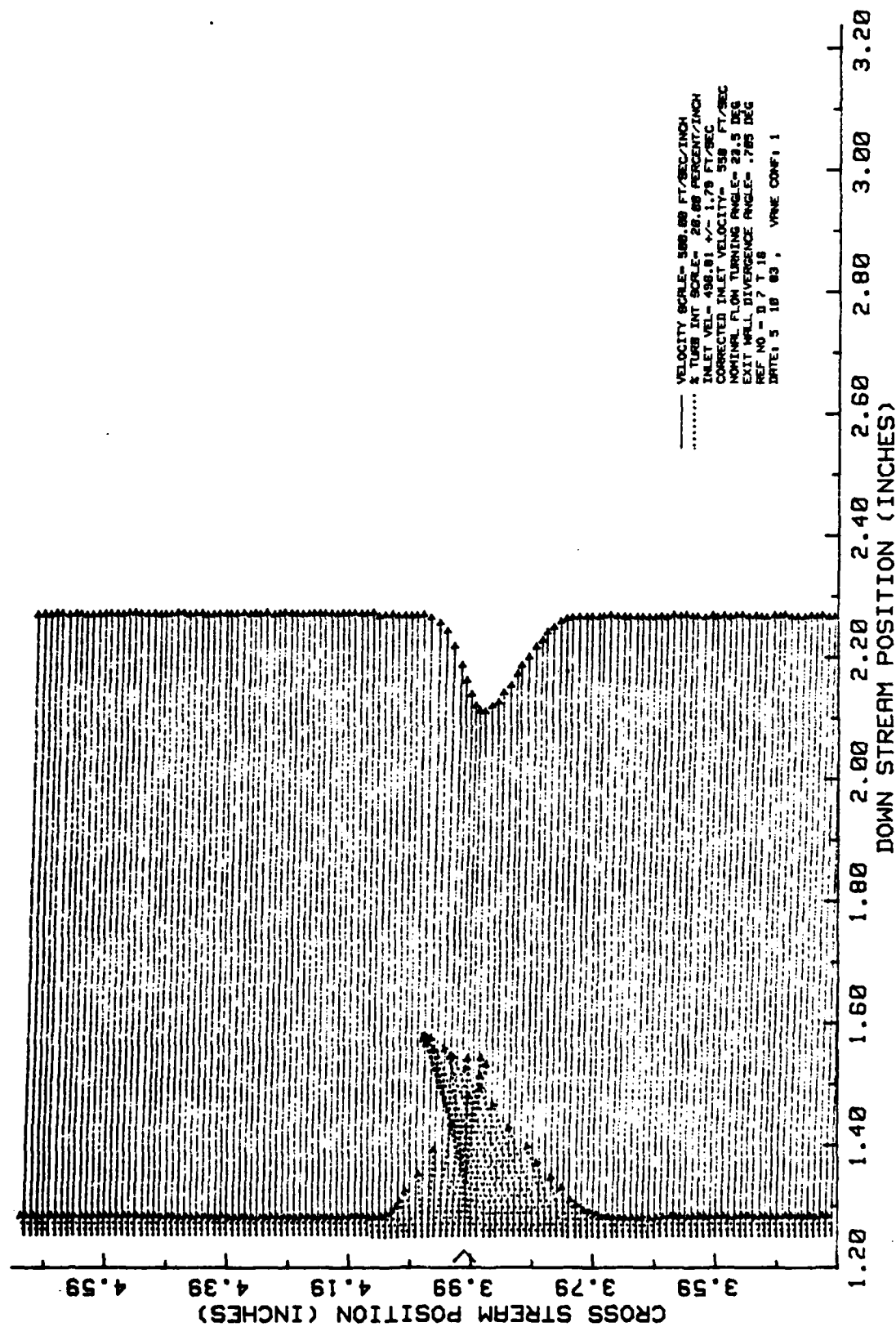
APPENDIX B: Velocity and Turbulence Intensity Profiles

VANE WAKE: CONF. NO.1, EVAL. NO.7



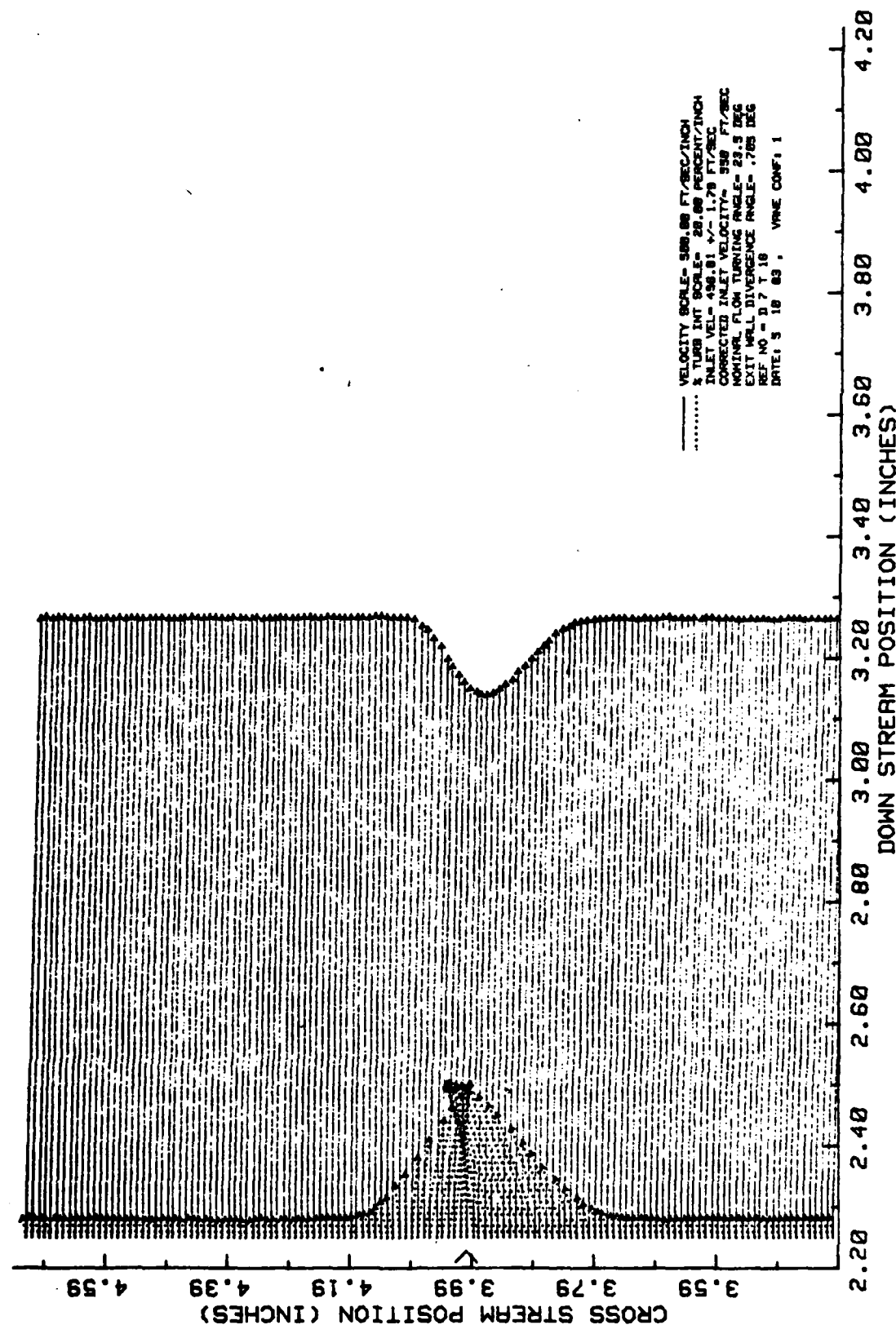
(A) Traverse#1
 Figure 28: Velocity and Turbulence Intensity Profile
 Conf#1 Eval#7: Smooth Baseline Blade

VANE WAKE: CONF. NO.1, EVAL. NO.7



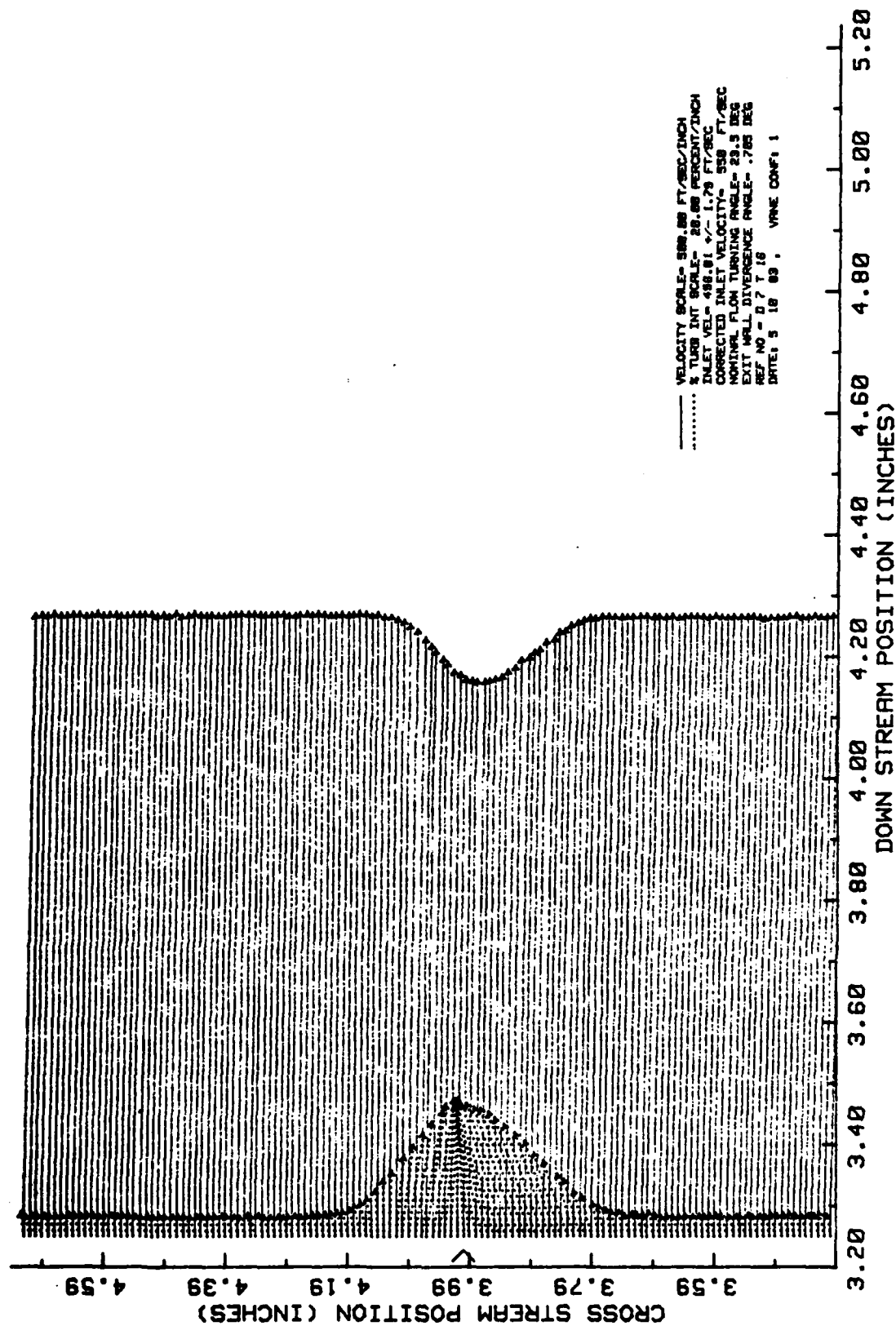
(B) Traverse#2
Figure 28: Continued

VANE WAKE: CONF. NO.1, EVAL. NO.7



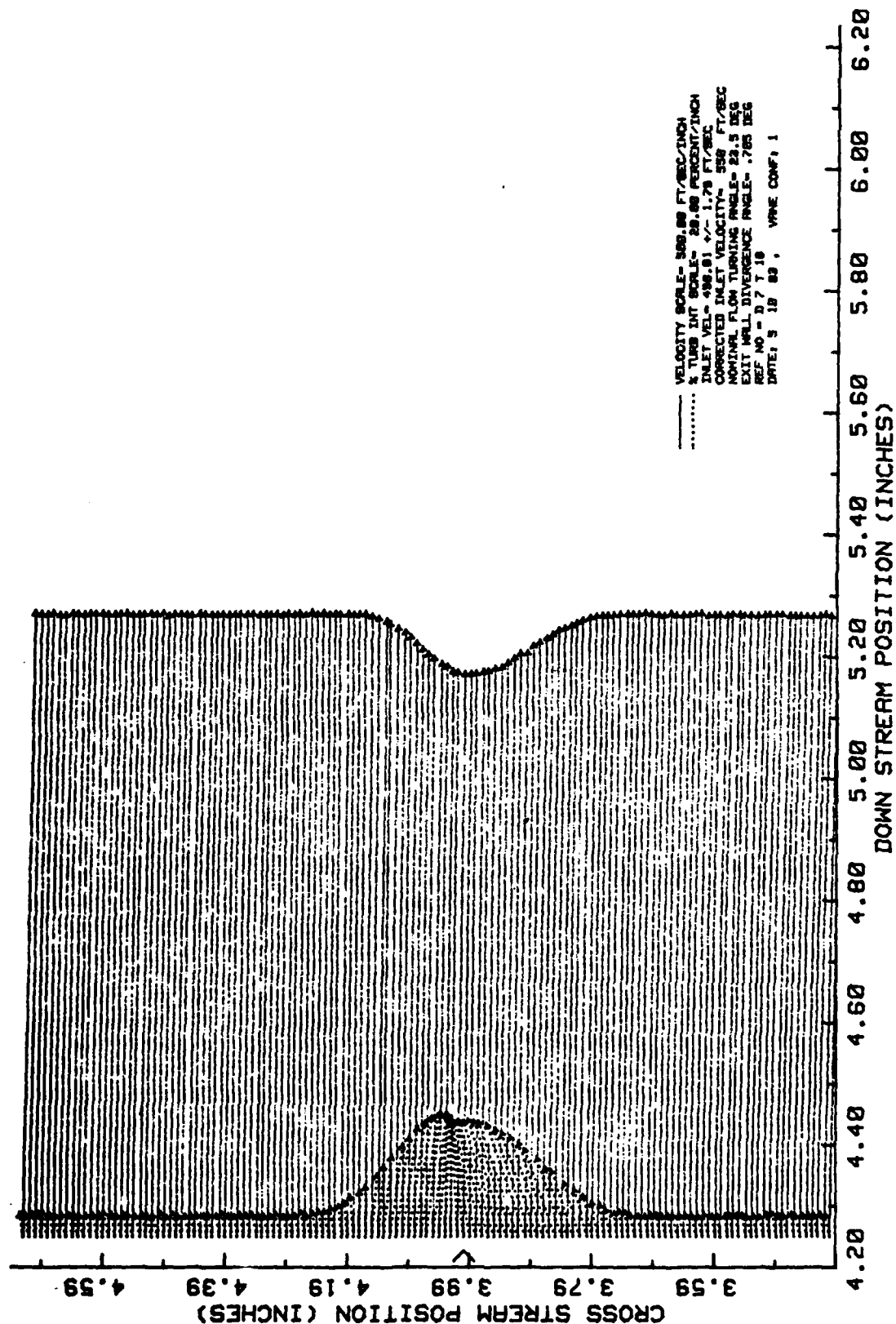
(C) Traverse#3
Figure 28: Continued

VANE WAKE: CONF. NO.1, EVAL. NO.7



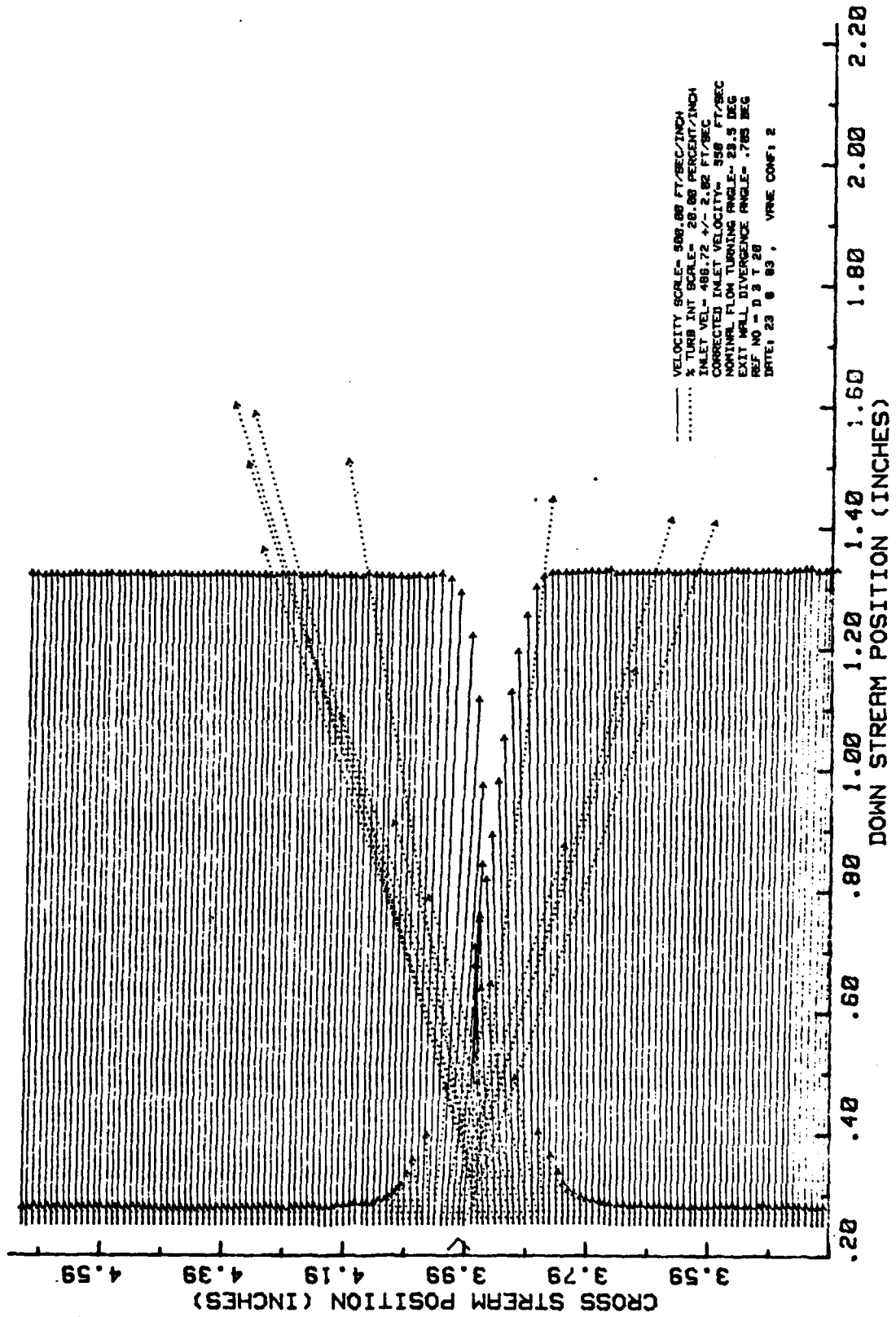
(D) Traverse #4
Figure 28: Continued

VANE WAKE: CONF. NO.1, EVAL. NO.7



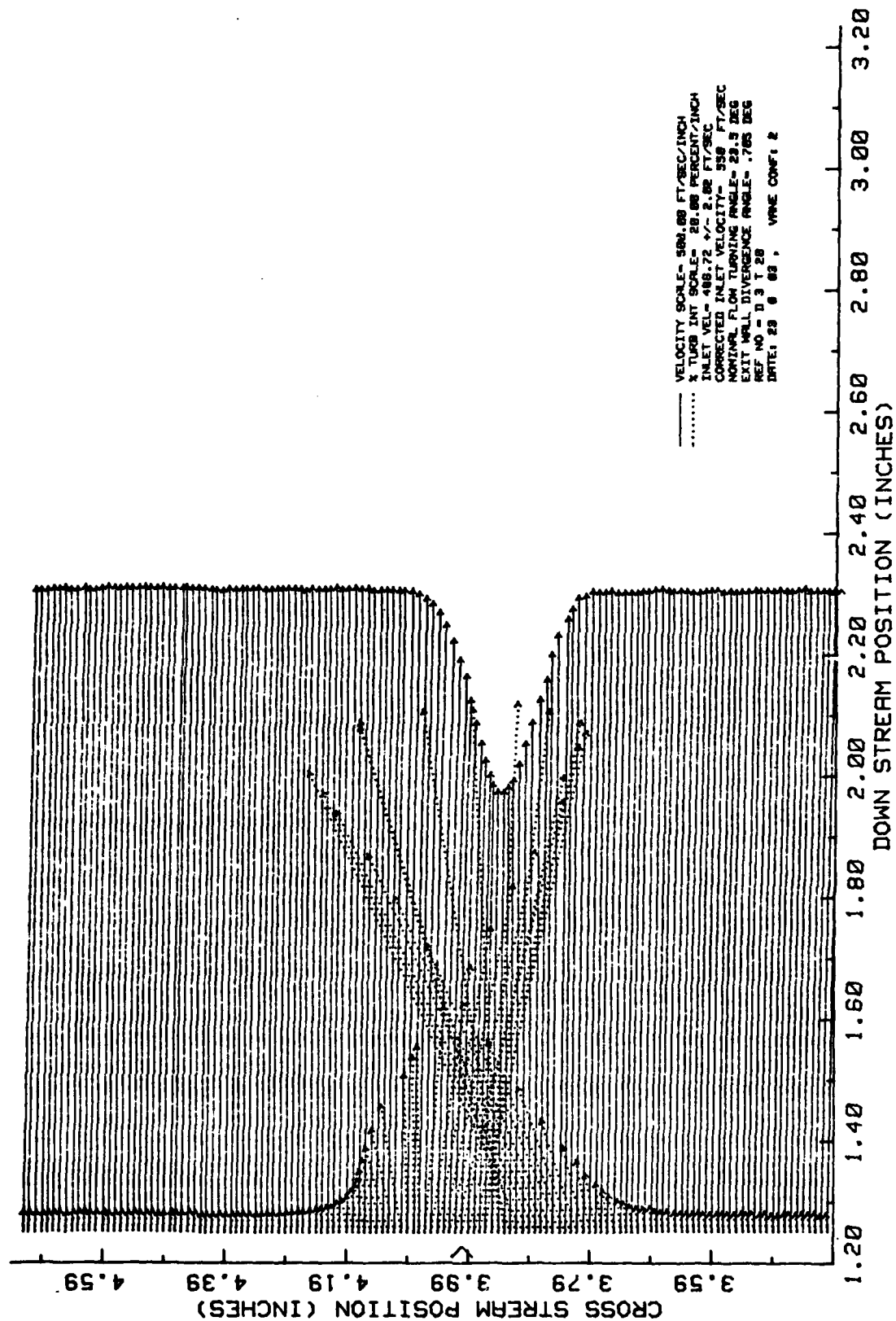
(E) Traverse#5
Figure 28: Continued

VANE WAKE: CONF. NO.2, EVAL. NO.1



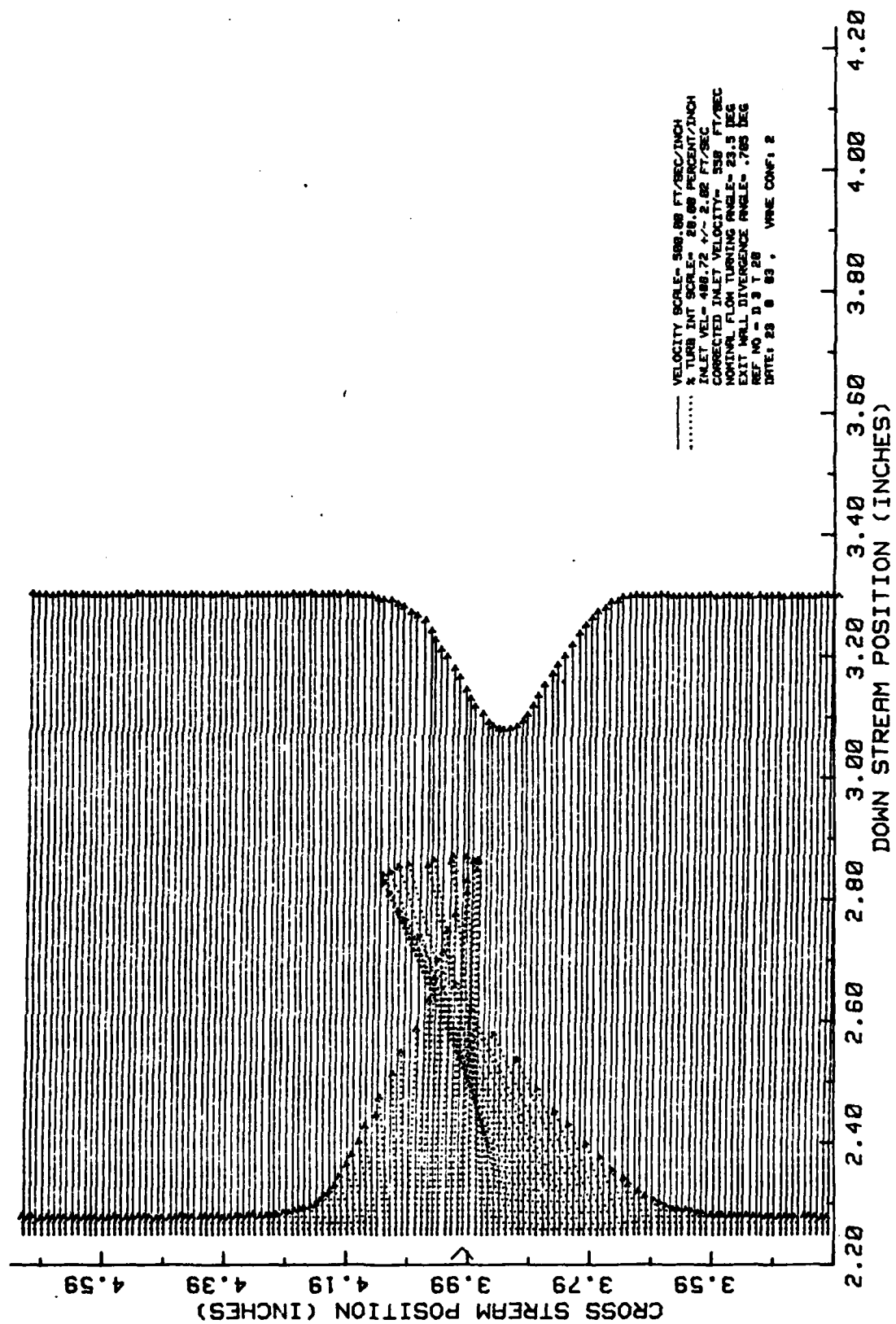
(A) Traverse#1
 Figure 29: Velocity and Turbulence Intensity Profile
 Conf#2 Eval#1: 27 micro-meter Ra Roughness from L.E.-1/4Chord

VANE WAKE: CONF. NO.2, EVAL. NO.1



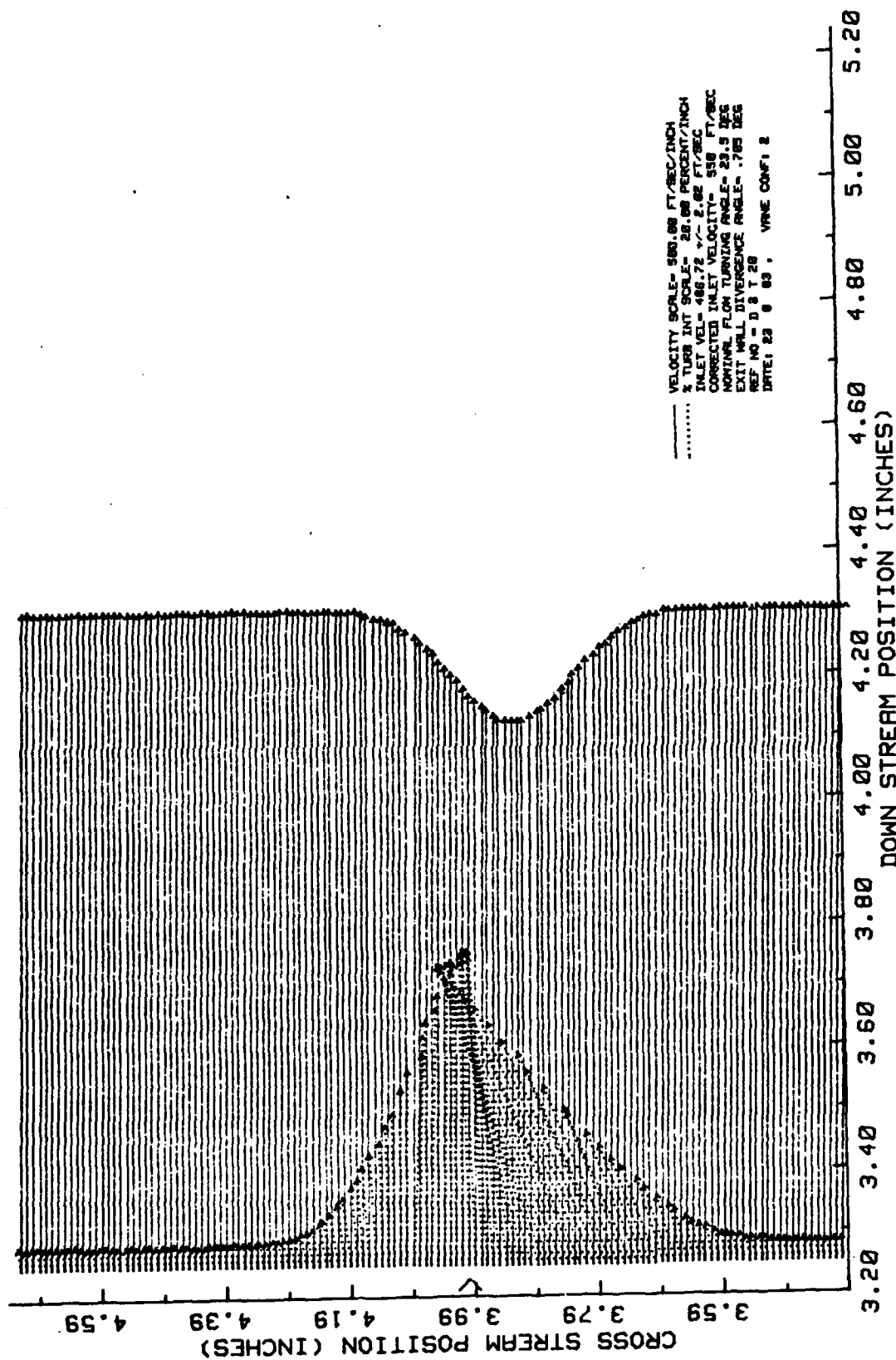
(B) Traverse#2
Figure 29: Continued

VANE WAKE: CONF. NO.2, EVAL. NO.1



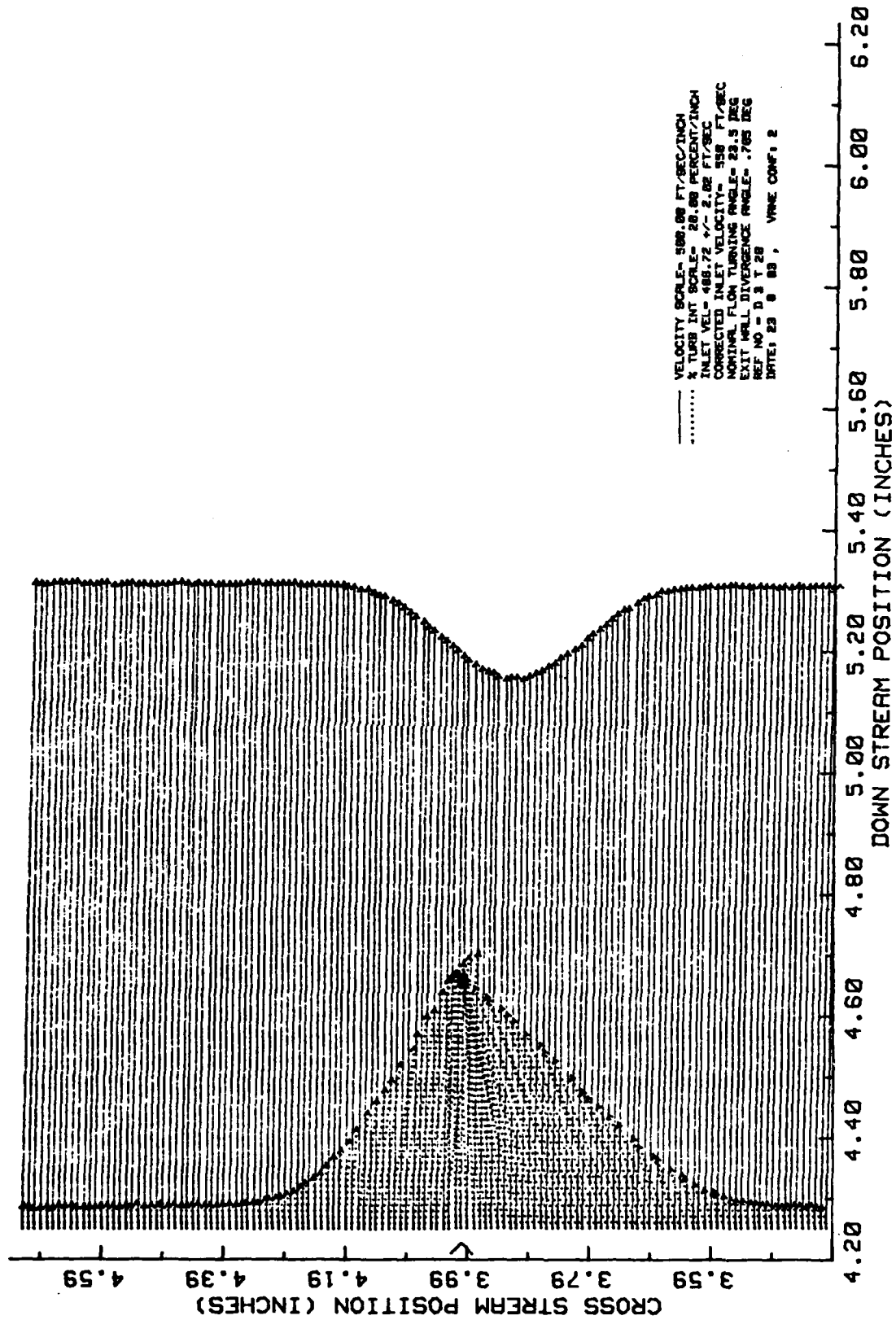
(C) Traverse#3
Figure 29: Continued

VANE WAKE: CONF. NO.2, EVAL. NO.1



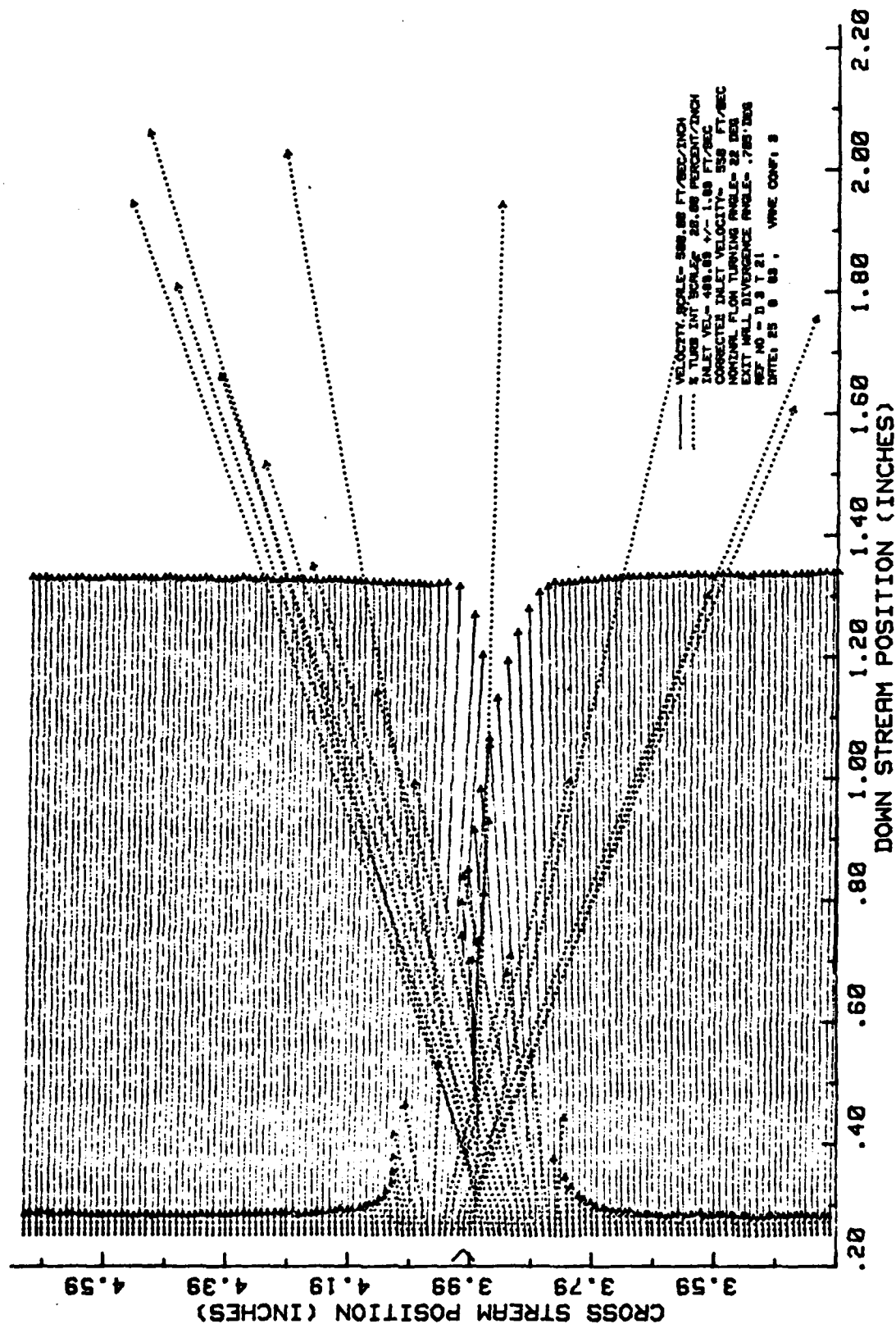
(D) Traverse#4
Figure 29: Continued

VANE WAKE: CONF. NO.2, EVAL. NO.1



(E) Traverse#5
 Figure 29: Continued

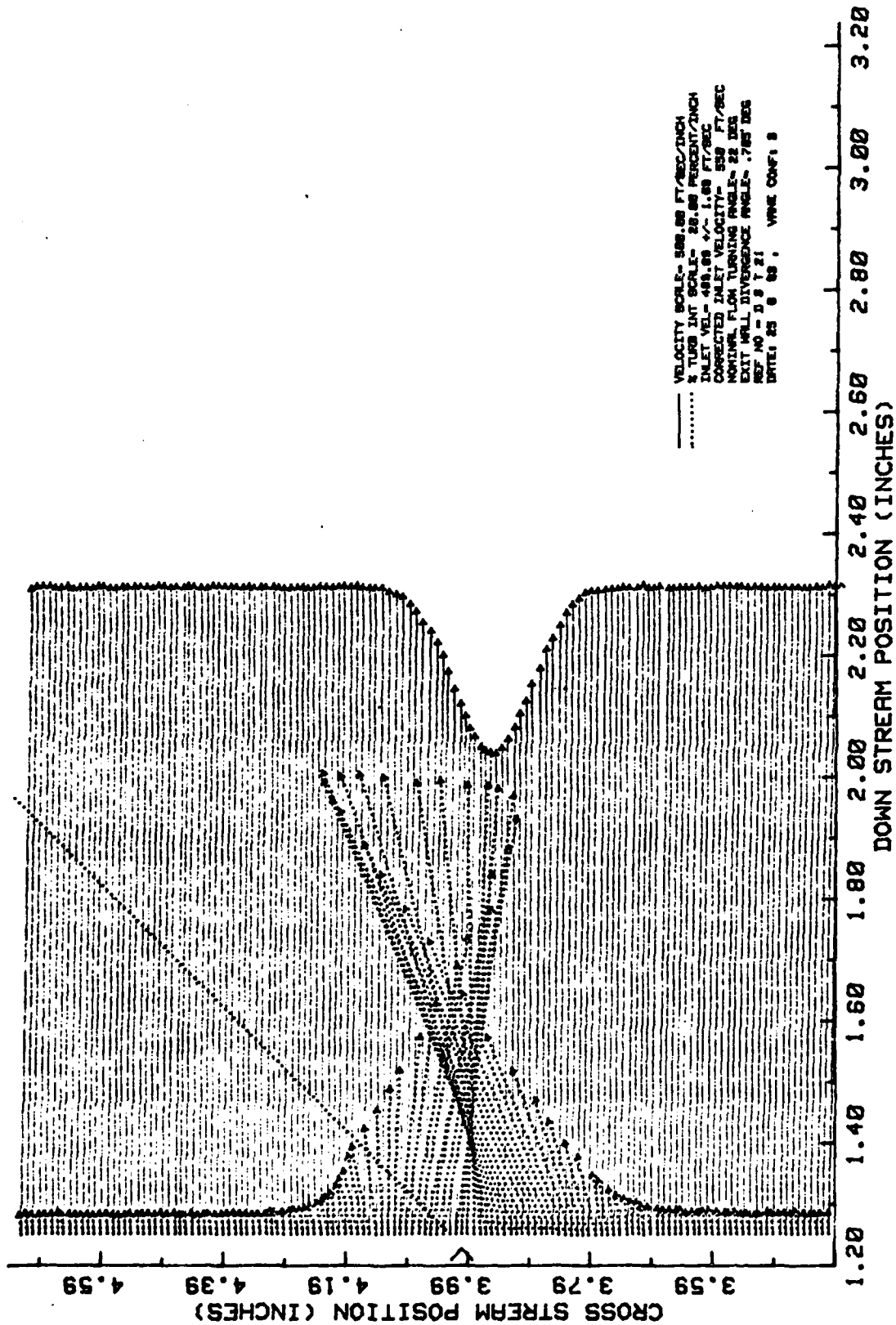
VANE WAKE: CONF. NO.3, EVAL. NO.1



(A) Traverse #1

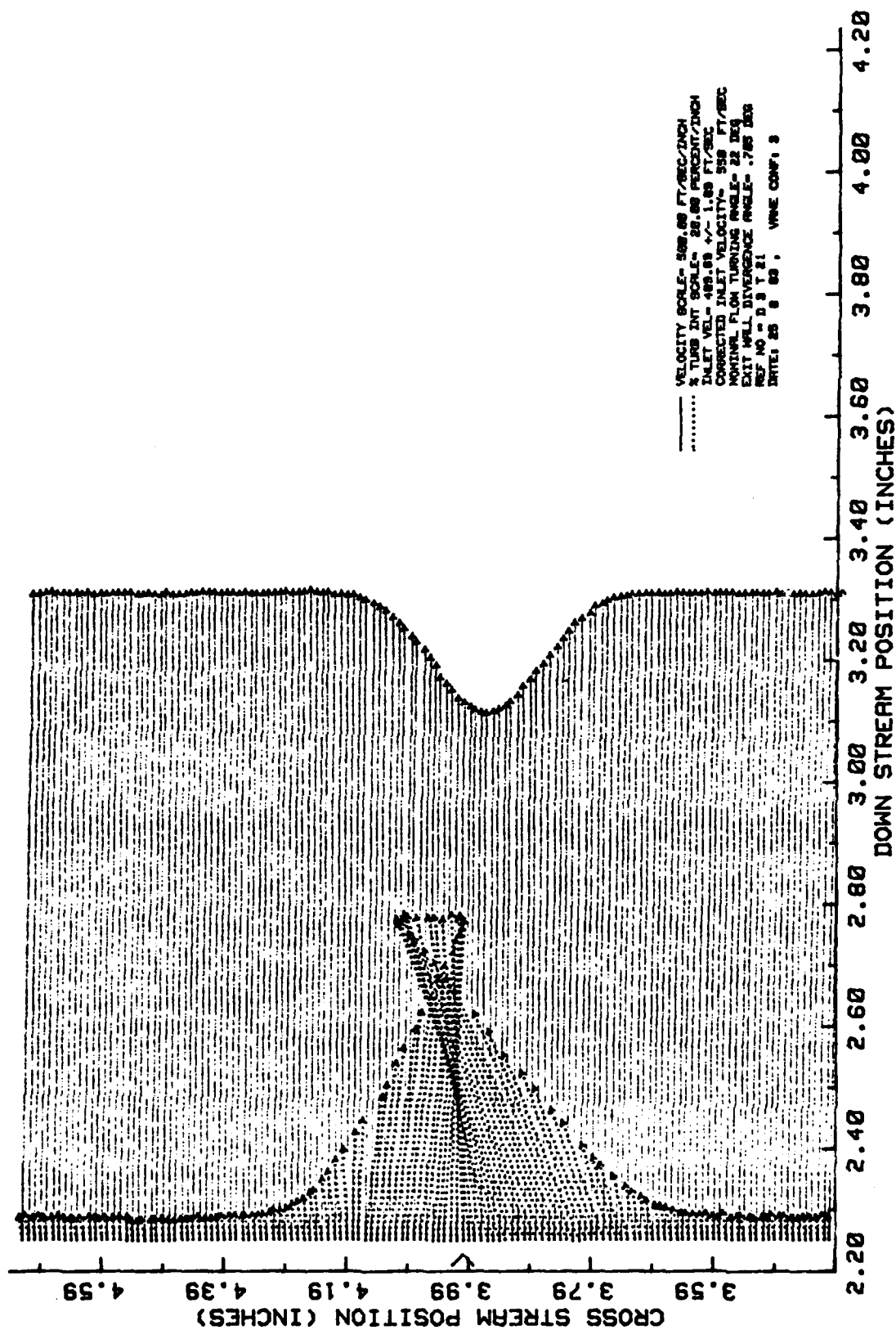
Figure 30. Velocity and Turbulence Intensity Profile
 Conf#3 Eval#1: 44 micro-meter Ra Roughness from 1/2Chord-T.E.

VANE WAKE: CONF. NO.3, EVAL. NO.1



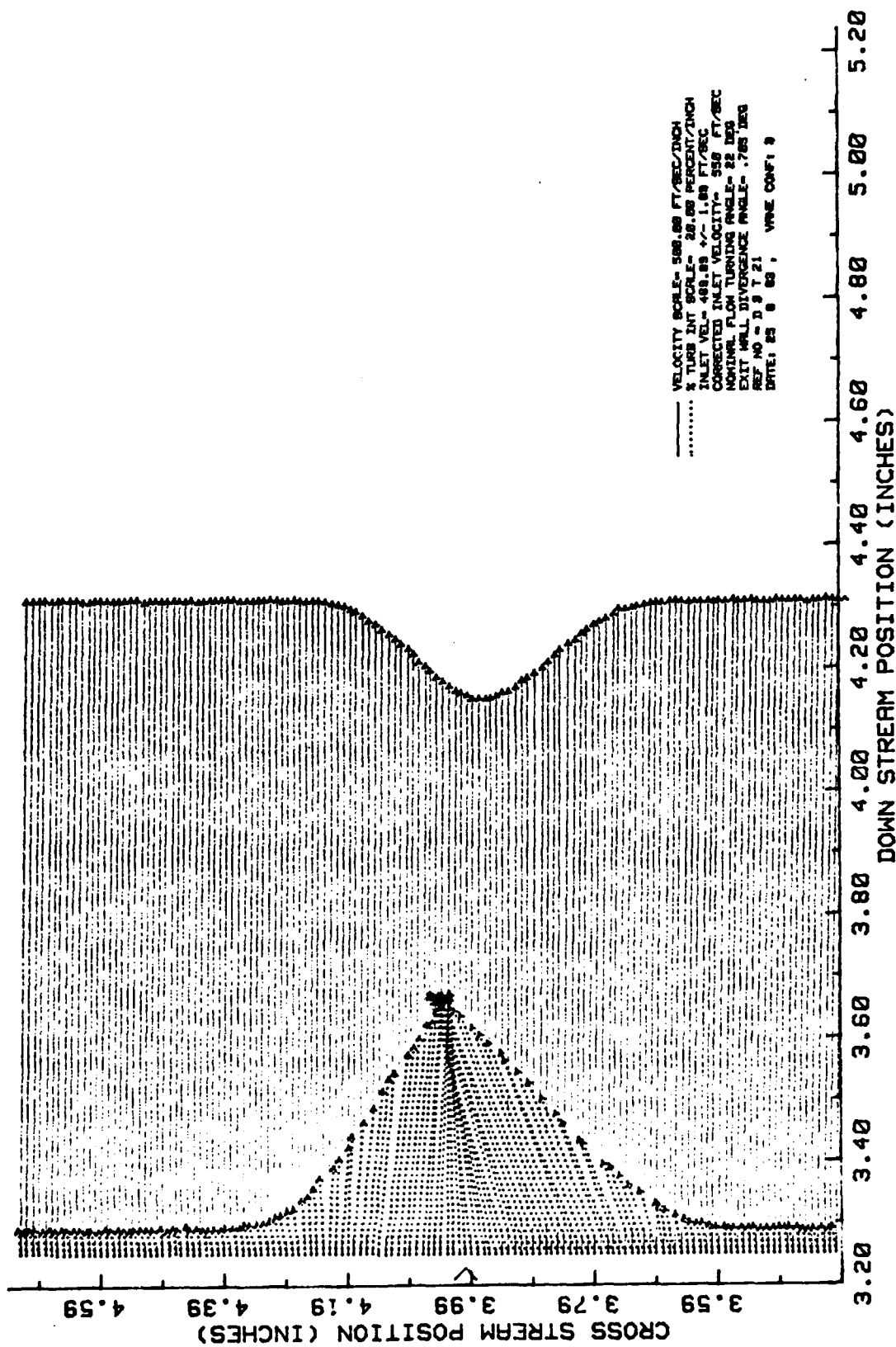
(B) Traverse#2
Figure 30: Continued

VANE WAKE: CONF. NO.3, EVAL. NO.1



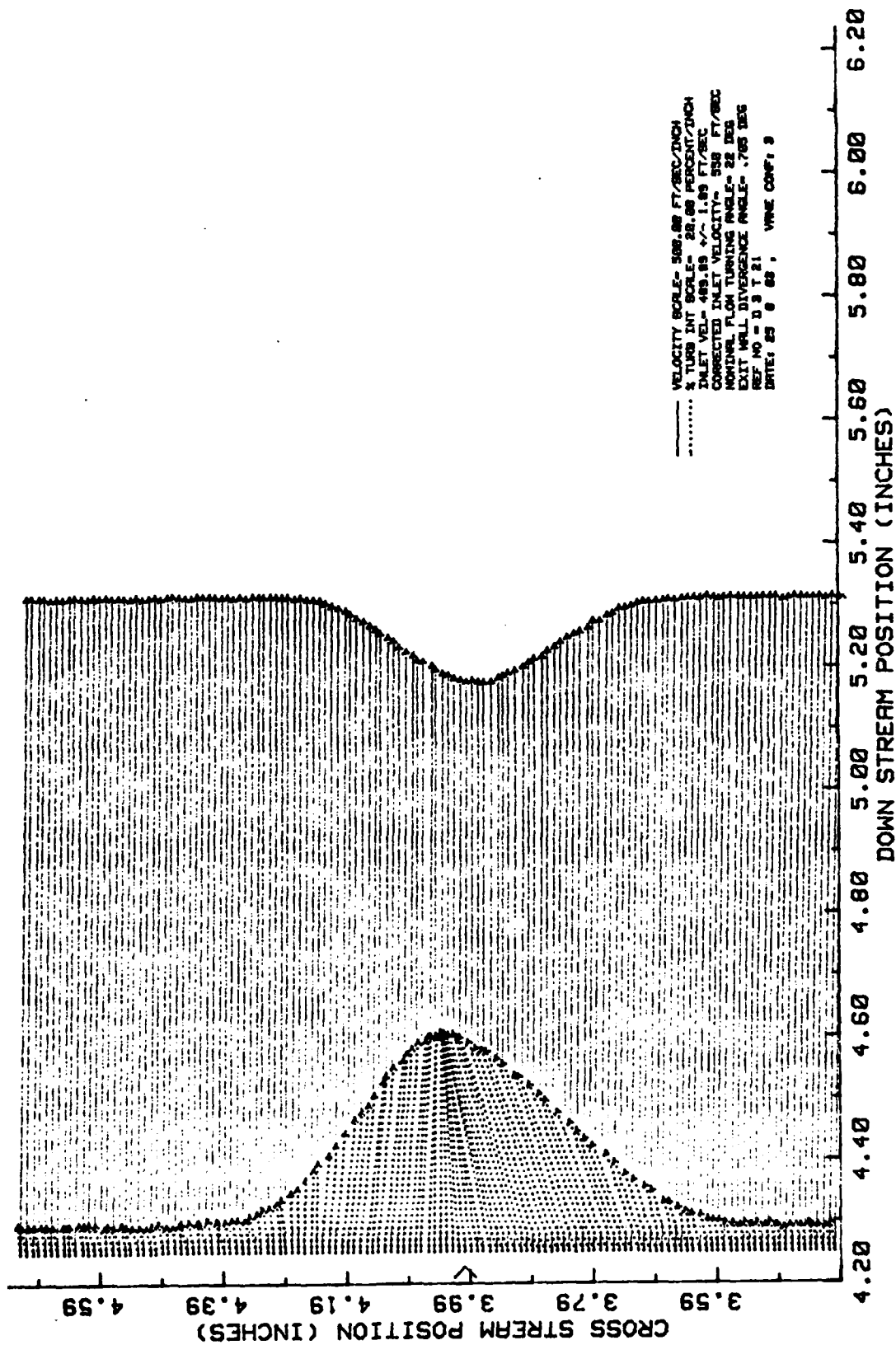
(C) Traverse#3
Figure 30: Continued

VANE WAKE: CONF. NO.3, EVAL. NO.1



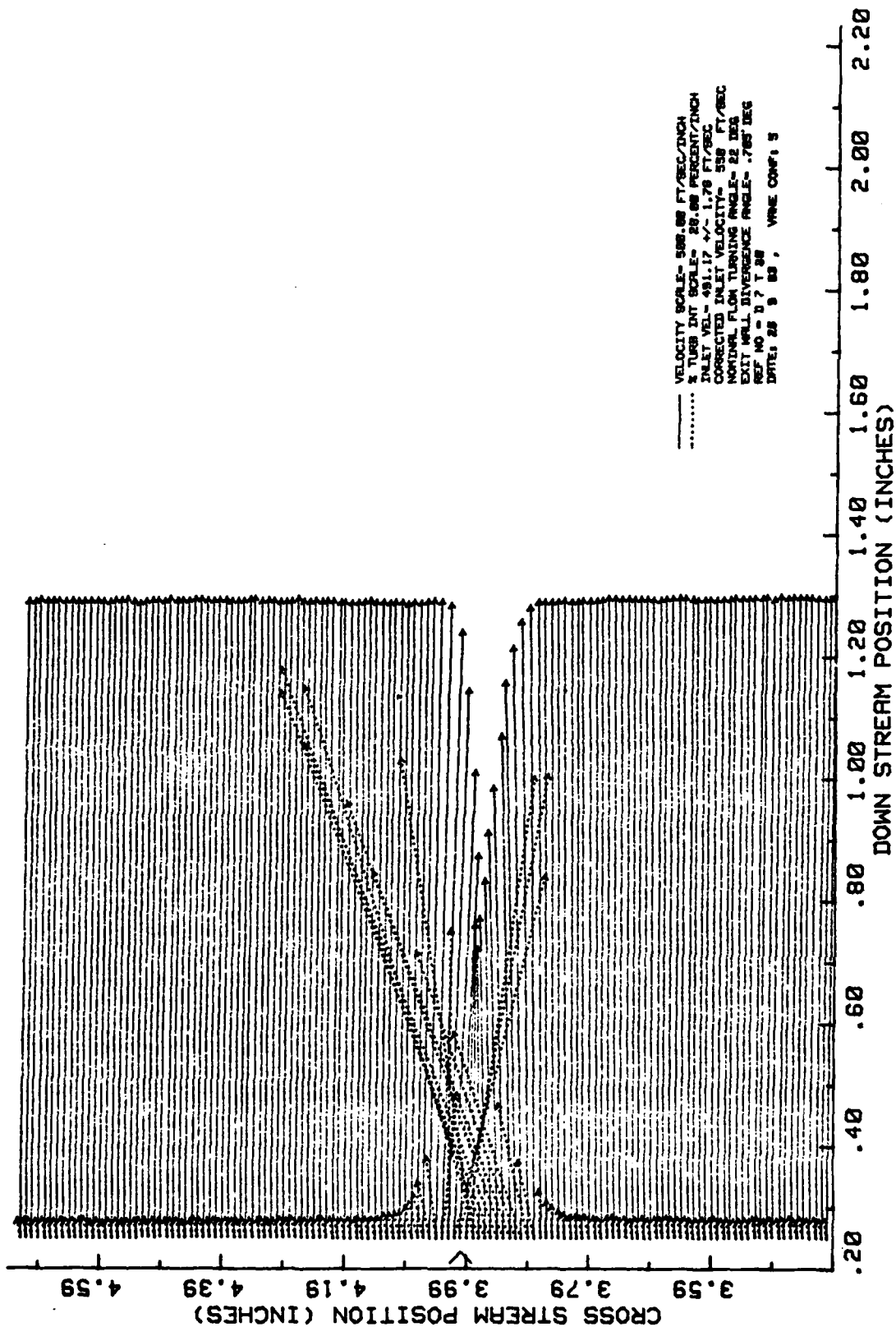
(D) Traverse#4
Figure 30: Continued

VANE WAKE: CONF. NO.3, EVAL. NO.1



(E) Traverse#5
Figure 30: Continued

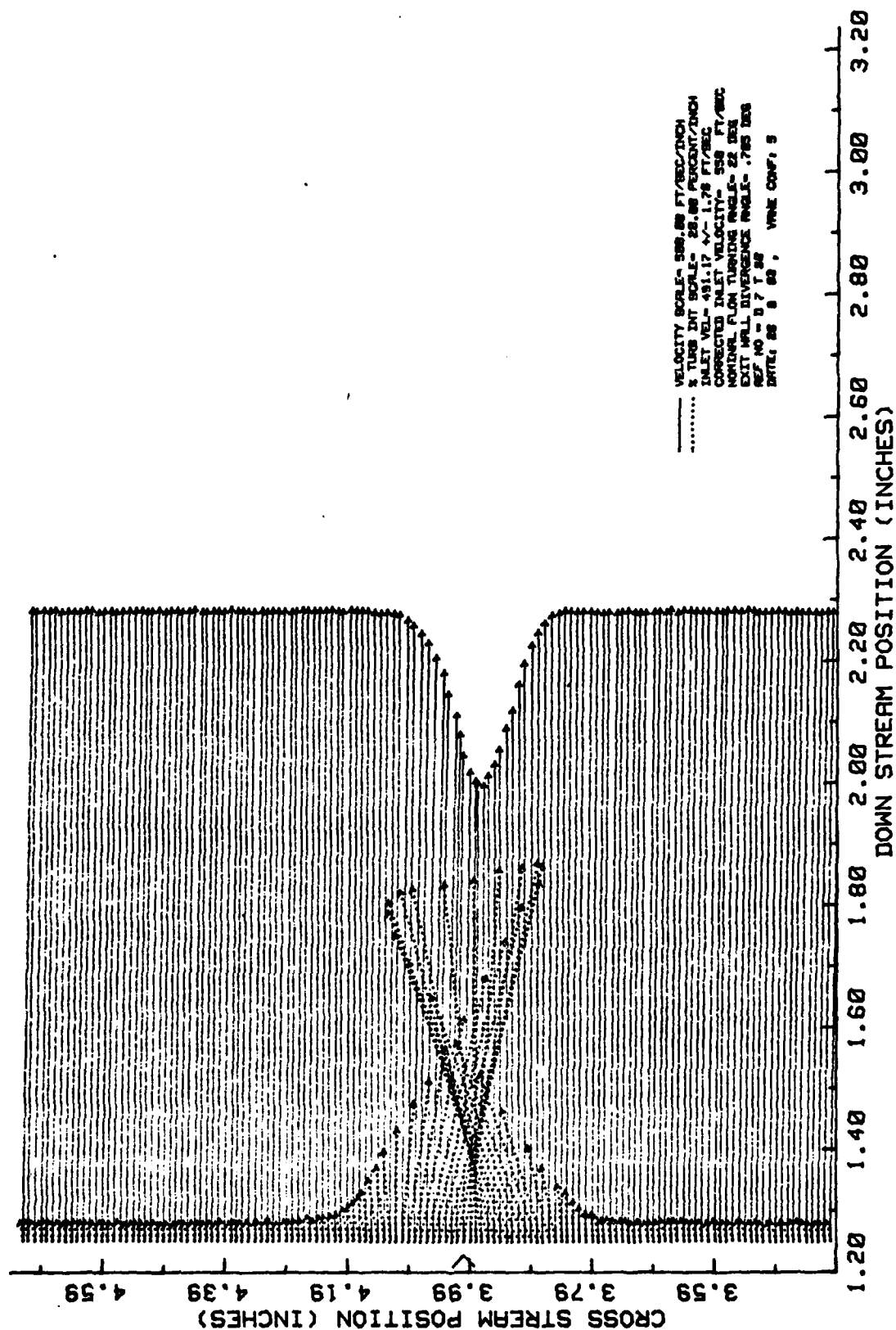
VANE WAKE: CONF. NO.5, EVAL. NO.2



(A) Traverse #1

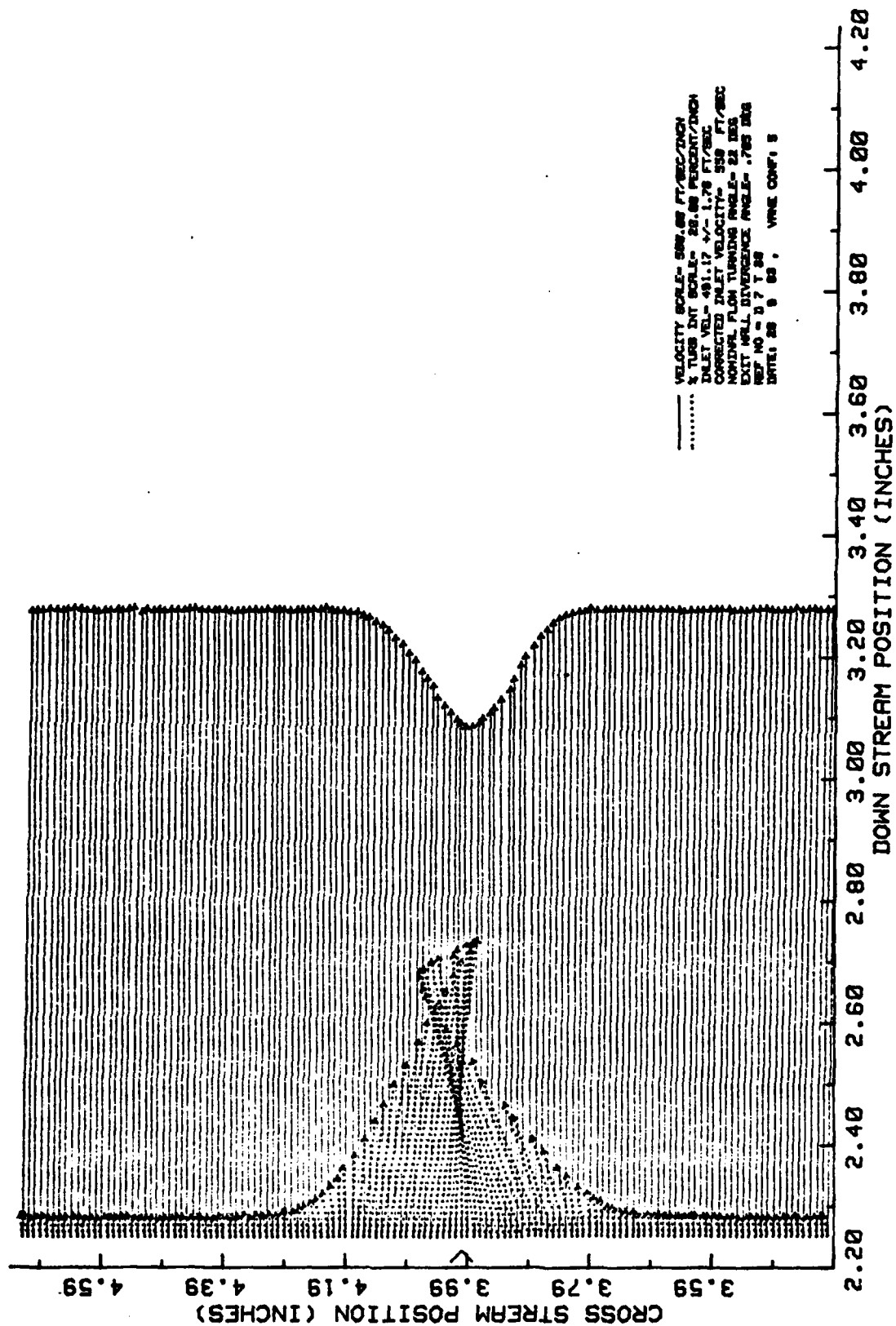
Figure 31: Velocity and Turbulence Intensity Profile
 Conf#5 Eval#2: 20 micro-meter Ra Roughness from L.E.-1/4Cord

VANE WAKE: CONF. NO.5, EVAL. NO.2



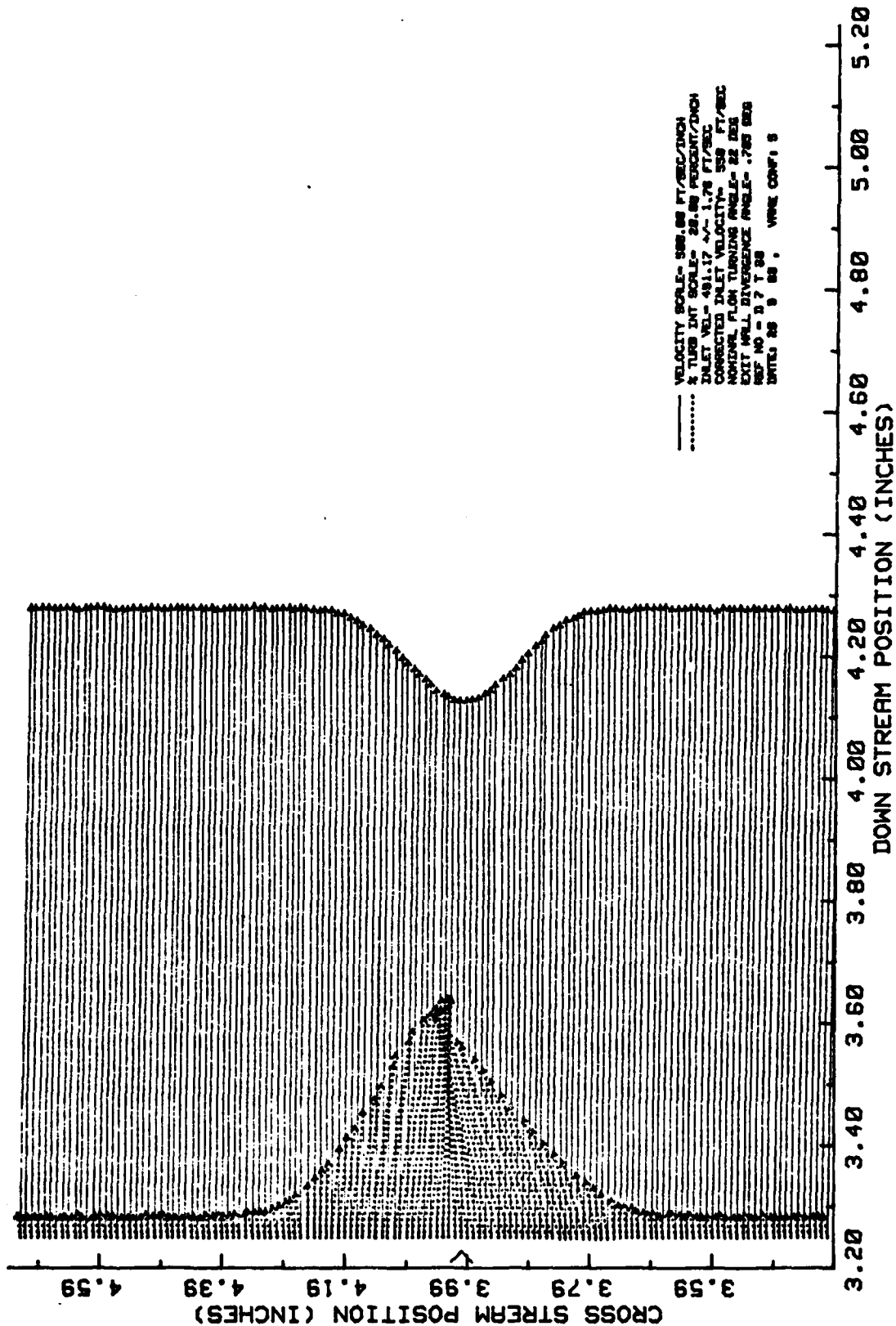
(B) Traverse#2
 Figure 31: Continued

VANE WAKE: CONF. NO.5, EVAL. NO.2



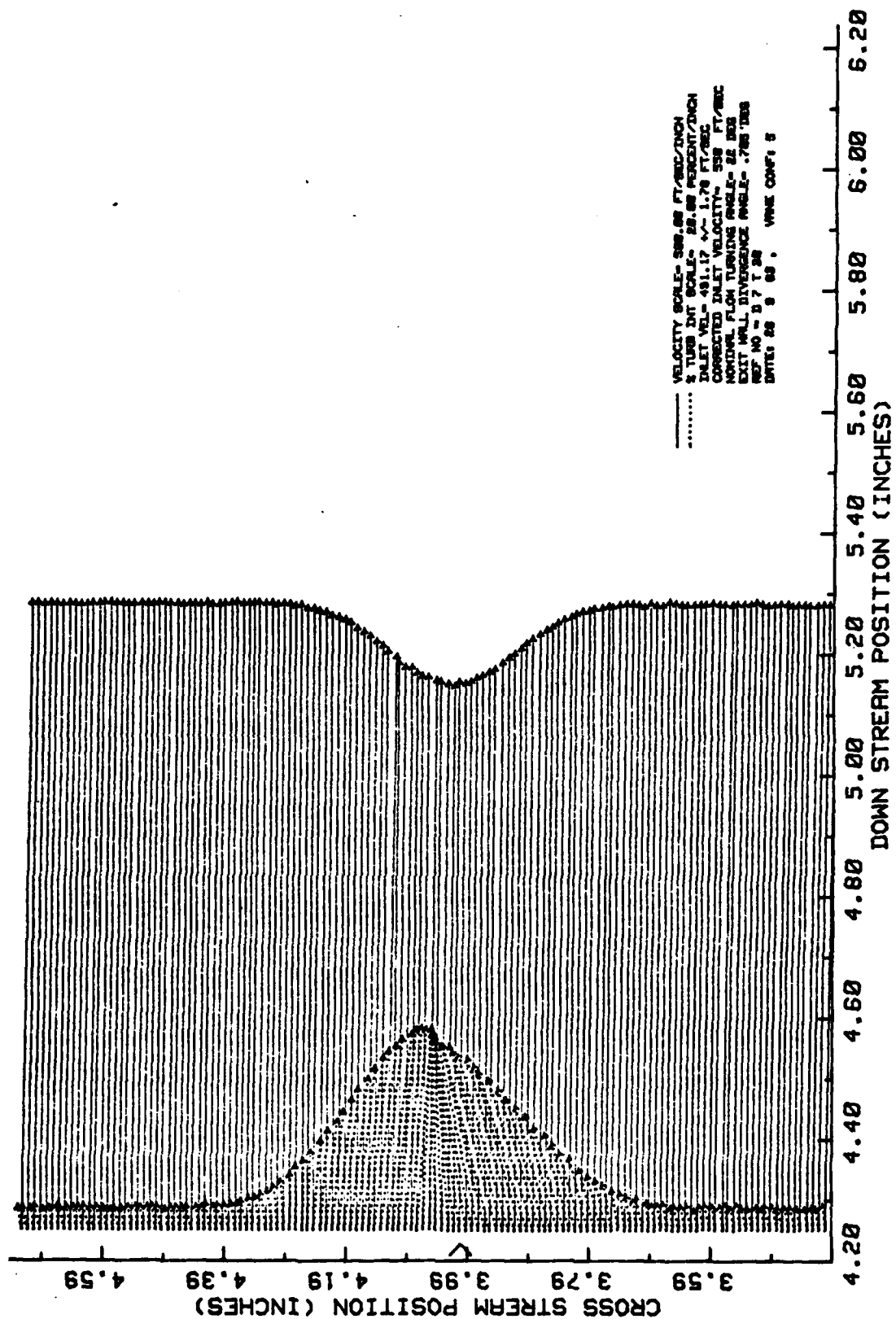
(C) Traverse#3
Figure 31: Continued

VANE WAKE: CONF. NO.5, EVAL. NO.2



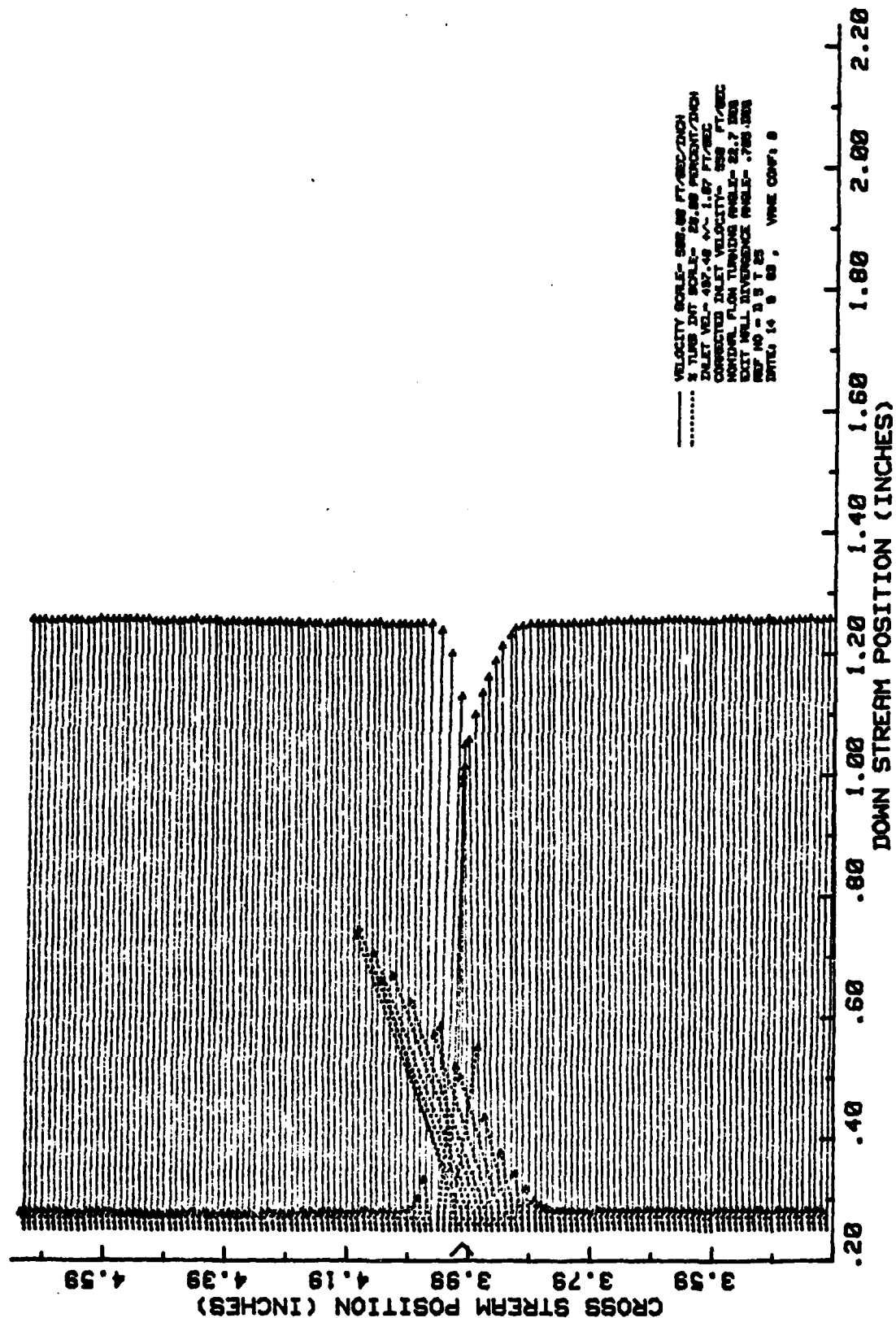
(D) Traverse#4
Figure 31: Continued

VANE WAKE: CONF. NO.5, EVAL. NO.2



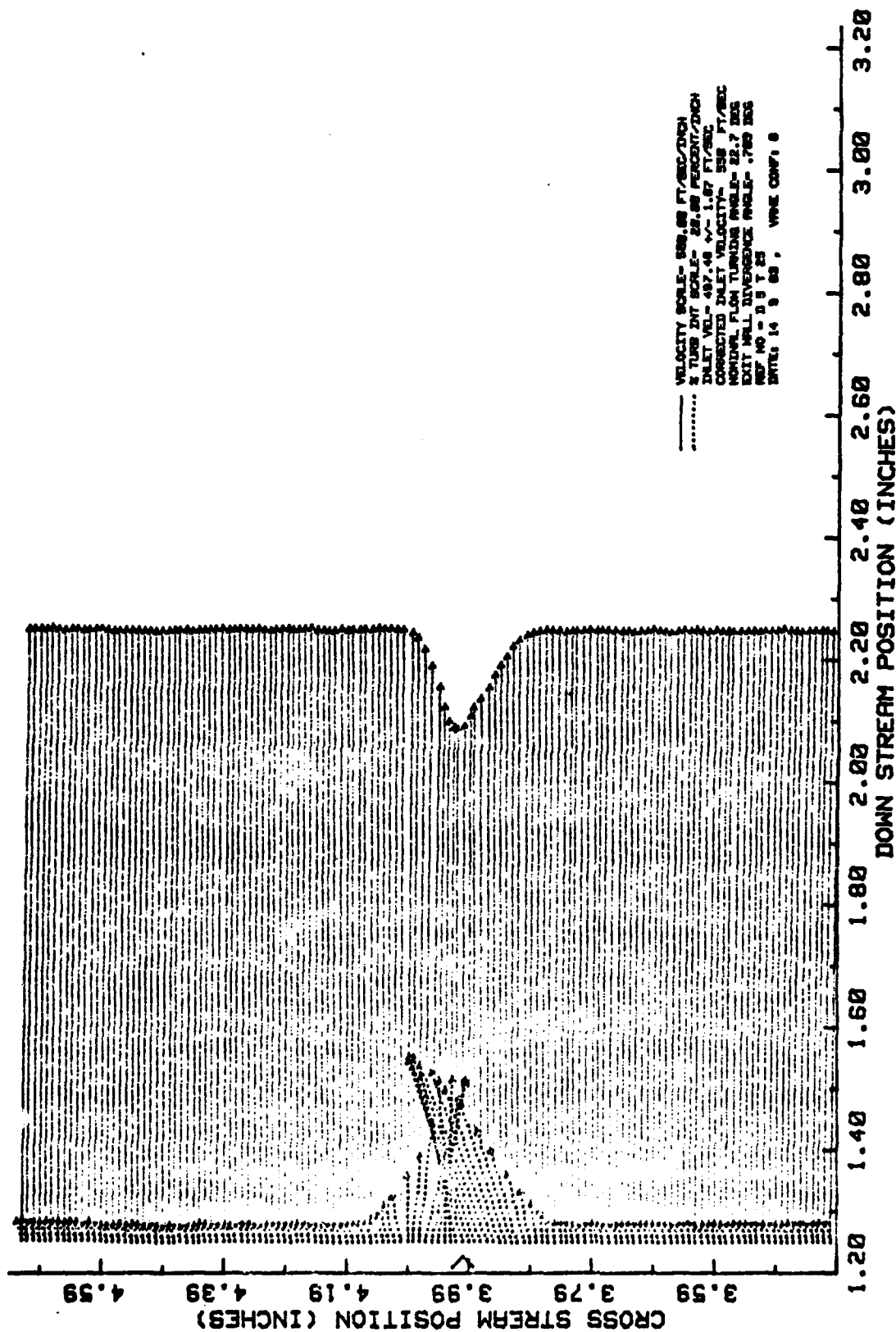
(E) Traverse#5
Figure 31: Continued

VANE WAKE: CONF. NO.6, EVAL. NO.2



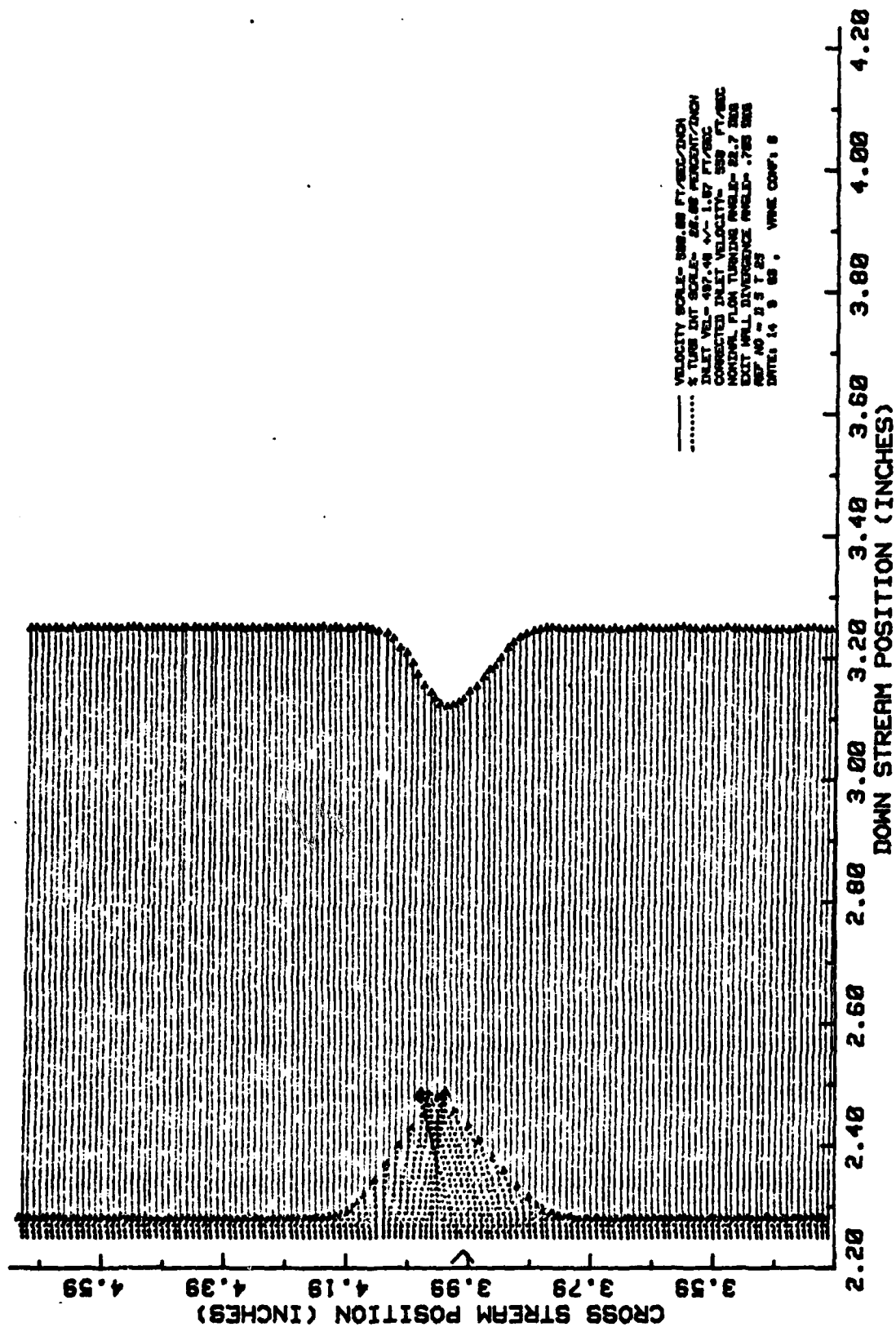
(A) Traverse #1
 Figure 32: Velocity and Turbulence Intensity Profile
 Conf#6 Eval#2: 3 micro-meter Ra Roughness from L.E.-1/4Cord

VANE WAKE: CONF. NO.6, EVAL. NO.2



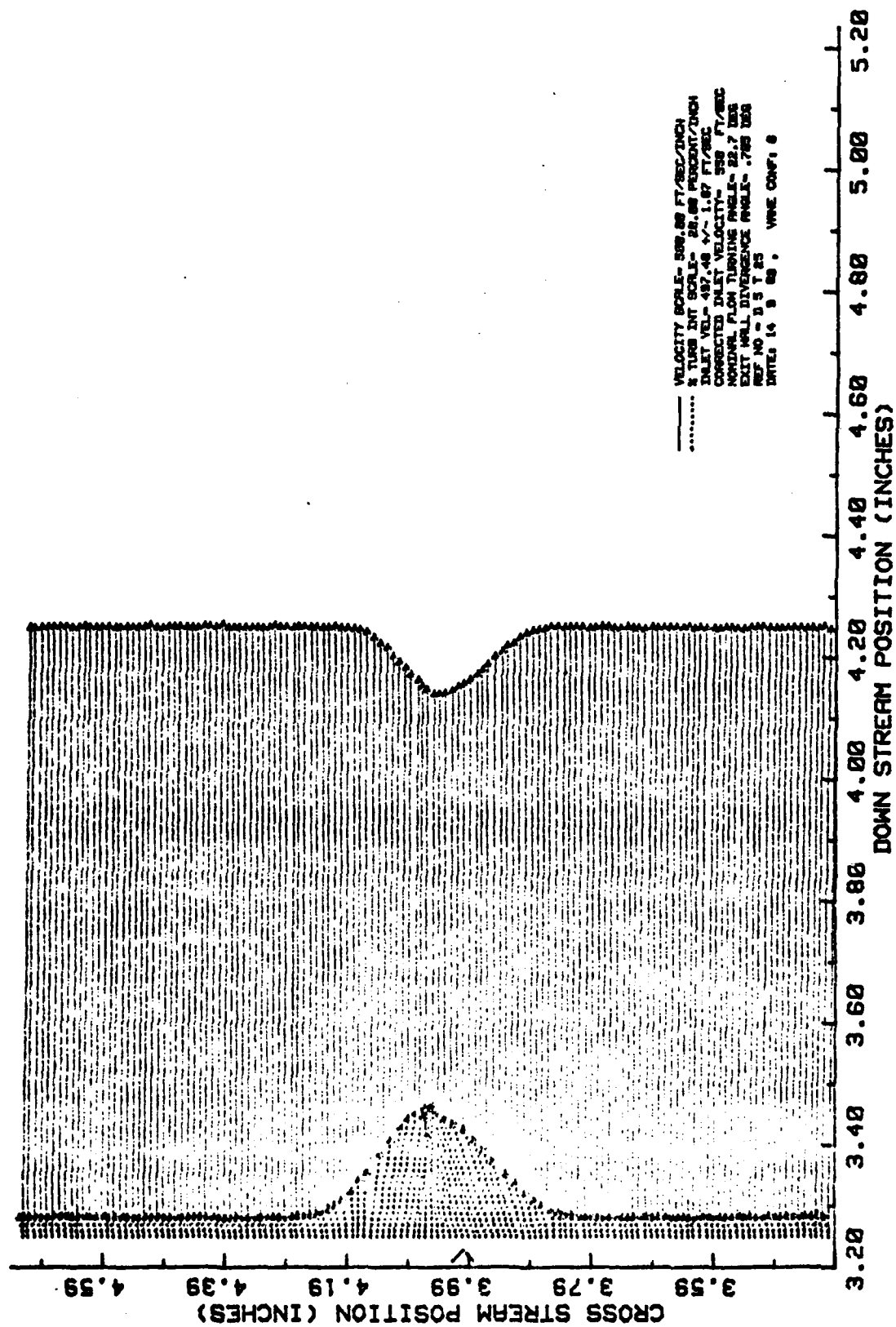
(B) Traverse#2
Figure 32: Continued

VANE WAKE: CONF. NO.6, EVAL. NO.2



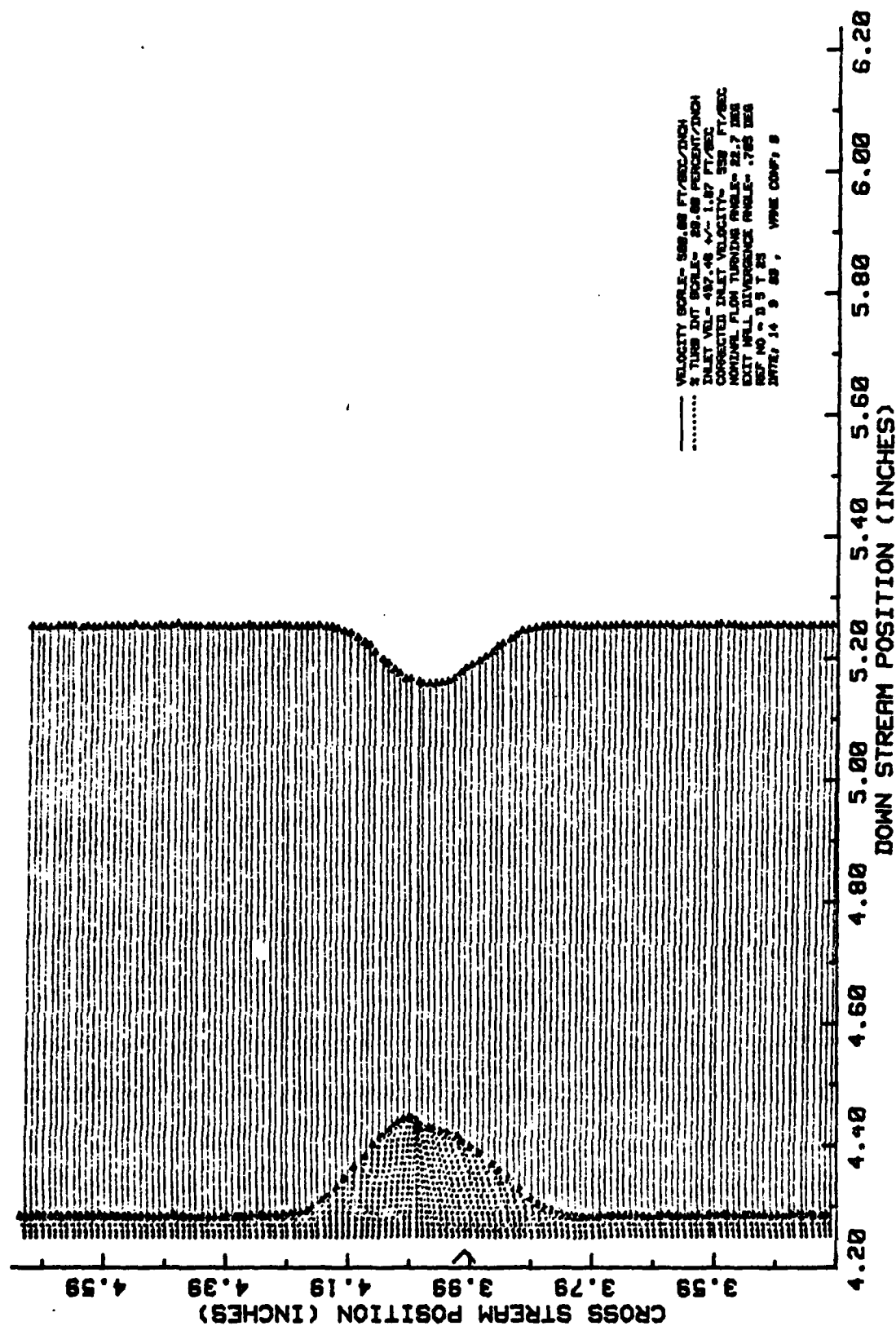
(C) Traverse #3
Figure 32: Continued

VRNE WAKE: CONF. NO.6, EVAL. NO.2



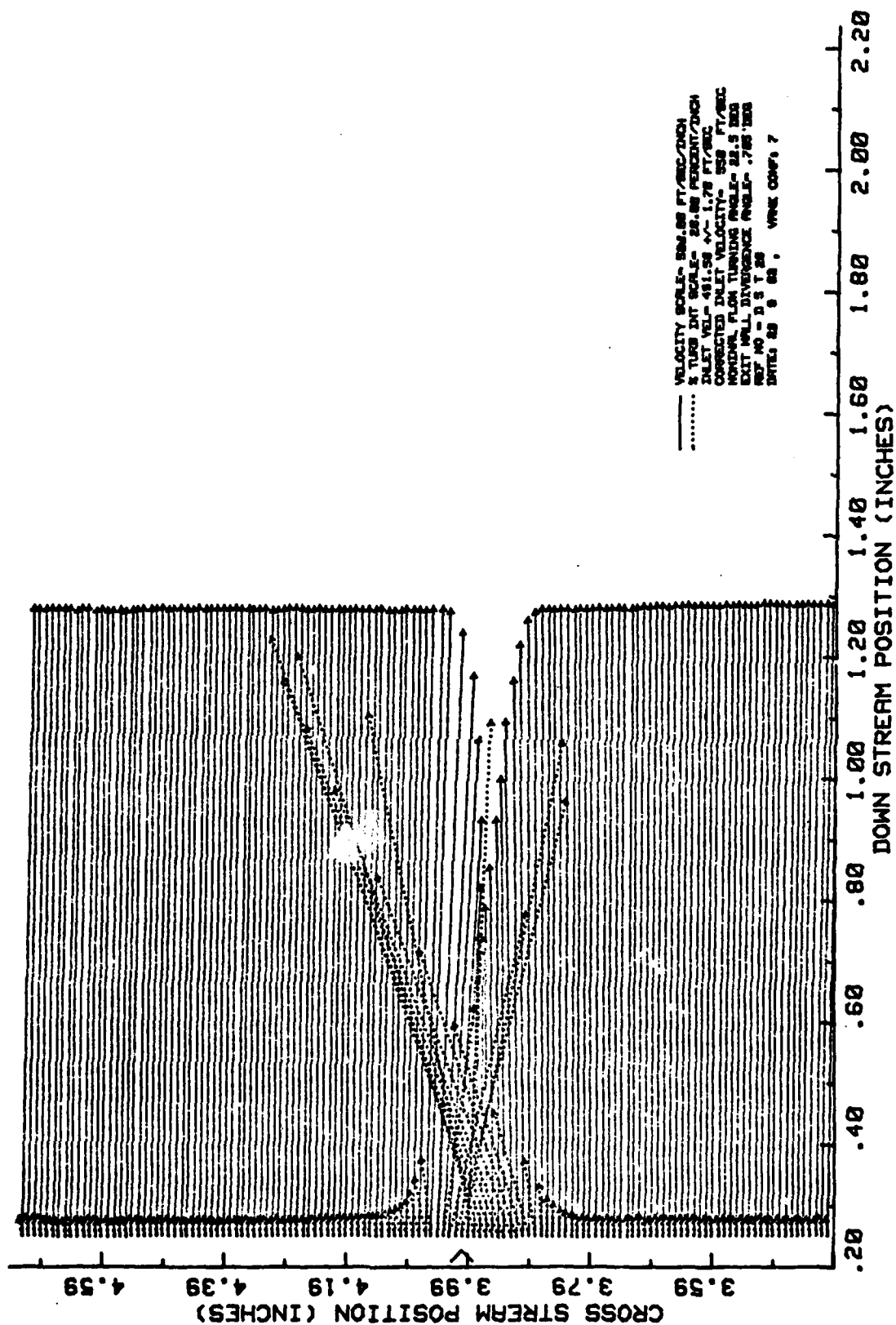
(D) Traverse#4
Figure 32: Continued

VANE WAKE: CONF. NO.6, EVAL. NO.2



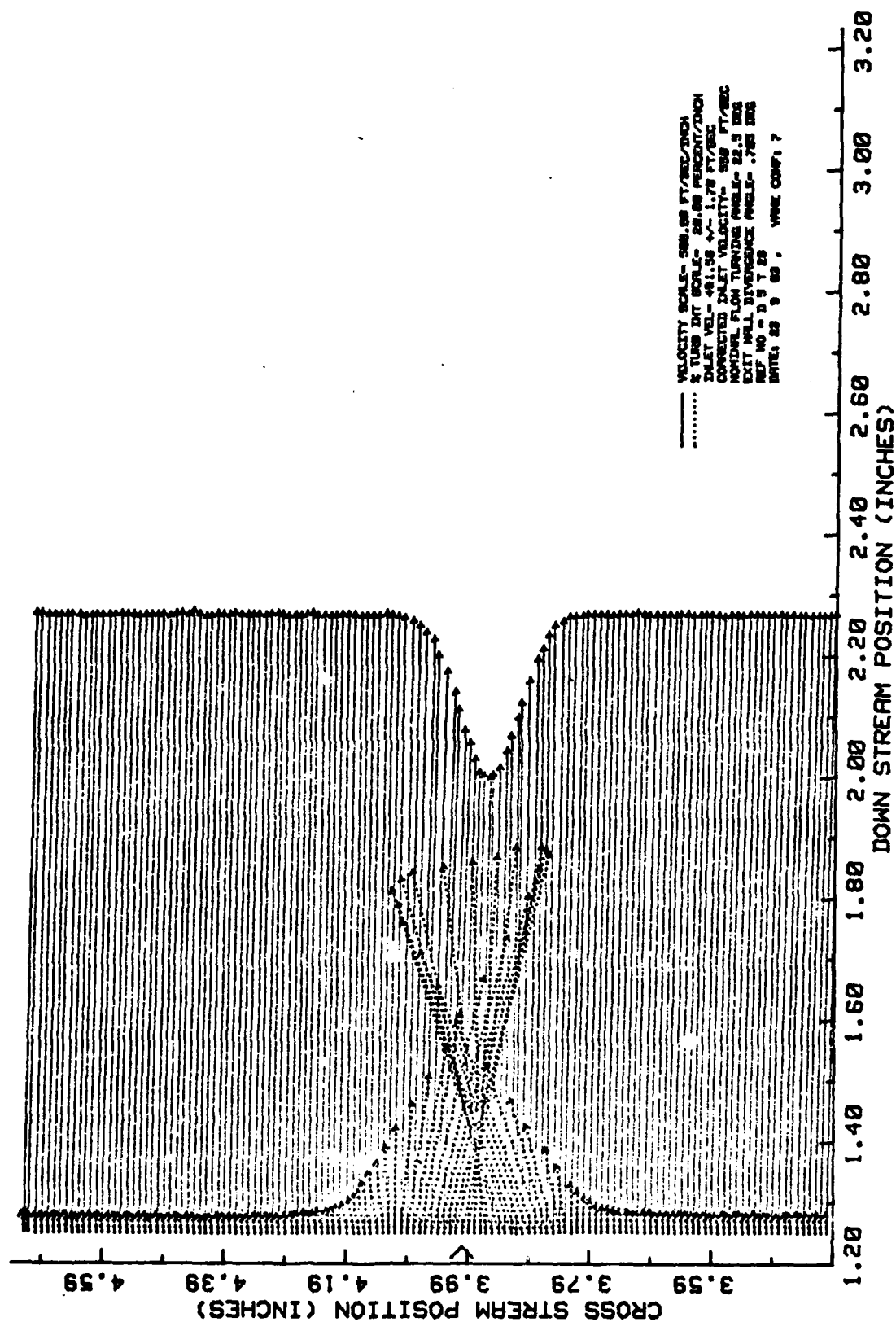
(E) Traverse#5
Figure 32: Continued

VANE WAKE: CONF. NO.7, EVAL. NO.1



(A) Traverse #1
 Figure 33: Velocity and Turbulence Intensity Profile
 Conf#7 Eval#1: 20 micro-meter Ra Roughness from 1/8-3/8Chord

VANE WAKE: CONF. NO.7, EVAL. NO.1



(B) Traverse#2
Figure 33: Continued

AD-A136 896

ROUGHNESS EFFECTS ON COMPRESSOR BLADE PERFORMANCE IN
CASCADE AT HIGH REYN. (U) AIR FORCE INST OF TECH
WRIGHT-PATTERSON AFB OH SCHOOL OF ENGI. F J TANIS
NOV 83 AFIT/GAE/AA/83D-23

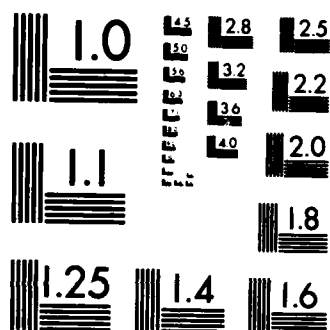
2/2

UNCLASSIFIED

F/G 20/4

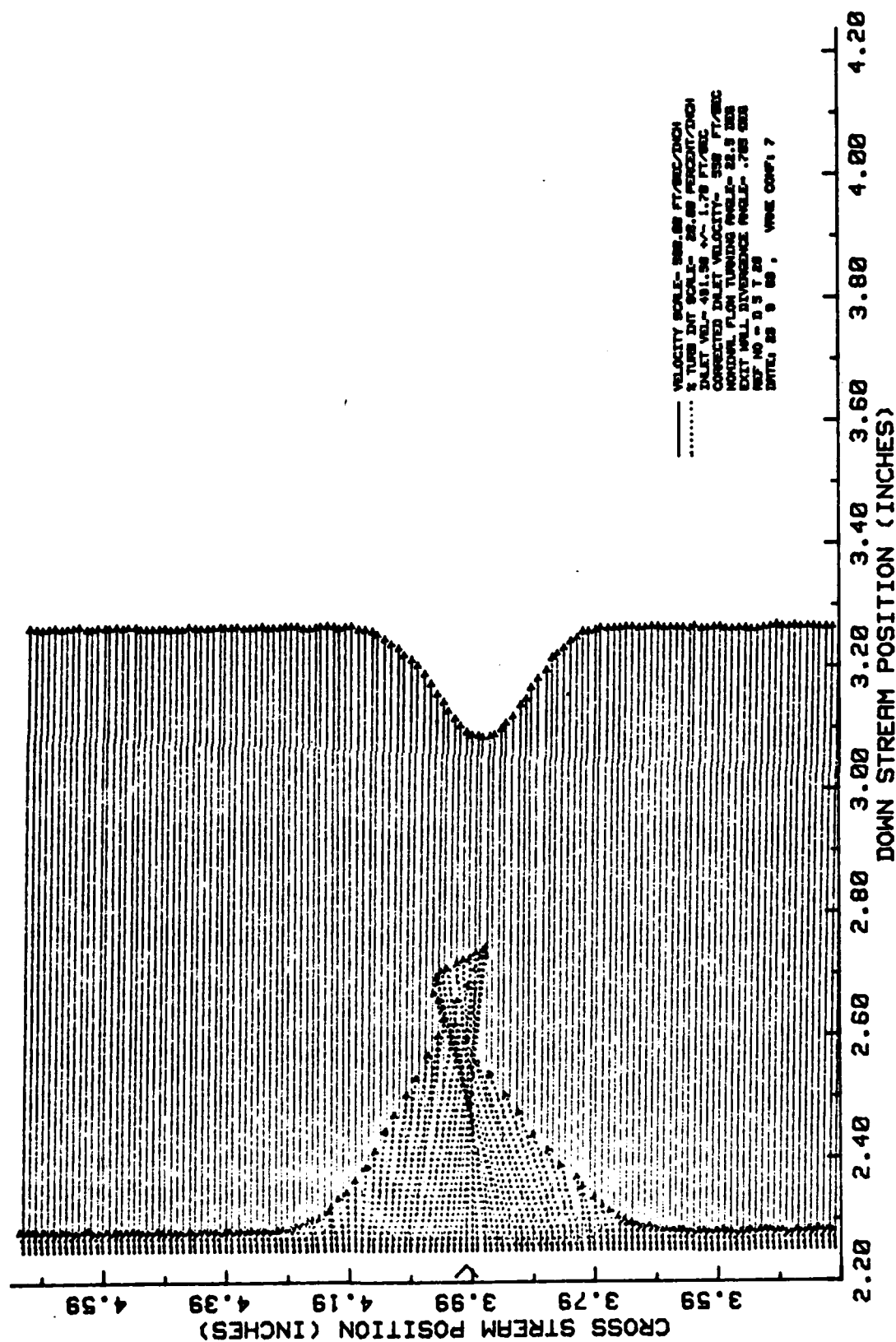
NL

END

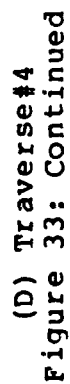


MICROCOPY RESOLUTION TEST CHART
NATIONAL BUREAU OF STANDARDS-1963-A

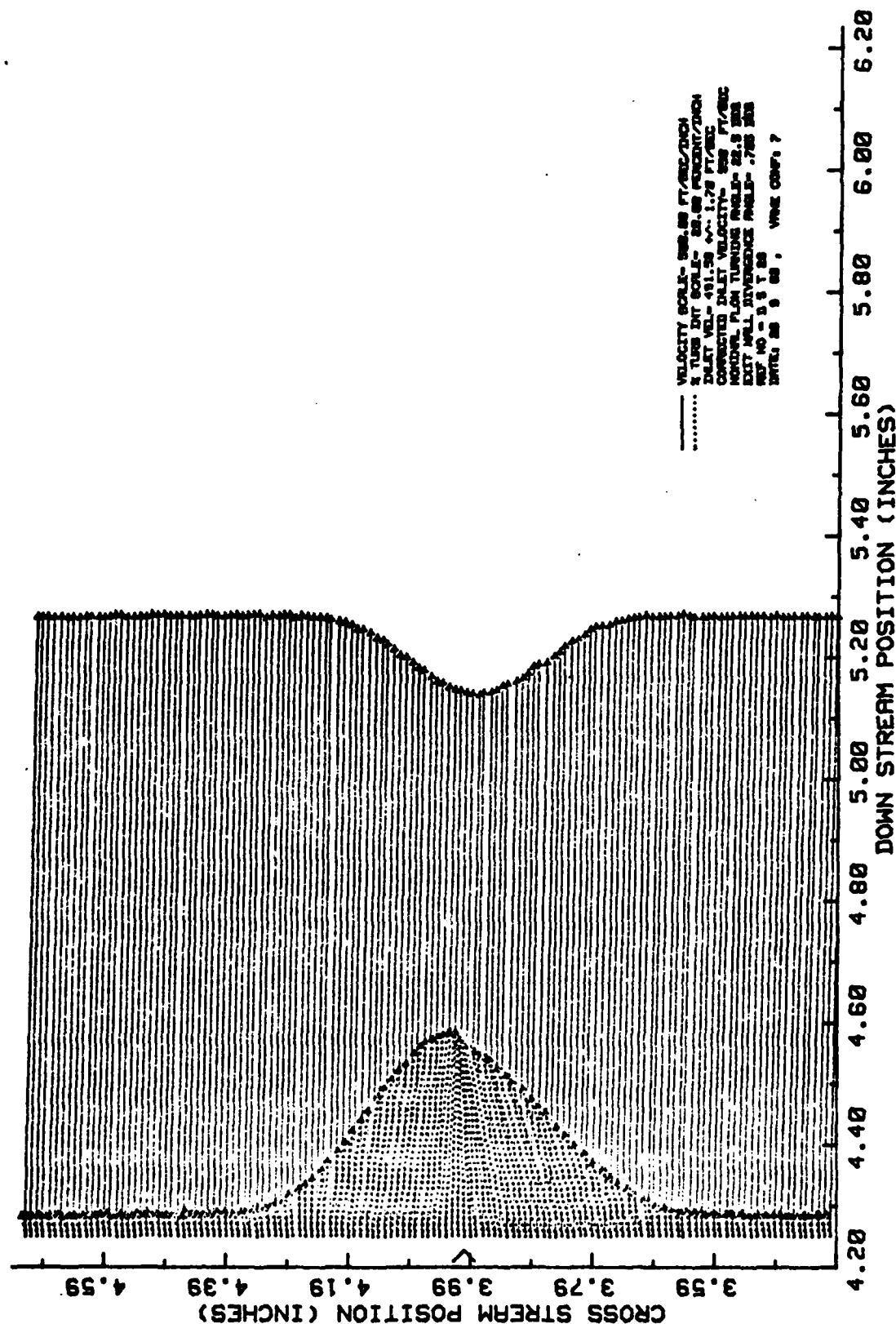
VANE WAKE: CONF. NO.7, EVAL. NO.1



(C) Traverse#3
Figure 33: Continued



VANE WAKE: CONF. NO.7, EVAL. NO.1



(E) Traverse #5

Figure 33: Continued

VANE WAKE: CONF. NO.8, EVAL. NO.1

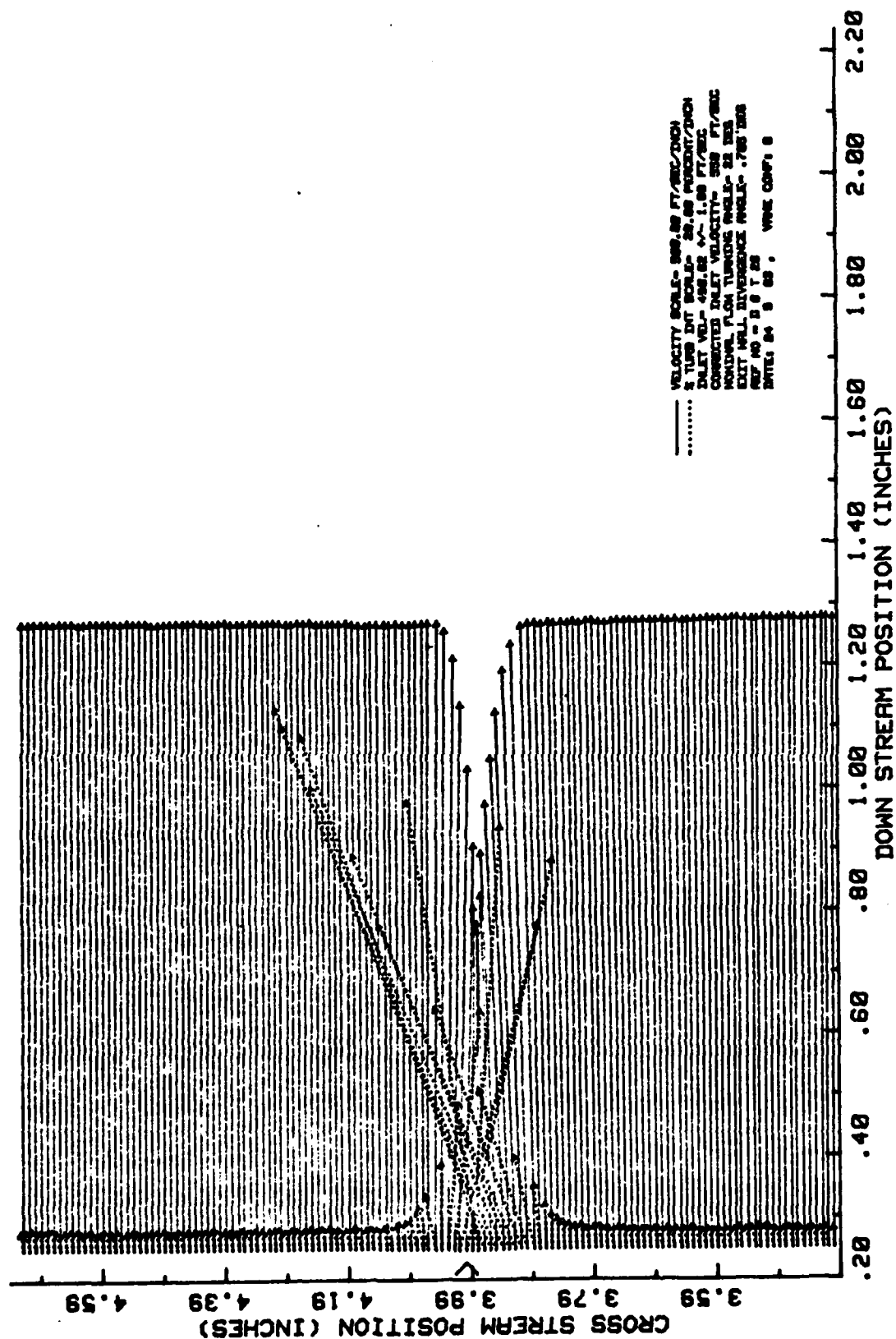
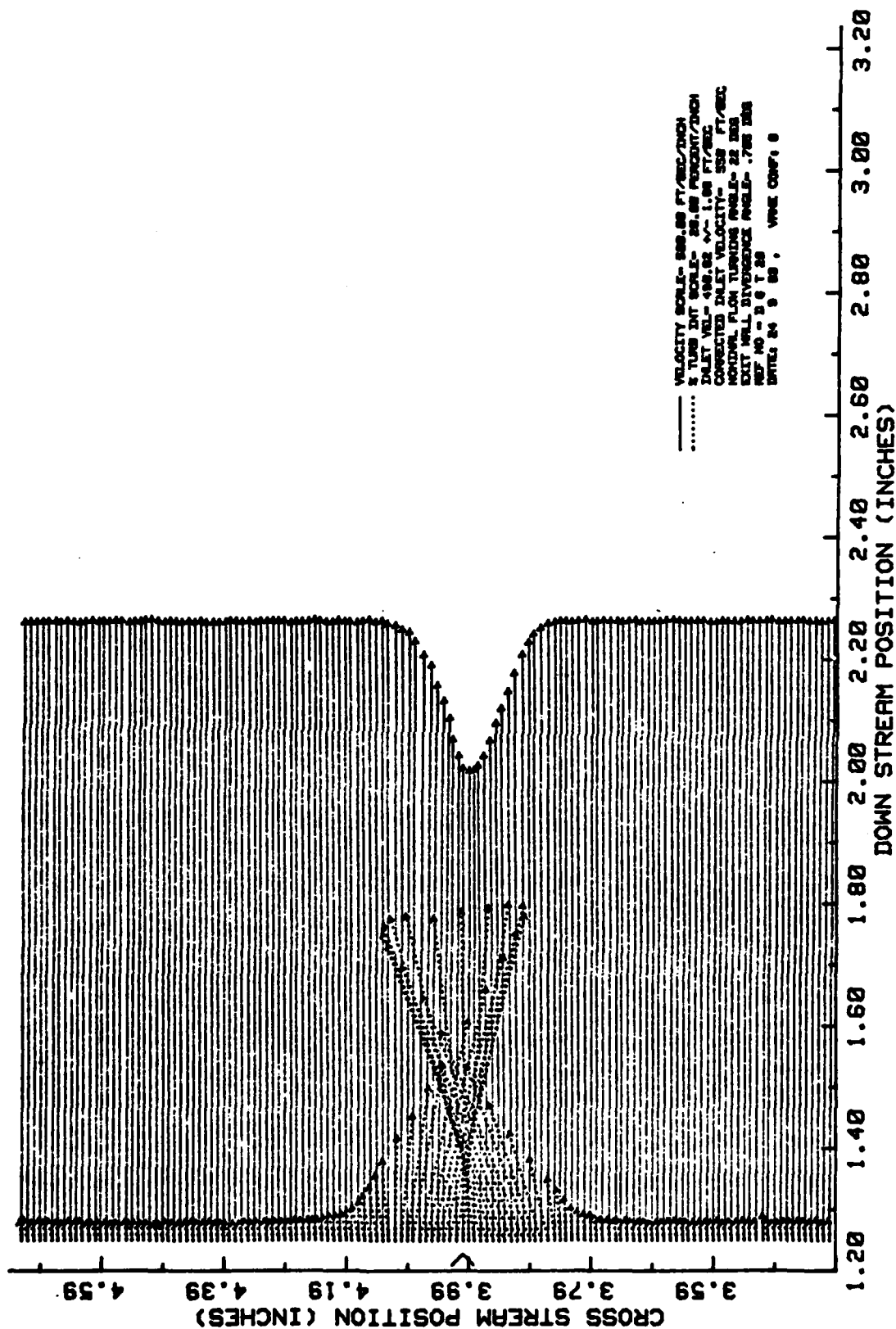


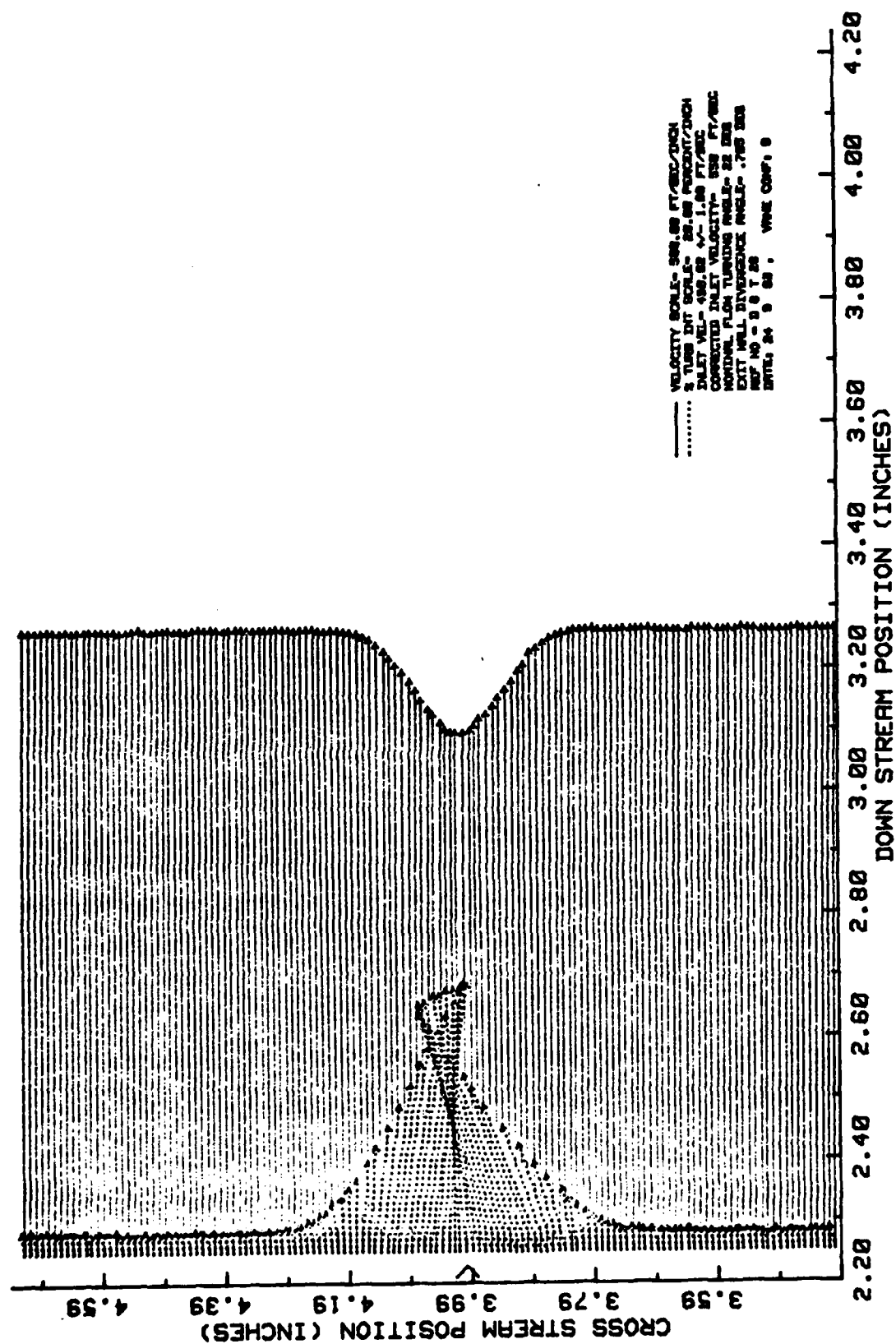
Figure 34: Velocity and Turbulence Intensity Profile
 Conf#8 Eval#1: 20 micro-meter Ra Roughness from 1/4-1/2Chord

VANE WAKE: CONF. NO.8, EVAL. NO.1



(B) Traverse#2
 Figure 34: Continued

VANE WAKE: CONF. NO.8, EVAL. NO.1



(C) Traverse#3
Figure 34: Continued

VRANE WAKE: CONF. NO.8, EVAL. NO.1

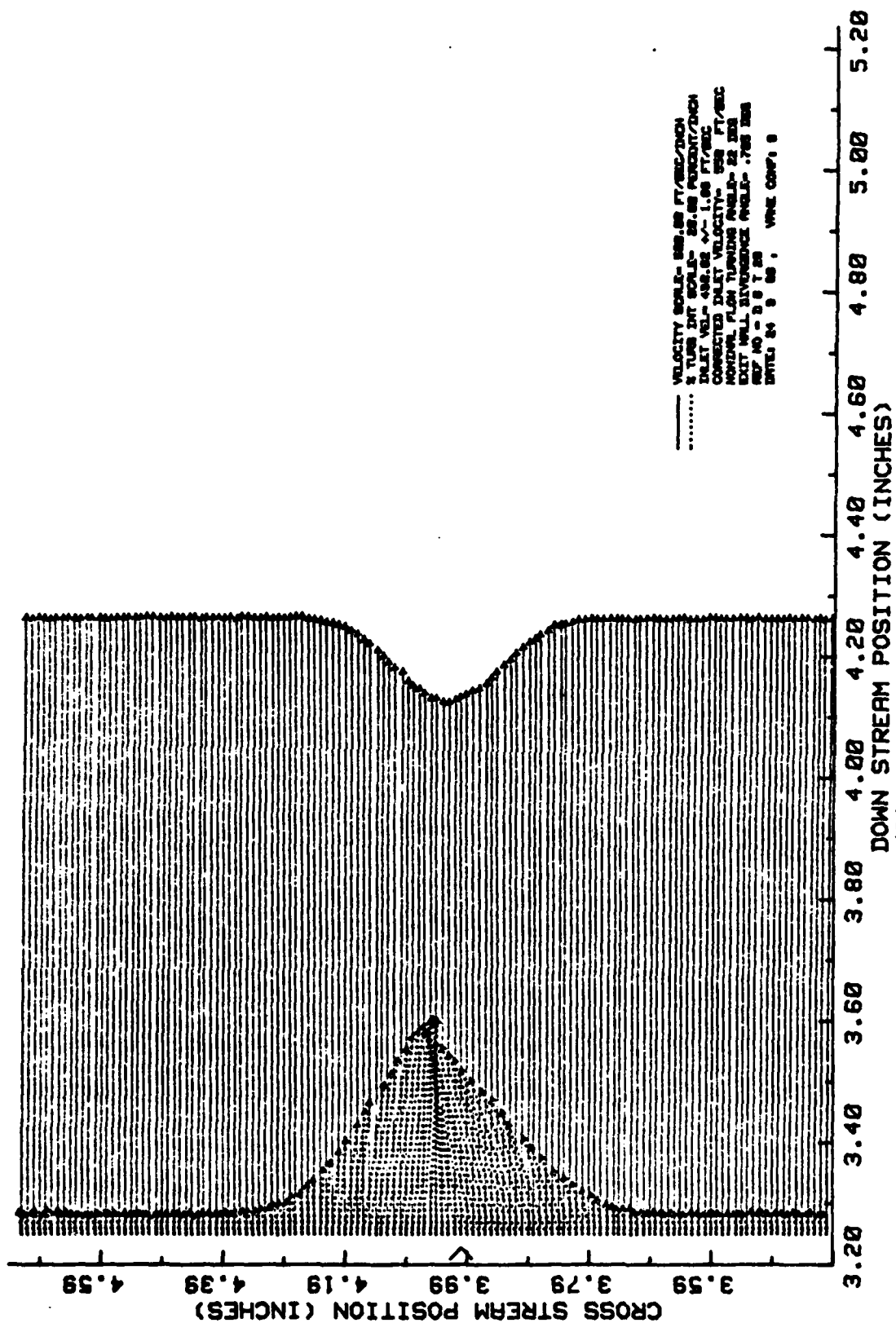
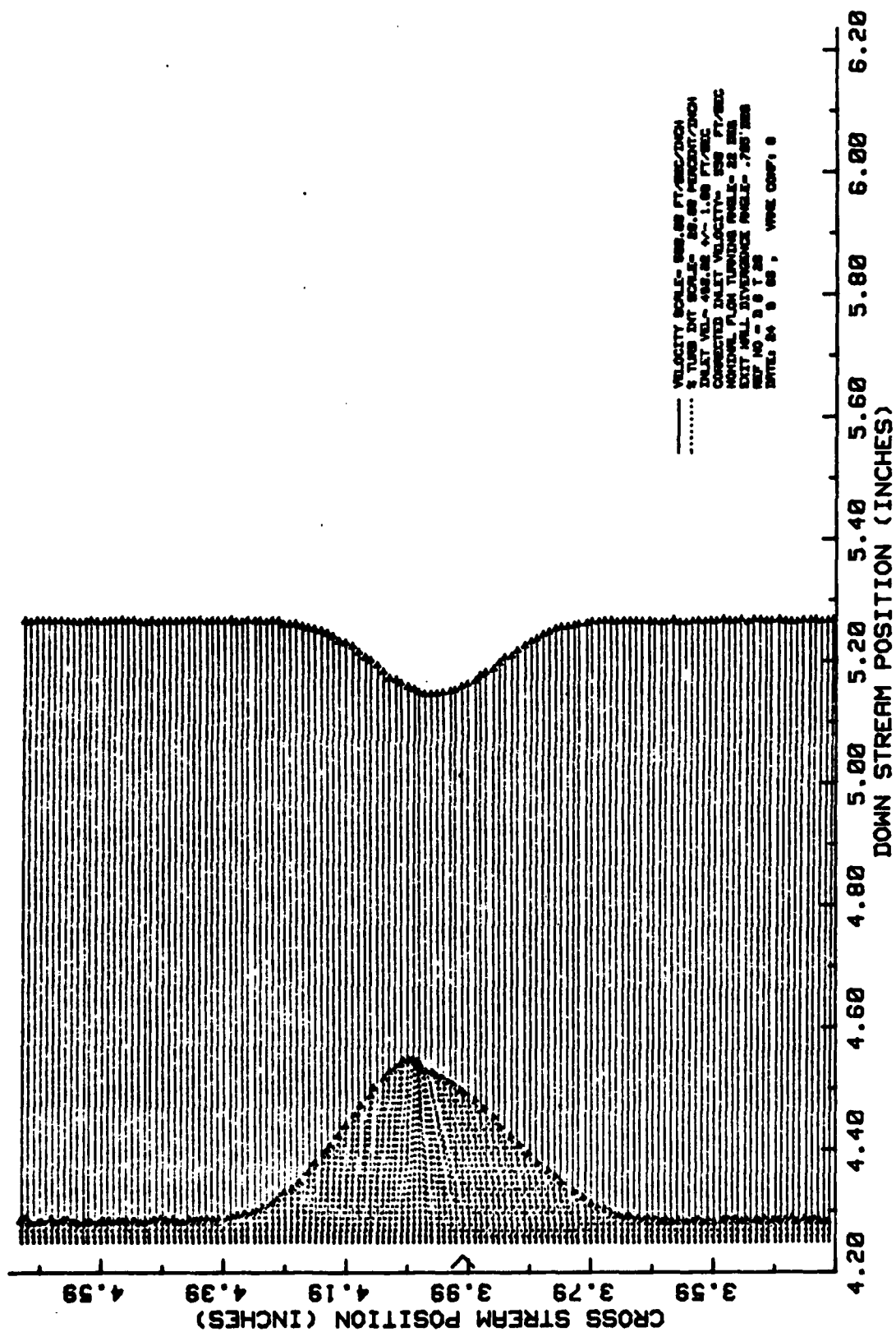


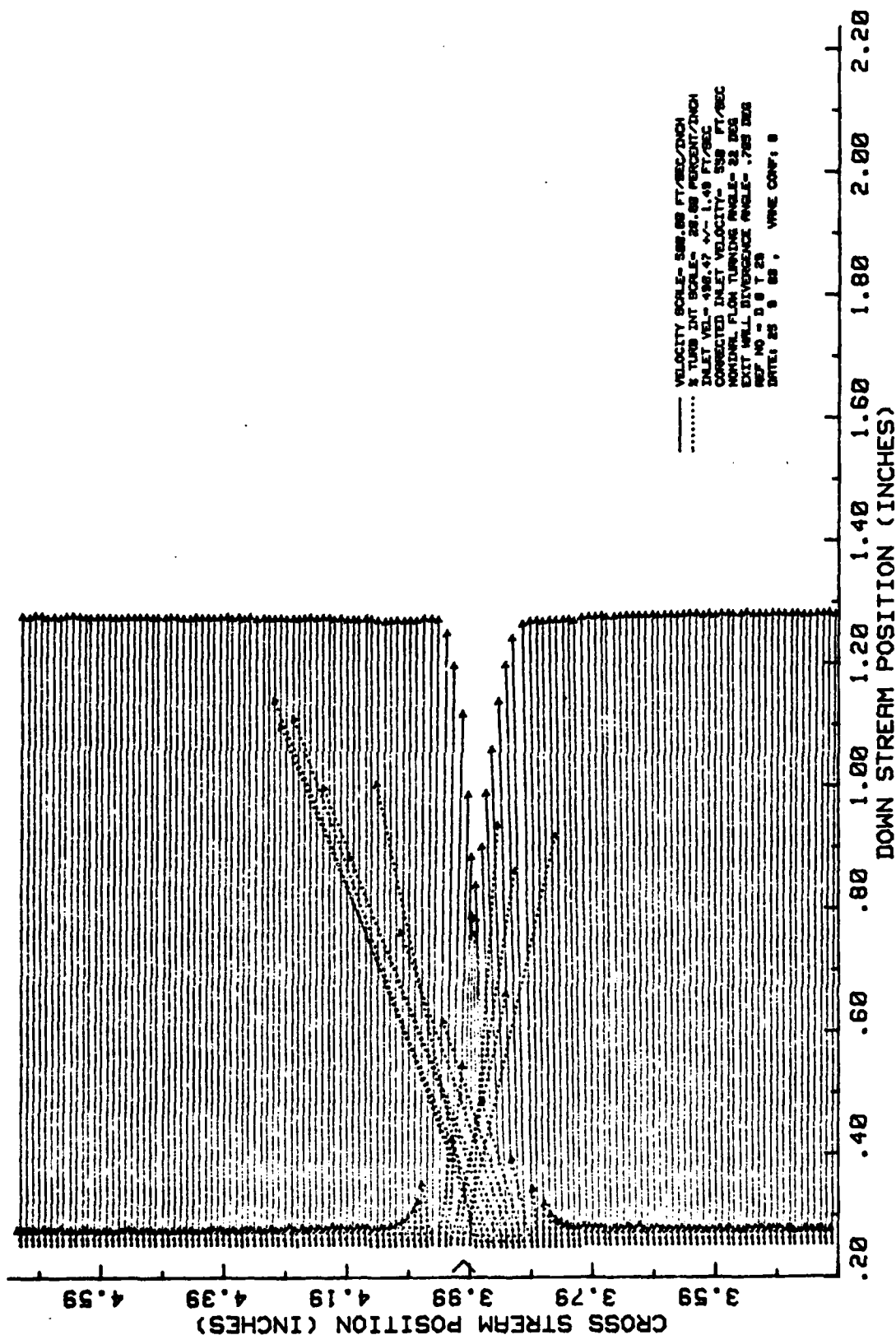
Figure 34: Continued
(D) Traverse#4

VANE WAKE: CONF. NO.8, EVAL. NO.1



(E) Traverse#5
Figure 34: Continued

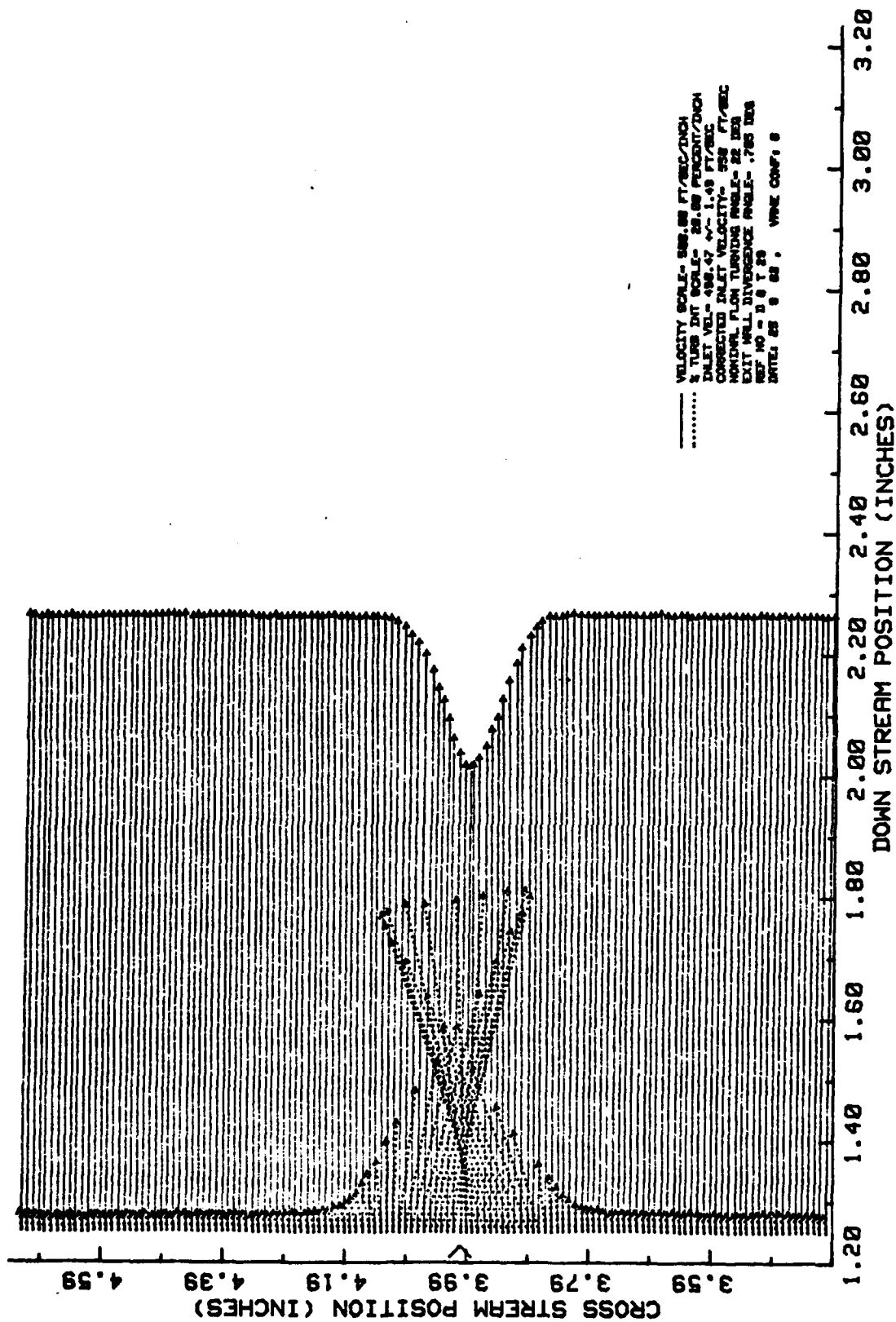
VANE WAKE: CONF. NO.8, EVAL. NO.2



(A) Traverse#1

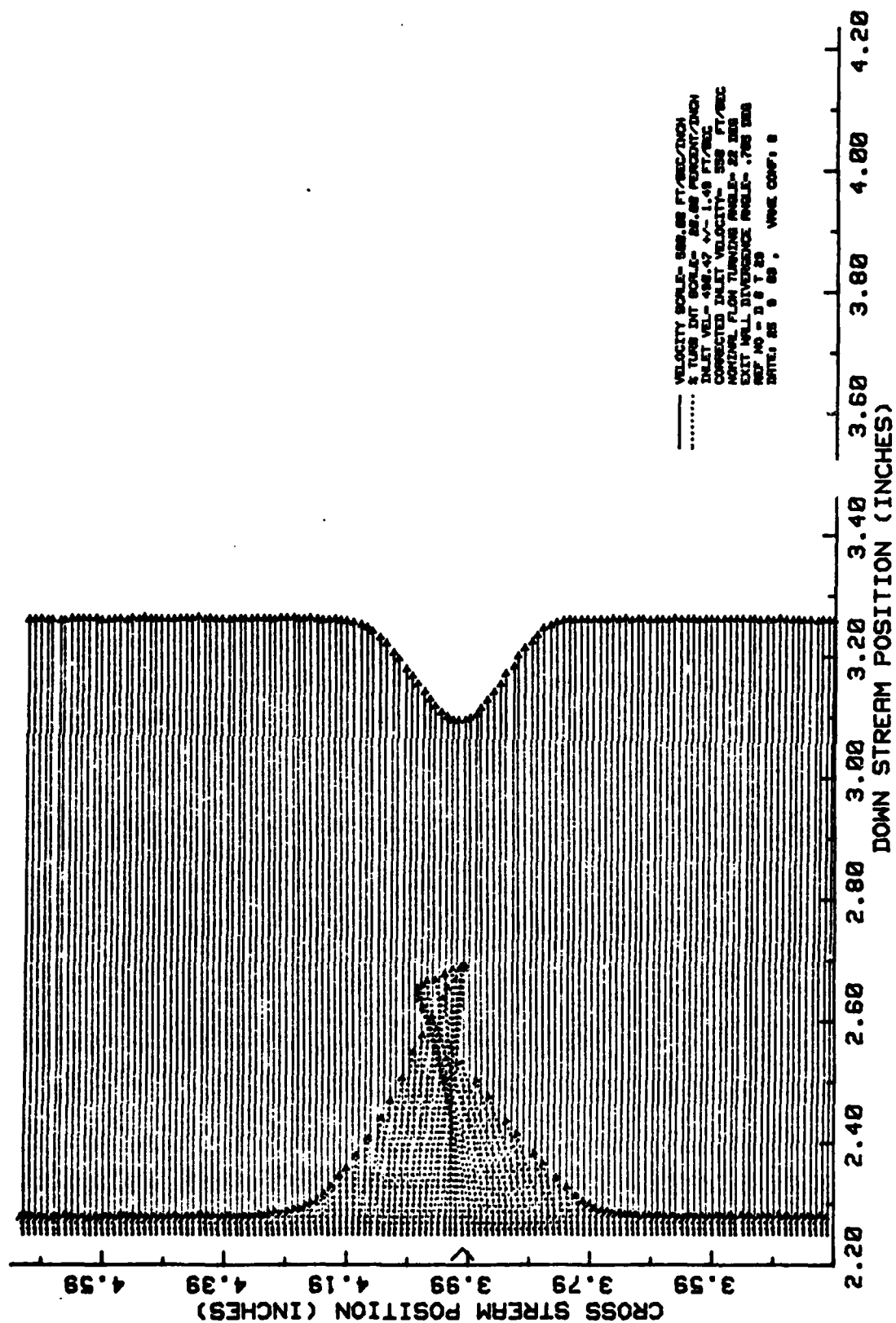
Figure 35: Velocity and Turbulence Intensity Profile
Conf#8 Eval#2: 20 micro-meter Ra Roughness from 1/4-1/2Chord

VRANE WAKE: CONF. NO.8, EVAL. NO.2



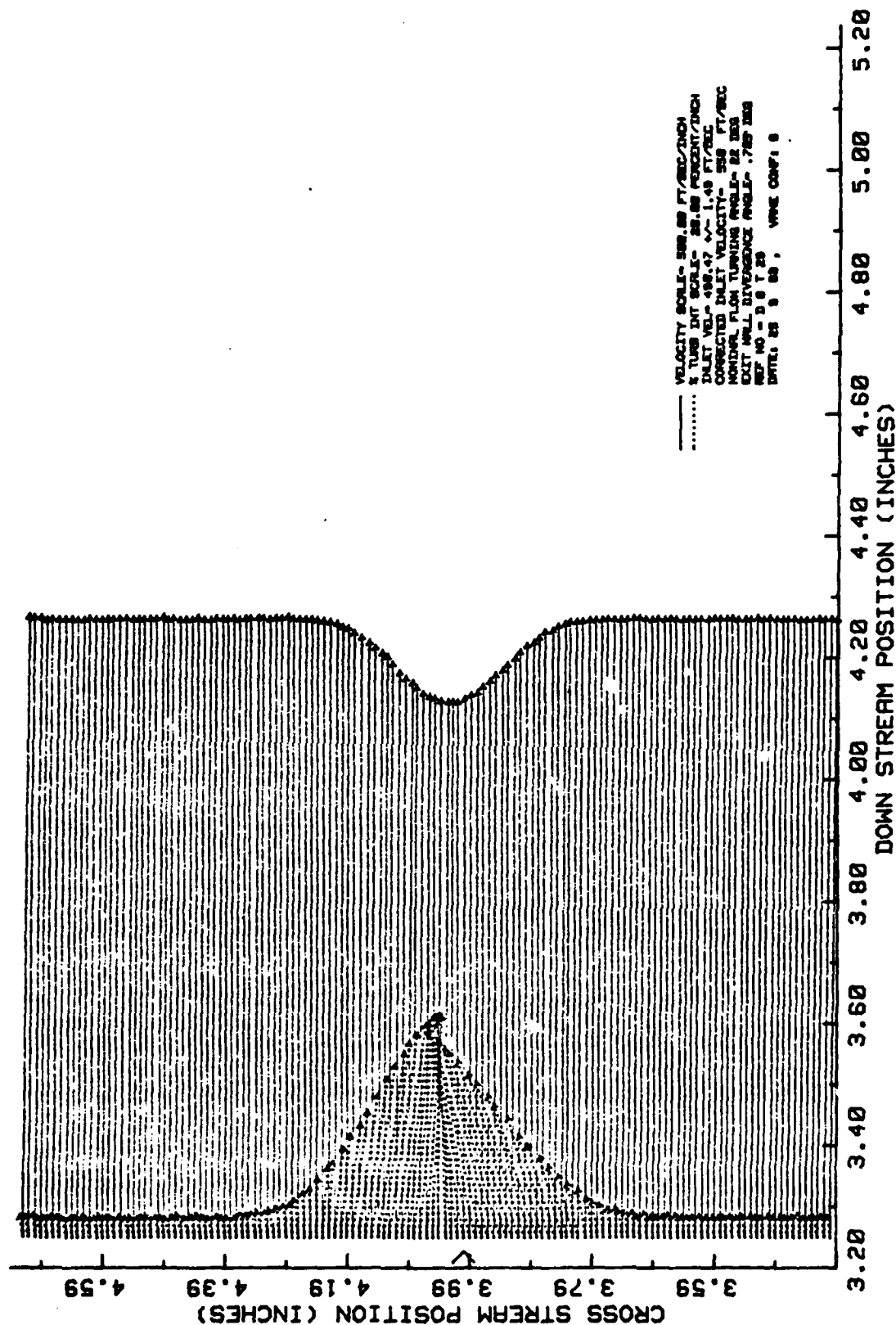
(B) Traverse#2
Figure 35: Continued

VANE WAKE: CONF. NO.8, EVAL. NO.2



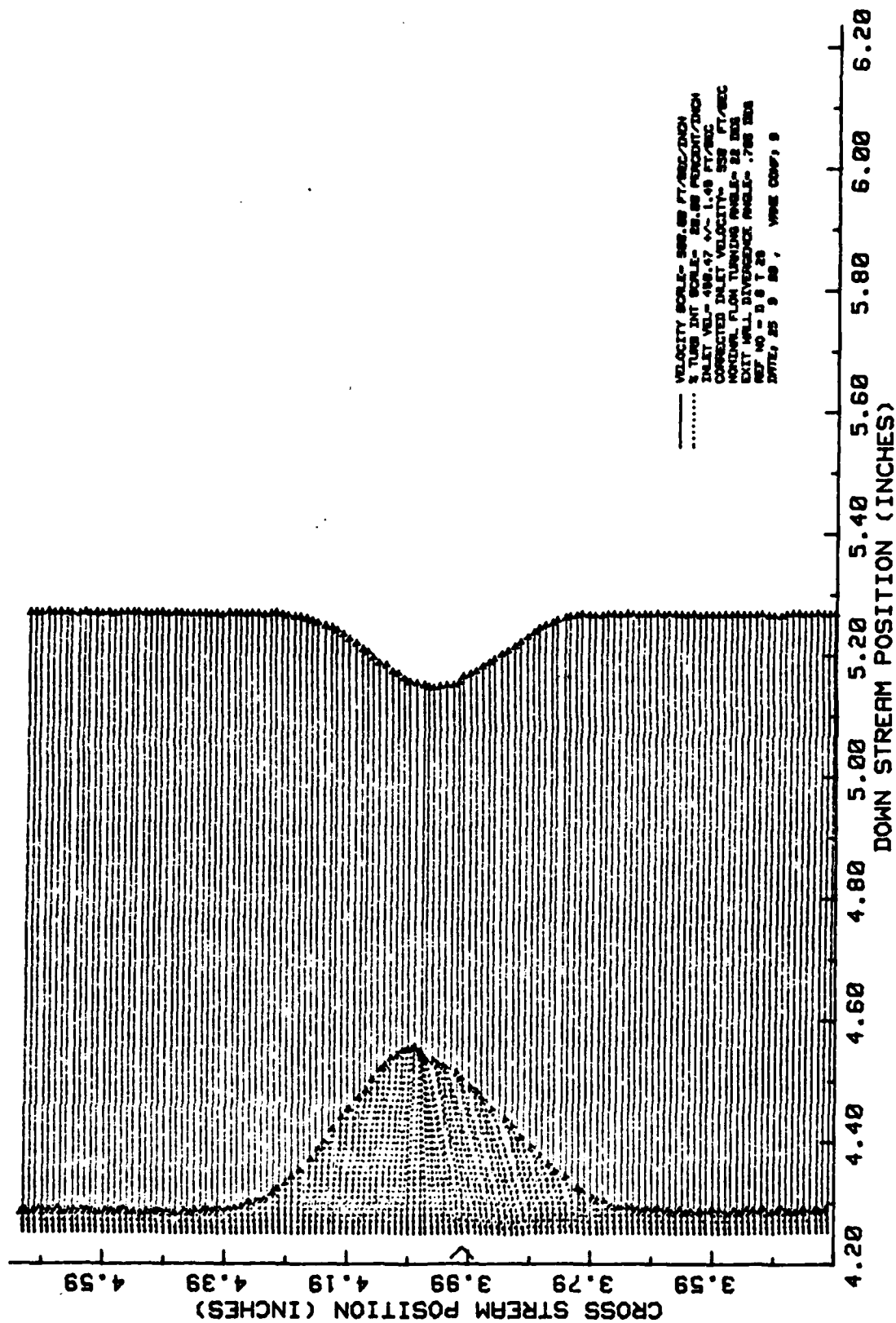
(C) Traverse#3
Figure 35: Continued

VANE WAKE: CONF. NO.8, EVAL. NO.2



(D) Traverse #4
Figure 35: Continued

VANE WAKE: CONF. NO.8, EVAL. NO.2



(E) Traverse #5
Figure 35: Continued

VITA

Frederick Johnson Tanis Jr. was born on 29 July 1960 in Red Bank New Jersey. After graduating from Middletown High School South in 1978 he attended Lafayette College in Easton Pennsylvania. He graduated from Lafayette College Cum Laude with a Bachelor of Science degree in Mechanical Engineering in May of 1982. He received his commission in the United States Air Force Reserve through the Reserve Officer Training Corps at Lehigh University in June of 1982. As his first assignment Lt Tanis entered the Air Force Institute of Technology at Wright Patterson AFB in June of 1982.

Permanent Address:

500 Newman Springs Rd.

Lincroft New Jersey 07738

UNCLASSIFIED

SECURITY CLASSIFICATION OF THIS PAGE

REPORT DOCUMENTATION PAGE

1a. REPORT SECURITY CLASSIFICATION UNCLASSIFIED			1b. RESTRICTIVE MARKINGS				
2a. SECURITY CLASSIFICATION AUTHORITY			3. DISTRIBUTION/AVAILABILITY OF REPORT Approved for public release; distribution unlimited				
2b. DECLASSIFICATION/DOWNGRADING SCHEDULE							
4. PERFORMING ORGANIZATION REPORT NUMBER(S) AFIT/GAE/AA/83D-23			5. MONITORING ORGANIZATION REPORT NUMBER(S)				
6a. NAME OF PERFORMING ORGANIZATION School of Engineering		6b. OFFICE SYMBOL (If applicable) AFIT/ENY		7a. NAME OF MONITORING ORGANIZATION			
6c. ADDRESS (City, State and ZIP Code) Air Force Institute of Technology Wright-Patterson AFB, Ohio 45433			7b. ADDRESS (City, State and ZIP Code)				
8a. NAME OF FUNDING/SPONSORING ORGANIZATION		8b. OFFICE SYMBOL (If applicable)		9. PROCUREMENT INSTRUMENT IDENTIFICATION NUMBER			
8c. ADDRESS (City, State and ZIP Code)			10. SOURCE OF FUNDING NOS.				
11. TITLE (Include Security Classification) See Box 19			PROGRAM ELEMENT NO.		PROJECT NO.	TASK NO.	WORK UNIT NO.
12. PERSONAL AUTHOR(S) Frederick J. Tanis Jr., B.S., 2d Lt, USAF							
13a. TYPE OF REPORT MS Thesis		13b. TIME COVERED FROM _____ TO _____		14. DATE OF REPORT (Yr., Mo., Day) 1983 December		15. PAGE COUNT 108	
16. SUPPLEMENTARY NOTATION <div style="text-align: right;">Approved for public release: 14W AFH 190-17. <i>J. E. Wolan</i> Lieut. E. Wolan Dept. of Engineering and Professional Development Air Force Institute of Technology (AFIT) Wright-Patterson AFB, Ohio 45433</div> <div style="text-align: right;">3 JAN 1984</div>							
17. COSATI CODES			18. SUBJECT TERMS (Continue on separate page if necessary and identify by block number)				
FIELD	GROUP	SUB. GR.	Cascade Testing, Compressor Blades, Roughness Effects High Reynolds Number, Total Pressure Loss				
21	1						
19. ABSTRACT (Continue on reverse if necessary and identify by block number)							
<p>Title: Roughness Effects on Compressor Blades Performance in Cascade at High Reynolds Number</p> <p>Thesis Chairman: Dr. William C. Elrod</p>							
20. DISTRIBUTION/AVAILABILITY OF ABSTRACT UNCLASSIFIED/UNLIMITED <input checked="" type="checkbox"/> SAME AS RPT. <input type="checkbox"/> DTIC USERS <input type="checkbox"/>				21. ABSTRACT SECURITY CLASSIFICATION UNCLASSIFIED			
22a. NAME OF RESPONSIBLE INDIVIDUAL William C. Elrod			22b. TELEPHONE NUMBER (Include Area Code) 513-255-3517		22c. OFFICE SYMBOL AFIT/ENY		

An experimental investigation of the effects of roughness on compressor blade performance in cascade at high reynolds number was performed. A seven blade cascade of NACA 64-A905 blades with a chord of 2 in and an aspect ratio of 1 was tested in a linear cascade. The blades were mounted with a stagger angle of 31 deg and an angle of attack of 15 deg. The spacing between the blades was 1.33 in which gave a solidity of 1.5.

This study was divided into two parts, first to determine the importance of the location of the roughness on the blade performance and second to determine how the degree of roughness affects blade performance. The velocity and turbulence intensity profiles of the flow region down stream of the center blade and the non-dimensional total pressure loss parameter, ω , were used to evaluate blade performance. Hot wire anemometry was used to measure the velocity and turbulence intensity profiles down stream of the blade. The measured exit velocity and static pressure were used to derive the exit total pressure.

Roughness located near the leading edge of the blade caused the greatest impact on ω and the velocity and turbulence intensity profiles. Changes in the magnitude of the roughness did not affect the blade performance until a threshold was exceeded then the performance decreased rapidly.

END

FILMED

2-84

DTIC